HCMUTE

Graphic Arts and Media

Sponsored by:

The 12th Asian Symposium on Printing Technology (ASPT 2022)
September 15th and 16th, 2022

Advancements in Printing Engineering Technology

Ho Chi Minh City University of Technology and Education
Thu Duc City, Ho Chi Minh City, Vietnam

The 12th Asian Symposium on Printing Technology (ASPT 2022)

Advancements in Printing Engineering Technology

Host

Ho Chi Minh City University of Technology and Education,

Printing Association of Ho Chi Minh City,

Vietnam Printing Association

Co-hosts

The Japanese Society of Printing Science and Technology (JSPST)

Chiba University

University of Tsukuba

Department of Engineering, Tokyo Polytechnic University

Department of Imaging and Printing Technology, Chulalongkorn University

September 15th and 16th, 2022

Ho Chi Minh City University of Technology and Education

Thu Duc City, Ho Chi Minh City, Vietnam

The 12th ASIAN SYMPOSIUM ON PRINTING TECHNOLOGY (ASPT 2022)

We are pleased to inform the 12th Asian Symposium on Printing Technology (ASPT 2022) for the first time since the successful 4th 2013 Asian Symposium (ASPT 2013) on Printing Technology in Vietnam. ASPT 2022, with the main topic Advancements in Printing Engineering technology, will be held on September 15th and 16th, 2022, at Ho Chi Minh City University of Technology and Education. The representative topics this year related to printing engineering technology are listed as follows:

- Eco-friendly printing
- Plastic-free packaging
- Functional and security printing
- Digital printing
- Prepress, pre-media and image processing
- Color management
- Print quality assessment
- Environment-friendly materials
- Printed electronic devices
- Others related to printing or imaging

The studied results from researchers as key sector players will be presented at the conference. To accomplish this symposium, we also cordially invite researchers and experts who are active in related fields to printing and packaging as well as keynote and speakers to enhance fruitful international exchange. In addition, this conference will provide oral and poster presentations in the sessions for more technical information and interactive discussion. We welcome many international attendees to this technical symposium, particularly from Asian countries.

Host: Ho Chi Minh City University of Technology and Education, Printing Association of Ho Chi Minh City, and Vietnam Printing Association.

Conference: The 12th Asian Symposium on Printing Technology (ASPT 2022).

Advancements in Printing Engineering Technology

Date: 15th and 16th September 2022

Venue: Ho Chi Minh City University of Technology and Education, Vietnam.

Contact: ASTP2022@hcmute.edu.vn

giangnl@hcmute.edu.vn (Chair)

phuongnt@hcmute.edu.vn (Secretary)

ngocntm@hcmute.edu.vn (Secretary)

Co-hosts: The Japanese Society of Printing Science and Technology (JSPST), Chiba University

Faculty of Life and Environmental Sciences, University of Tsukuba.

Department of Engineering, Tokyo Polytechnic University

Department of Imaging and Printing Technology, Chulalongkorn University

Homepage: http://www.aspt2022.hcmute.edu.vn

※This symposium was supported by JSPS Core-to-Core Program, (grant number: JPJSCCB20220006 ）

Committee:

A. Organizing Committee

Le Hieu Giang (HCMC University of Technology and Education)	Vice Rector of UTE
Nguyen Van Dong (Vietnam Printing Association)	President of VPA
Ngo Anh Tuan (Printing Association of Ho Chi Minh City)	President of HPA
Yoshihiko Azuma (Tokyo Polytechnic University)	President of JSPST
Nguyen Long Giang (HCMC University of Technology and Education)	Symposium Chair
Aran Hansuebsai (Chulalongkorn University)	Co-Chair
Suda Kiatkamjornwong (Chulalongkorn University)	Co-chair
Toshiharu Enomae (University of Tsukuba)	Co-chair
Shigeru Takahara (Chiba University)	Co-chair)
Toshifumi Satoh (Tokyo Polytechnic University)	Co-chair
Nguyen Thanh Phuong (HCMC University of Technology and Education)	Secretary
Nguyen Thi Minh Ngoc (HCMC University of Technology and Education)	Secretary

B. Program Advisory Committee

• Domestic members

Hoang An Quoc (HCMC University of Technology and Education)

Nguyen Vu Lan (HCMC University of Technology and Education)

Do Thanh Trung (HCMC University of Technology and Education)

Le Cong Danh (HCMC University of Technology and Education)

Cao Xuan Vu (HCMC University of Technology and Education)

• Asian Members (Invited Keynote speakers in the past ASPTs)

Adisorn Tuantranont (TOPIC, Thailand)

Guangxue Chen (South China University of Technology, P.R. China)

Tan Jit Khoon (Winson Press, Singapore)

Hirokazu Shimizu (Shimizu printing, Japan)

Chinmay Bhattacharya (Indian Statistical Institute, Kolkata, India)

Hamidin Abdullah (University of Technology MARA, Malaysia)

Rolando F. Rocha (Philippine Center for Print Excellence Foundation, Inc., Philippines)

Taufan Hidayat (Center for Pulp and Paper, Indonesia)

ADORA S. PILI (Technological University of the Philippines, Philippines)

Muhammad Yusuf Bin Masod (Universiti Teknologi MARA, Malaysia)

Tohru Sugiyama (Dai Nippon Printing Co., Ltd. Japan)

Michinari Kohri (Chiba University, Japan)

Tsuyoshi Hotta (Dai Nippon Printing Co., Ltd., Japan)

Komkrit Sajja-Anantakul (Haydale Technologies, Thailand Co., Ltd), Thailand)

Krairop Charoensopa (Suan Sunandha Rajabhat University, Thailand)

Tae-Wook Kim (Jeonbuk National University, Korea)

Youngshin Kwak (Ulsan national institute of science and engineering, Korea)

Yoko Mizokami (Chiba University, Japan)

Registration fee:

Speakers/Poster presenters: Free of charge

Oversea participants: VND 1.000.000 / US$ 50

- Oversea student including residents in Vietnam: Free of charge

Vietnamese academics/students: Free of charge.

The 12th Asian Symposium on Printing Technology (ASPT 2022)

(September 15th -16th, 2022)

"Advancements in Printing Engineering Technology"

At Faculty of Graphic Arts & Media, Ho Chi Minh City University of Technology and Education, Vietnam

Program

15th September

9.00 - 9.15 Opening Remarks by the Rector, JSPST president.

Session I

9.15 - 9.35 **The growth of the printing industry: An investigation of the Malaysian printing industry performance and responses to COVID 19**

Author: Muhammad Yusuf B. Masod
College of Creative Arts,
Printing Technology Department,
University Teknologi MARA (UiTM) Cawangan Selangor,
Kampus Puncak Alam, 42300, Bandar Puncak Alam, Selangor Darul Ehsan,
MALAYSIA

9.40 - 10.00 **Effect of the spatial frequency of skin texture on the conspicuousness of a pigmented spot**

Author: Akane Takahashi
Graduate School of Science and Engineering, Chiba University

10.05 - 10.25 **Tea Break**

Session II

10.30 - 10.50 **Fast Degradation of Synthesized Maleic Anhydride-Grafted-Polycaprolactone (MA-g-PCL) with Lipase**

Author: Kotchaporn Thangunpai
Graduate school of Science and Technology, University of Tsukuba

10.55 - 11.15 **Combined effects of lighting diffuseness, object surface and curvature on the object impression**

Author: Haruya Shiba
Graduate school of Science and Engineering, Chiba University

10.20 - 11.40 **Applying the G7 method to color calibration for Offset printing machines**
Author: Cuong Nguyen Viet
Department of Printing Technology, Chemical Engineering, Hanoi University of Science and Technology

11.45 - 13.00 **Lunch Time**

Session III

13.00 -13.20 **Advancement of Paper-based Eco-friendly Material Sciences**
Author: Prof. Toshiharu Enomae
Laboratory of Paper Device and Eco-friendly Material Sciences
Division of Biomaterial Engineering, Faculty of Life and Environmental Sciences, University of Tsukuba, JAPAN

13.25 - 13.45 **Investigation on the effect of different papers on the total area coverage of inks in offset color printing**
Author. Anh Tuan Phung
Department of Printing Technology, Hanoi University of Science and Technology
Address: No 1, Dai Co Viet str., Hanoi, Vietnam

13.50 – 14.40 **Break (Poster presentation)**

Session IV

14.45 - 15.05 **Optimization of Printing Conditions to Achieve Effective Ink Transfer in Flexographic Printing**
Author: Phornanan Keawkul
School of Science and Technology
Sukhothai Thammathirat Open University

15.10 -15.30 **Prediction of Color Discrimination in Color Vision Deficiency based on the Cone-Sensitivity Shift Model**
Author: Yoka Onozaki
Graduate School of Science and Engineering, Chiba University

15.35 - 15.55 **Digital transformation on business operation and internal administration of printing houses focusing on the problem of adjustable work processes of employees**
Authors: Koravit Sriwongsa, Banchar Arnonkijpanich and Aran Hansuebsai
Department of Imaging and Printing Technology, Faculty of Science, Chulalongkorn University, Bangkok, Thailand 10330

16.00-16.05 **Closing remark**
Nguyen Long Giang
Faculty of Graphic Arts and Media, Ho Chi Minh City University of Technology and Education, Vietnam

16.05-17.00 **ASEAN printing academy network forum**
Prof. Dr. Aran Hansuebsai,
Chulalongkorn University, Thailand

16th September

8.00 - 11.00 **Visit Printing Joint Stock Company No.7 –** (Pick up at 8:00 in front of Hotel)

11.00 - 12.30 **Welcome lunch hosted by HCMUTE.**

12.30 – 16.00 **Ho Chi Minh City tour**

Fast Degradation of Synthesized Maleic Anhydride-Grafted-Polycaprolactone (MA-g-PCL) with Lipase

Kotchaporn Thangunpai,[1] Donghao Hu,[2] Toshiharu Enomae,[3]

[1]Graduate school of Science and Technology, University of Tsukuba
[2]Department of Chemistry & State Key Laboratory of Molecular Engineering of Polymers, Fudan University
[3]Faculty of Life and Environmental Science, University of Tsukuba
[1,3]1-1-1 Tennodai, Tsukuba, Ibaraki 305-8572, Japan
[2] Shanghai 200433, P. R. China

Abstract

Nowadays, plastic wastes are causing a huge impact on the environment and ecosystem. To find a solution of the problem on plastics remaining on earth unresolved, the development of polyesters that can be easily degraded in the natural environment is studied. Polycaprolactone (PCL) is one of the aliphatic synthetic polyesters widely used owing to high resistance to solvents including water and oil but commonly degrade by microorganisms, or more accurately, enzymes they produce; however, it takes 2–3 years to completely degrade in natural conditions. Lipase is a common enzyme that hydrolyzes ester groups. There are many factors for studying the degradation reaction such as crystalline morphology and molecular weight. Chemical modification of PCL is one of the methods for improving the biodegradability. Maleic Anhydride (MA) was grafted onto PCL to produce PCL-g-MA. As a result of the grafting reaction, the crystallinity of PCL decreased, indicating the MA addition concurrently scissored PCL chains during the reaction. In this study, we focused on the degradation factors of PCL by comparison to PCL-g-MA. The results in this study were characterized by scanning electron microscopy for observation and differential scanning calorimetry for measuring and calculating the crystallinity.

Introduction

Plastics are one of the materials most substantially used in the world because of their low cost, lightweight, a variety of functions, and so on. The plastic production until 2017 worldwide reached 300 million t. Then, the use of plastic still remains as a trend in society through economic and industrial demands. It was possible to recycle only 9% of the plastic waste and almost 90% of it has ended up in landfill or left in nature around 1950. The final disposal has caused a critical environmental problem because some of the plastic waste ended up in the ocean. Moreover, plastics production produces the greenhouse effect gases which cause global warming [1-3]. To deal with and resolve all of these problems, biodegradable materials are considered and studied to solve all of these problems. Biodegradable materials are substances that are able to decompose easily into CO_2, CH_4, water, inorganic compounds, or biomass through enzymatic action with living microorganisms (ex. Bacteria, fungi, and so on) under the appropriate condition [4-6].

Poly(ε-caprolactone) (PCL) is an aliphatic polyester widely used as a biomaterial and sustainable packaging because of its high mechanical and good adhesion to a broad range of substrates [7-9]. PCL always occurs around us and degrades in the environment through microorganisms and/or an enzymatic reaction. However, it took a few years to completely degrade in natural conditions [10, 11]. To improve the rate of degradation of PCL, the idea of modifying of PCL structure was introduced. Maleic anhydride (MA) is a polar substance which helps interfacial adhesion between two or more substances and reduce the crystallinity of the structure. [12].

Lipase is a common enzyme occurring in plant and animal tissues and can also be produced by microorganisms during fermentation. PCL could be hydrolysed to esters. Many researchers have studied degradation of PCL by Lipase [13, 14] and paid attention to several parameters such as molecular weight, crystalline morphology, film thickness, and so on [15].

In this research, we focused on the study of the degradation factors of PCL by comparison to synthesized PCL-g-MA by Lipase. Two factors (surface morphology and crystallinity) were chosen to study in this experiment. Surface morphology before and after degradation was observed by using Field Emission Scanning Electron Microscopy (FESEM). Crystallinity was determined from differential Scanning Calorimetry (DSC).

Materials and Methods

Materials

PCL with M_w = 10,000 g/mol, Benzoyl peroxide (BPO), Maleic Anhydride (MA), tetrahydrofuran (THF), hexane, potassium hydroxide (KOH), ethanol (C_2H_5OH), phenolphthalein ethanol solution (1.0% w/v), Lipase PS, Sodium azide (NaN_3), and 0.1M Phosphate Buffer Solution (PBS) pH =7.4 were purchased from Fujifilm Wako Pure Chemical (Osaka, Japan). Filter paper (No.4, Kiriyama, Japan) was utilized for the experiment.

Synthesized PCL-g-MA

A total of 3.375 g PCL and 3.000g MA were dissolved in 40mL THF at 40± 2°C for 30 min in an oil bath under an N_2 atmosphere. BPO was added to the reactants 18 h after initiation. After that, the THF mixture solution was poured into hexane (1:10 v/v) and was gently stirred to precipitate the compounds at 25°C for 10 min. Finally, the precipitated polymer was filtrated and dried in a vacuum desiccator at 25°C.

Preparation of sample films

PCL and PCL-g-MA film were prepared by hot-pressing. First, PCL and PCL-g-MA were pressed at 20 MPa between two flat steel plates at room temperature for 10 min. While the pressure was kept, the steel plates were heated to 70 °C. Subsequently, those films were kept pressed at 70 °C for 10 min followed by cold-pressing at room temperature for 10 more min. PCL and PCL-g-MA films were finally obtained.

Enzymatic degradation by Lipase

Degradation test samples were categorized into three groups: (I) PCL with enzyme (II) PCL-g-MA without enzyme and (III) PCL-g-MA with enzyme groups. A total of 0.01 mg sodium azide was added to each PCL-containing tube to prevent the normal substrate-enzyme combination and the catalytic reaction. A 15 mL PBS solution of 0.025 M was added to every tube. For groups (I) and (III), 0.01 mg lipase PS was used in the experiment. All samples were heated and shaken at 37 °C at a speed of 100 rpm in a water bath. The PBS solution was changed every 24 h to simulate the natural condition. Finally, the samples were washed with distilled water and dried until a constant weight is reached. The remining weight of films (%) was calculated by Eq.1 [16].

$$\textbf{\textit{Remaining weight}}\ (\%) = \mathbf{100} - \left(\frac{w_i - w_f}{w}\right)\mathbf{x100}, \quad \ldots (1)$$

where w_i and w_f are the initial and final weights of the film

Characterization

Surface morphology of the film before and after degradation were observed with a field-emission scanning electron microscope (SU8020, Hitachi, Japan). Samples were coated with sputtered platinum (Pt) before observation.

Crystallinity of all samples before and after lipase degradation was studied and calculated using the standard enthalpy of PCL (ΔH_m = 139.5 J/g) [17]. X_c was calculated based on the ratio of the enthalpy of all samples to that of pure PCL.

Results and Discussions

Enzymatic Degradation

Figure 1 shows the remaining weight of a PCL film with enzyme, PCL-g-MA film with the degradation time in the presence and absence of the enzyme, namely, lipase. The PCL-g-MA and PCL with enzyme started to lose its weight until approx. 60% and 30% for 1 d, continued to degrade, and finally disappeared within 3 d and 5 d, respectively. However, the PCL-g-MA even without lipase lost the weight approx. 30% for the initial 1 d and kept it for additionally 2 d. The weight loss might be due to MA grafted on PCL that decreased the crystallinity index and the amorphous region was easily degraded by lipase.

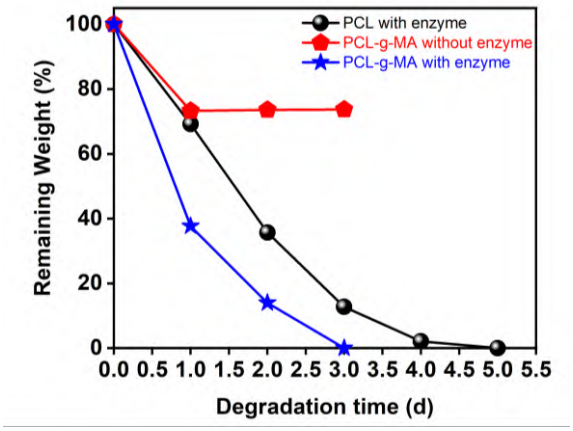

Figure 1 Remaining weight of PCL with enzyme and PCL-g-MA film with and without enzyme with time of degradation by lipase.

Surface Morphology

The surface morphology of PCL and PCL-g-MA films before and after degradation are shown in Fig. 2. The PCL surface is smooth before enzymatic reaction (Fig.2a). Moreover, with increased degradation time, the weight loss increased. The PCL film degraded by lipase for the initial 1 d incurred holes on the surface (Fig.2b). The surface roughness and crack depth increased with increasing degradation time. Cylindrical holes are also observed around the cracks (Fig. 2c). In addition, the degradation process understood through the FESEM observation could be concluded such that the first attack was given to the center of each crystal and then, the whole structure was cracked due to the microbial invasion mechanisms [18, 19].

The surface of PCL-g-MA film is slightly rough comparing to the PCL film (Fig.2a) before enzymatic reaction (Fig.2d). The PCL-g-MA film was degraded by lipase for the initial 1 day and the surface is observed to have clearly become rougher. (Fig.2g). The surface roughness and crack depth also increased with increasing degradation time (Fig.2h). However, PCL-g-MA films without enzyme also seems to show a crack inside the film in 1 d and 2 d (Fig.2e and 2f). This may be a degraded amorphous structure of MA moieties grafted on PCL.

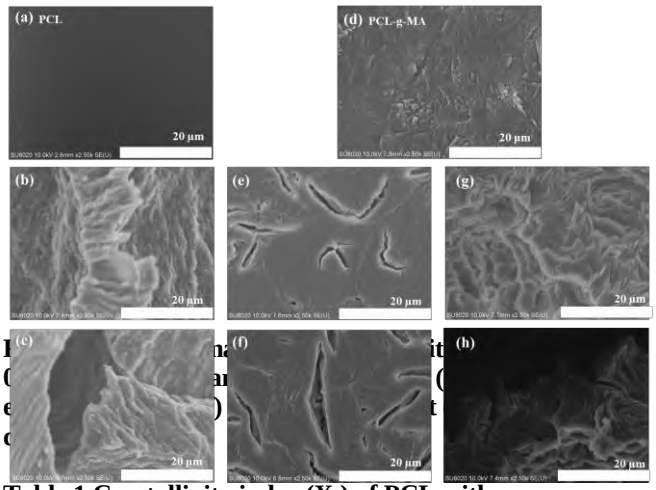

Table 1 Crystallinity index (X_c) of PCL with enzyme group and PCL-g-MA before and after degradation without and with enzyme group

Degradation time (d)	Crystallinity Index (X_c) of PCL-g-MA		
	PCL with enzyme	PCL-g-MA without enzyme	PCL-g-MA with enzyme
0	59.50	11.60	11.60
1	53.39	49.65	46.36
2	51.61	47.75	41.84

Table 1 shows the crystallinity index (X_c) of PCL with enzyme and PCL-g-MA compared between without enzyme and with enzyme groups before and after degradation for 1 and 2 d. X_c of PCL film decreased with increasing degradation time because the enzyme attacked the crystal region and transformed to the amorphous region [14]. X_c of synthesized PCL-g-MA tends to decrease compared to that of plain PCL (X_c of PCL = 59.5%) because MA interacted with plain PCL and inhibited the crystal growth [20]. After the degradation by lipase within 1 d, X_c was increased by approx. 25% because the enzymatic hydrolysis process took place in the amorphous phase. The other reason is also confirmed by Yoshioka et al. that the amorphous chains are in a rubber-like state under the enzymatic-phosphate buffer condition, then possible to crystallize [21]. X_c tended to slightly decrease from 1 d until 2 d by approx. 9.7%, implying the crystal region is also attacked by enzyme and hydrolyzed. It appears that the crystal region was transformed into an amorphous structure. In addition, PCL macromolecules are also partially and randomly arranged and loosely stacked. For all these reasons, lipase can efficiently catalyze PCL and destroy its crystal structure [14]. The PCL-g-MA without enzyme samples are also observed to show the same tendency as the group of PCL-g-MA with enzyme.

Figure 3 shows DSC curves of PCL film with enzyme (Fig.3a) and PCL-g-MA films without enzyme (Fig.3b) and with enzyme groups (Fig.3c) before and after degradation within 2d. DSC is commonly used to characterize the PCL and PCL-g-MA hydrolysis by lipase. The PCL with enzyme group is observed to have the melting point (T_m) of PCL at approx. 70 °C and T_m is shifted to a lower melting point of approx. 60 °C on the second day, corresponding to the chemi-crystallisation process where shorter chain segments with enough mobility tend to realign and crystallize [22].

The result of the PCL-g-MA without enzyme group is shown the degradation on day 1 change the shape of DSC curve due to the amorphous part from MA being degraded. And there is no significant change of exothermic curves during 1d to 2d. of the group without enzyme. These facts imply that the longest PCL chains were not broken and oligomeric species were not formed [23]. In the case of the enzymatic hydrolysis group of PCL-g-MA (Fig.3c), The degraded polymer samples show a lower melting point (T_m) than the initial PCL-g-MA. T_m of the degraded polymer on day 2 is also shifted to the low melting point of about 50 °C compared to the tended of PCL with enzyme, it seems to be that the results of DSC also be the same trends. However, T_m of shifted PCL-g-MA is lower than PCL due to the crystal region of PCL-g-MA decreased from MA grafted reaction [14].

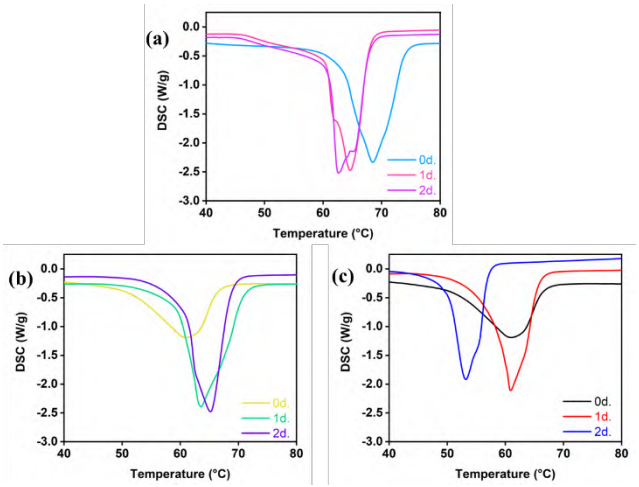

Figure 3 DSC curves of (a) PCL with enzyme and PCL-g-MA film before and after degradation (b) without enzyme and (c) enzymatic group within 2d

Conclusions

A film of PCL and PCL-g-MA was penetrated and degraded by lipase then lost 30% and 60% of the initial weight within 1 d, respectively. And both of PCL-g-MA and PCL lost completely 100% within 3 and 5 d, respectively. It seemed to be the synthesized PCL-g-MA degraded faster than PCL 2d. Moreover, the DSC analysis showed that during degradation by lipase, the crystalline and amorphous regions of PCL and PCL-g-MA were partially destroyed and this reaction transformed crystal regions into amorphous regions. Supplementally, FESEM images also confirmed the result of DSC that the roughness of the surface and depth of the cracks increased with increasing degradation time,

and cylindrical holes are also observed around the cracks with degradation of lipase**.**

Acknowledgement

This research was funded by a joint-research fund of academic-industrial alliance (CDI03138) and the funding from the operating budget of University of Tsukuba. T. Kotchaporn acknowledges to the Ministry of Education, Culture, Sports, Science and Technology (MEXT) of Japan to provide the scholarship under the Trans-world Professional Human Resources Development Program on Food Security & Natural Resources Management (TPHRD) for Doctoral Course. JSPS Core-to-Core Program, (grant number: JPJSCCB20220006) Formation of a Strategic Base in Asia Creating and Developing of Global Minded Imaging Science (Base of Asian Global Imaging Science, BAGIS) centered by Department of Imaging Sciences, Faculty of Engineering, Chiba University is greatly thanked for a financial support to travel fee.

References

1. d'Ambrières, W., *Plastics recycling worldwide: current overview and desirable changes.* Field Actions Science Reports. The journal of field actions, 2019(Special Issue 19): p. 12-21.
2. Coleman, F. and D. Wehle, *Plastic Pollution: A worldwide oceanic problem.* Parks, 1984. **9**(1): p. 9-12.
3. Comăniță, E.-D., et al., *Occurrence of plastic waste in the environment: ecological and health risks.* Environmental Engineering & Management Journal (EEMJ), 2016. **15**(3).
4. Vroman, I. and L. Tighzert, *Biodegradable Polymers.* Materials, 2009. **2**(2): p. 307-344.
5. Chiellini, E. and R. Solaro, *Biodegradable Polymeric Materials.* Advanced Materials, 1996. **8**(4): p. 305-313.
6. Raclavská, H., et al., Definitions and Procedures for Characterization of Biodegradable Waste, in Biodegradable Waste Management in the Circular Economy. 2022. p. 55-67.
7. Pitt, C.G., *Poly-ε-caprolactone and its copolymers.* Drugs and the pharmaceutical sciences, 1990. **45**: p. 71-120.
8. Chandra, R. and R. Rustgi, *Biodegradable polymers.* Progress in polymer science, 1998. **23**(7): p. 1273-1335.
9. Okada, M., *Chemical syntheses of biodegradable polymers.* Progress in polymer science, 2002. **27**(1): p. 87-133.
10. Bartnikowski, M., et al., Degradation mechanisms of polycaprolactone in the context of chemistry, geometry and environment. Progress in Polymer Science, 2019. **96**: p. 1-20.
11. Lu, B., et al., Comparison of PCL degradation in different aquatic environments: Effects of bacteria and inorganic salts. Polymer Degradation and Stability, 2018. **150**: p. 133-139.
12. Roumeli, E., et al., *Effect of maleic anhydride on the mechanical and thermal properties of hemp/high-density polyethylene green composites.* Journal of Thermal Analysis and Calorimetry, 2015. **121**(1): p. 93-105..
13. Tsutsumi, C., et al., The enzymatic degradation of commercial biodegradable polymers by some lipases and chemical degradation of them. Macromolecular Symposia, 2003. **197**(1): p. 431-442.
14. Gan, Z., et al., Enzymatic degradation of poly(ε-caprolactone) film in phosphate buffer solution containing lipases. Polymer Degradation and Stability, 1997. **56**(2): p. 209-213.
15. Sekosan, G. and N. Vasanthan, *Morphological changes of annealed poly-ε-caprolactone by enzymatic degradation with lipase.* Journal of Polymer Science Part B: Polymer Physics, 2010. **48**(2): p. 202-211.
16. Wongnarat, C. and P. Srihanam, Degradation behaviors of Thai bombyx mori silk fibroins exposure to protease enzymes. 2013.
17. Ma, Q., et al., Biodegradation of polycaprolactone (PCL) with different molecular weights by Candida antarctica lipase. Journal of Polymers and the Environment, 2020. **28**(11): p. 2947-2955.
18. Tansengco, M. and Y. Tokiwa, *Thermophilic microbial degradation of polyethylene succinate.* World Journal of Microbiology and Biotechnology, 1997. **14**(1): p. 133-138.
19. Zumstein, M.T., et al., Enzymatic hydrolysis of polyester thin films at the nanoscale: effects of polyester structure and enzyme active-site accessibility. Environmental Science & Technology, 2017. **51**(13): p. 7476-7485.
20. Morais, D.D., et al., *Grafting maleic anhydride onto polycaprolactone: influence of processing.* Materials Research Express, 2019. **6**(5): p. 055315.
21. Yoshioka, T., et al., Structural changes and biodegradation of PLLA, PCL, and PLGA sponges during in vitro incubation. Polymer Engineering & Science, 2010. **50**(10): p. 1895-1903.
22. Sammon, C., J. Yarwood, and N. Everall, *An FT–IR study of the effect of hydrolytic degradation on the structure of thin PET films.* Polymer Degradation and Stability, 2000. **67**(1): p. 149-158.
23. Hermanová, S., et al., *Biodegradation study on poly(ε-caprolactone) with bimodal molecular weight distribution.* Journal of Applied Polymer Science, 2013. **127**(6): p. 4726-4735.

Influence of facial color on facial expression similarity recognition

Ryo Michishita[1], Makiko Yamada[2], Hirao Takahiro[2], Miyamae Mitsuhiro[2], Hiromi Sato[3], Yoko Mizokami[3]

[1]Graduate School of Science and Engineering, Chiba University
[2]National Institute of Radiological Sciences, National Institutes for Quantum Science and Technology
[3]Graduate School of Engineering, Chiba University
[1,3]1-33, Yayoicho, Inage-ku, Chiba-shi, Chiba, 263-8522 Japan
[2]4-9-1 Anagawa, Inage-ku, Chiba-shi 263-8555, Japan

Abstract

It is known that facial color affects facial expression recognition. However, it is not yet clear whether the influence of facial color changes with the intensity of the facial expression. In this study, we investigated the range of facial expression intensities affected by facial color. We examined the similarity of facial expression recognition using facial color modulation reproducing changes in skin hemoglobin concentration. We prepared seven facial expressions morphing images, which changed from angry to neutral and then to happy. Face color conditions are high hemoglobin concentration with reddish face color and low hemoglobin concentration conditions. Two images of facial expressions were presented in succession, and observers rated the similarity of the facial expressions in both images. A dissimilarity matrix was created from the similarity ratings and analyzed. The dissimilarity matrices were transformed into coordinates on a two-dimensional plane using the multidimensional scaling (MDS) method. The results showed that the combination of high and low hemoglobin had a low similarity. It was suggested that the effect of facial color on facial expression recognition is greater when the face is close to neutral. These results may be useful in expressing facial color more effectively for facial expression recognition.

Introduction

The human complexion is known to influence facial expression recognition[1-2]. Kato et al. showed that changes in skin tone in the direction of increasing hemoglobin facilitated the recognition of angry facial expressions. In contrast, changes in skin tone in the direction of decreasing hemoglobin facilitated the recognition of happy facial expressions[3]. Therefore, it is expected that the facial impressions would change between reddish faces with high hemoglobin and reddish faces with low hemoglobin, even for the same facial stimulus. In particular, the categories of facial expression recognition may change depending on facial color since it is difficult to determine the emotion in ambiguous facial expressions. Therefore, we expect a strong reddish face to be recognized as angry and a weak reddish face as happy for intermediate facial expressions between anger and happiness. In this study, we investigate the effect of skin color on facial expression recognition. In the experiment, we examined the similarity of facial expression recognition during the sequential change from an angry to a happy face.

Experiment

Stimulus

As shown in Figure 1, average male faces with neutral, happy, and angry expressions were created from the face images in the ATR database. Morphing images were then made by changing the proportion of facial expressions from angry to neutral and neutral to happy in steps of one-third, as shown in Figure 2. We modulated the face color for each facial stimulus in the direction of hemoglobin increase and decrease. Therefore, 14 facial expression morphing images were used in the experiment; seven face stimuli in which facial expressions changed from anger to happiness and two skin tone conditions of high and low hemoglobin

（a）angry　（b）neutral　（c）happy

Figure 1. Facial expression

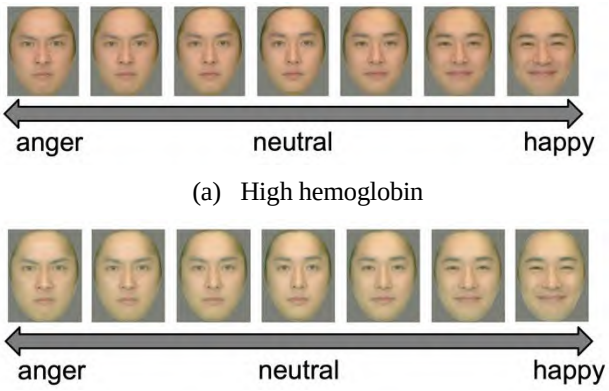

(a) High hemoglobin

(b) Low hemoglobin

Figure 2. Facial expression morphing image

Procedure

Stimuli were presented on an LCD monitor in a dark room. The first stimulus, fixation point, and the second stimulus were presented for 0.5 seconds each. Then, observers responded to the similarity of facial expressions between the first and second stimuli. The response time was unlimited. Similarity responses were rated on an 8-point scale from 1 to 8. Points 1 and 8 corresponded to the maximum similarity, "the same," and the lowest similarity, "quite different," respectively. Point 5 was "rather similar," and 4 was "rather different." The stimuli were presented in random order. A total of 196 trials for all combinations of stimulus images were considered in one session. Two sessions were conducted for each observer. The five male observers participated.

Results and Discussion

The similarities obtained from each face stimuli pair were arranged in a dissimilarity matrix. Each element of the matrix was the average of four similarity responses. The dissimilarity matrices were classified into three types: between stimuli with the same skin tone condition (high hemoglobin vs. high hemoglobin, low hemoglobin vs. low hemoglobin) and between stimuli with different skin tone conditions (high hemoglobin vs. low hemoglobin).

Figure 3 shows a heatmap of the dissimilarity matrix averaged across observers. Ag represents anger, Ne neutral, and Hp happy, and the number of each label, such as Ag1, indicates the percentage of anger or happiness. Since the matrix represents dissimilarity, the higher number means the lower similarity. The whiter color on the heatmap indicates a higher similarity response. The comparison between high hemoglobin in Figure 3 (a) shows that the overall similarity is higher in the upper left angry region. This is consistent with the results of Kato et al.[3], finding that the high hemoglobin skin color condition enhanced the perception of anger. On the other hand, in (b), the low hemoglobin condition had little effect on the similarity response for both anger and happiness, which is different from the results of Kato et al. Finally, in (c), a comparison of high and low hemoglobin under different skin color conditions showed that the same facial expressions were less similar when the facial color was different. The similarity was particularly low for Ag1, Ne, and Hp1. Considering that it was particularly high for Ag1 and Ne in (a), it is suggested that the effect of facial color is more pronounced for expressions close to neutral.

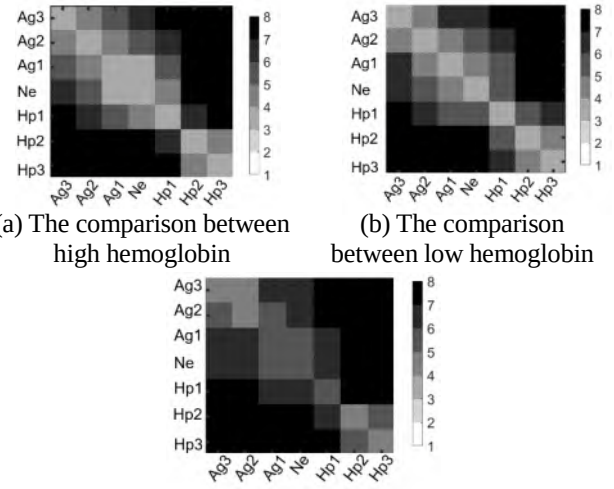

(a) The comparison between high hemoglobin

(b) The comparison between low hemoglobin

(c) The comparison between high and low hemoglobin

Figure 3. Overall average dissimilarity matrix (whiter color indicates greater similarity)

Figure 4 shows a two-dimensional plane transformed from the dissimilarity matrix using the multidimensional scaling (MDS) method. The red and blue symbols represent the high and low hemoglobin skin color conditions, respectively. The labels attached to each marker are the same as in Figure 3. In MDS, the similarity magnitude corresponds to the distance on the plane. The smaller distance indicates higher similarity. The elements are grouped according to the type of facial expression. Stimuli with the same facial expression were evaluated as having high similarity, indicating that observers could respond correctly. They were considered close and highly similar, even under different skin tone conditions. However, the high hemoglobin expressionless face stimulus, Ne, was located closer to the other angry stimuli than the low hemoglobin angry face stimulus, Ag1. Again, it suggests that the high hemoglobin skin color condition facilitated the recognition of anger. On the other hand, low hemoglobin did not enhance the perception of happiness in MDS.

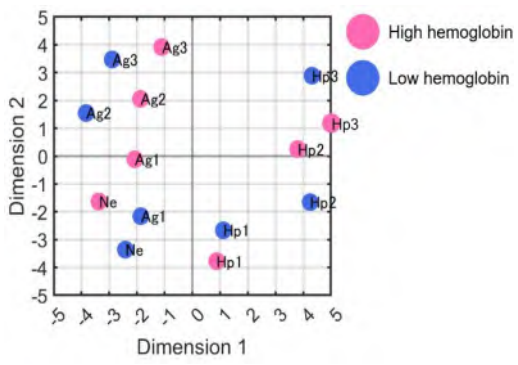

Figure 4. MDS of the overall average for facial expression similarity

Conclusion

The effect of skin color on facial expression recognition was investigated by examining the similarity of facial expression recognition. Experimental results showed relatively high similarity under high hemoglobin conditions. This may be because the high hemoglobin complexion color facilitated the recognition of anger. In the present study, the low hemoglobin condition had little effect on the evaluation of similarity. Facial color's effect on facial expressions' recognition was greater in the conditions close to the neutral.

Acknowledgment

This work was supported by JSPS KAKENHI JP18H04183 and JP21H05805, and JSPS Core-to-Core Program (grant number: JPJSCCB20220006).

References

1. Kae Nakajima, Tetsuto Minami & Shigeki Nakauchi, Interaction between facial expression and color, Scientific Report, 7, 41019. (2017).
2. Masahiro Kato, Hiromi Sato & Yoko Mizokami, Effect of natural skin color change on facial expression recognition, Proceedings of the 6th Asia Color Association Conference, pp. 32-37. (2021).

Effect of the spatial frequency of skin texture on the conspicuousness of a pigmented spot

Akane Takahashi[1], Hiromi Sato[2], Yoko Mizokami[2]

[1]Graduate School of Science and Engineering, Chiba University, Japan
[2]Graduate School of Engineering, Chiba University, Japan
1-33, Yayoicho, Inage-ku, Chiba-shi, Chiba, 263-8522 Japan

Abstract

The homogeneity of the skin influences facial impressions. The conspicuousness of pigmented spots is influenced by many factors such as the number, area, density, location, and contrast with the skin. Besides, skin color and texture may affect the appearance of the spot. In this study, we examined how the conspicuousness of pigmented spots changed by the skin color and noise on the skin. A composite image of the face and pigmented spots was used as the stimulus. A face image with the average skin tone of a young Japanese woman with one pigmented spot was used as a reference stimulus. The skin tone of the test stimulus was modulated by increasing and decreasing melanin and hemoglobin in five steps in each direction. In addition, Gaussian noise with 256 shades of gray was synthesized on the skin at five skin tone levels. The conspicuousness of pigment spots in each stimulus image was evaluated on a 10-point scale compared to the reference stimulus. The conspicuousness of the spots decreased in specific spatial frequency characteristics of the noise. This suggests that the spatial frequency of the skin texture influences a spot's conspicuousness.

Introduction

Pigmented spots of the skin influence impression such as age, health, and attractiveness[1)]. However, there is not much research on how pigmentation appears. In the previous study[2)], parameters such as concentration, number, position, and area affect the visibility of pigmented conspicuousness. Particularly concerning concentration, the conspicuousness of the pigmentation is due to the difference in lightness between the skin and the pigmentation. However, that study focused only on an evaluation of homogeneous skin. In real skin, many factors cause it to lose its homogeneities, such as fine spots, freckles, and wrinkles. This study aims to clarify how noise applied to the skin influences the conspicuousness of a pigmented spot.

Method

Five types of noise were added to a composite of a homogeneous face image and pigmented spots. Each face image was modulated in the direction of melanin and hemoglobin change and used as a stimulus. The conspicuousness of the pigment spots on the stimuli was evaluated.

Stimuli

The average face of Japanese women and a pigmented spot extracted from a cheek image were combined, as shown in Figure 1. The visual angle of the face image was 12.9° x 16.6°. This combined face was used as standard stimuli. The pigment spots were fixed on the upper cheeks. The background was gray, equivalent to Munsell value N5.

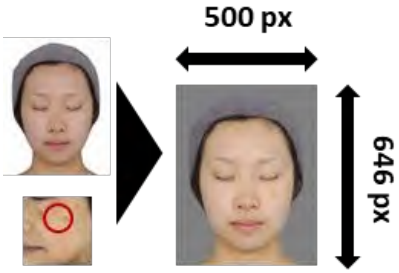

Figure 1. Standard Stimuli

Five types of Gaussian noise were used for skin noise. First, the noise was set to follow a normal distribution on a white image, as shown in Figure 2.

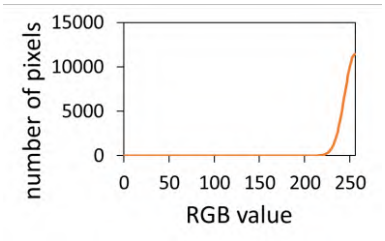

Figure 2. Normal distribution for face noise

Five different peak frequencies were set for the Gaussian noise in Figure 2 to vary the magnitude of the noise. The contrast was normalized, and the noise was synthesized on the skin area of the face image in Figure 1. We also prepared a face image with white gauss (without peak frequency) multiplied by noise according to Figure 2 and a homogeneous face image that has the same chromaticity with the average chromaticity of the skin multiplied by noise. A total of seven basic color face images were used in the experiment.

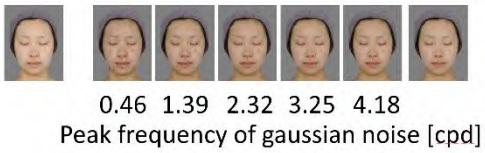

Figure 3. Basic color face images with noise

Face color modulation

We used a Monte Carlo simulation of skin spectral reflectance based on a nine-layer skin tissue model proposed by Maeda et al.[3] to reproduce color changes caused by changes in the amount of pigment in the skin. For all noise conditions, we prepared four types of skin color modulations shown in Figure 4. In this case, the contrast between the skin and noise/pigmentation was the same.

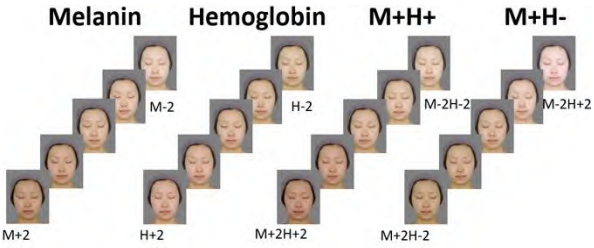

Figure 4. Face color modulation of homogeneous skin

Environment

The experiment was conducted in a dark room with a monitor (EIZO CG 247) for stimulus presentation and a numeric keyboard for a response. The viewing distance was fixed at 60 cm.

Procedure

First, dark adaptation was performed for 3 minutes, and the background color corresponding to Munsell value N5 was presented for 2 seconds. Then, two experimental stimuli were presented for 2 s. The left stimulus was the reference stimulus, and the right was the comparison stimulus, as shown in Figure 5.

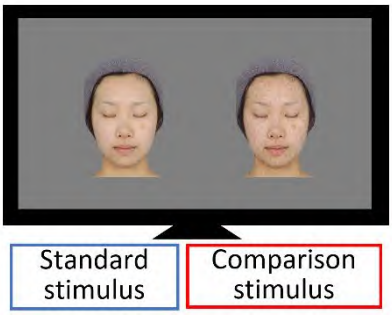

Figure 5. Display during the experiment

Observers evaluated the conspicuousness of the pigment spots in the comparison images. The observers rated the conspicuousness of the pigmented spots on a 10-point scale compared to the reference stimulus. The point of the reference stimulus was set at 5, and the conspicuousness of the pigmented spots in the comparison stimulus was rated as 0 (not noticeable) to 10 (noticeable).

After the response, the next experimental stimulus was presented, and this procedure was repeated until all comparison stimuli were evaluated. The reference stimulus was always the same image, and the comparison stimuli were presented randomly. Three sessions were conducted for each observer until all stimuli were evaluated.

Participants

Six students (3 male, three female) from Chiba University, with a mean age of 23.8 years (SD = 1.6). One female subject was of Chinese nationality, and the remaining subjects were of Japanese nationality. All reported normal or corrected-to-normal vision.

Results

Figure 6 shows the average evaluation results for all subjects. Seven different noise conditions were subjected to face color modulation, and the results were averaged for each face color condition because there was little variation among the levels of face color modulation. The horizontal axis is the evaluation score, and the vertical axis is the peak frequency of the noise [cpd (cycle per degree)]. Compared to the homogeneous patterns, most noise patterns had smaller evaluation scores. The evaluation score was significantly lower in the condition, with a peak frequency of 1.39. There was no significant difference in scores by skin color.

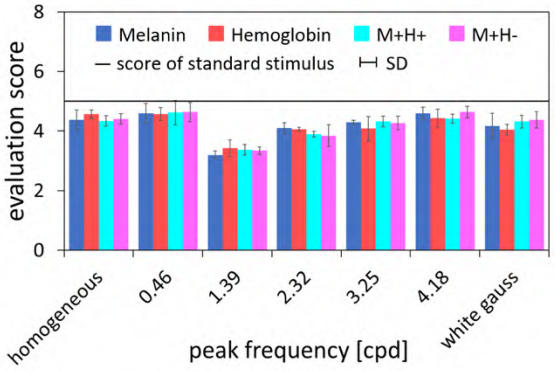

Figure 6. Evaluation score of the conspicuousness of the pigmentation

Discussion

The spatial frequency characteristics of pigments and noise are shown in Figure 7. Figure 8 shows the spatial frequency characteristics when the contrast sensitivity function (CSF) is applied to Figure 7. The mathematical model of the CSF shown in equation (1) was taken from Movshion et al. [4].

$$A(f) = 75f^{0.8}e^{-0.2f} \qquad (1)$$

Where A is CSF and f is the spatial frequency (cpd).

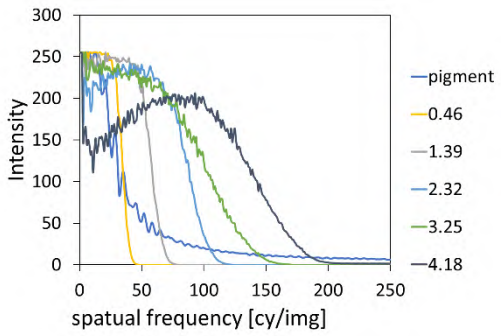

Figure 7. The power spectrum of pigmentation and skin added noise

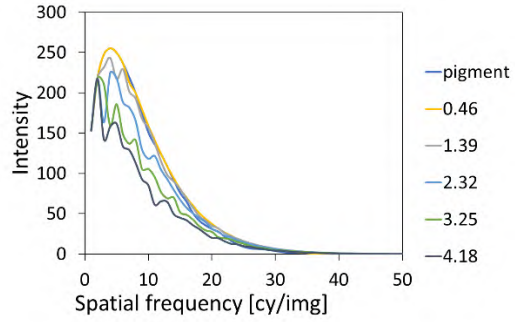

Figure 8. The power spectrum of the product of that in Figure 7 and CSF

The correlation coefficients and Euclidean distances between pigmentation and skin conditions with noises are shown in Figures 9 and 10 to indicate the spatial frequency similarity between the pigmented spots and the noise. The higher the correlation coefficient and the smaller the Euclidean distance, the similar power spectrum of pigmentation and each skin condition. Spectrum between pigmentation and the skin conditions of these are similar for the peak frequencies of 0.46 and 1.39. It is inconsistent with the visual evaluation result that the evaluation points significantly decreased at 1.39.

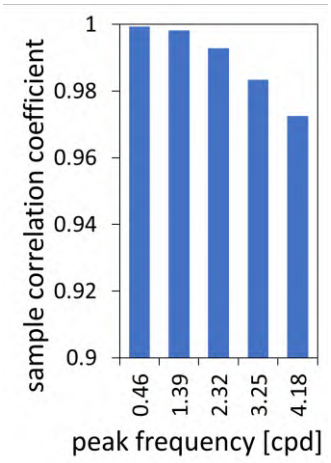

Figure 9. The correlation coefficient between the power spectrum of pigmentation and each skin conditions

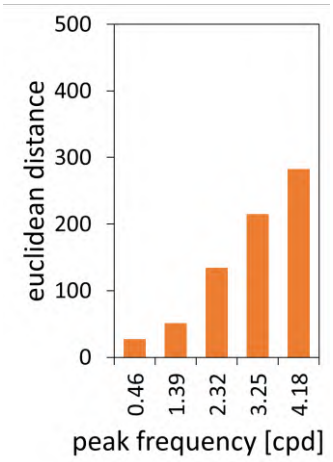

Figure 10. Euclidean distance between the power spectrum of pigmentation and each skin conditions

The luminance profile around the pigmented spot is shown in Figure 11. The area of the luminance profile is a circle with a radius of 40 pixels from the coordinates of the center of the spot. The luminance was extracted from an arbitrary straight line passing through the circle's center and averaged 180 degrees. When the peak frequency was 1.39 cpd, the area of luminance reduction was narrower, which may have made the pigmented spot appear smaller and lowered the evaluation score, but further quantitative analysis of the area of the pigmented spot is needed.

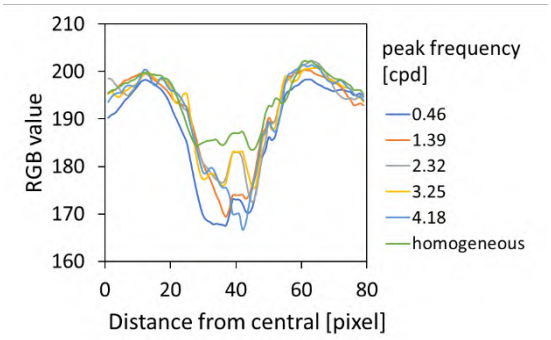

Figure 11. Profile pf RGB value around the pigment

Conclusion

We evaluated the conspicuousness of pigmented spots using face images with Gaussian noise added to the skin portion to simulate conditions more similar to actual skin. The results showed that the evaluation score was significantly lower when the peak frequency of the Gaussian noise was 1.39. It suggests the effect of the spatial frequency of skin texture on the conspicuousness of a pigmented spot. The possible reasons for this are the similarity between the spatial frequency of the pigment spots and the noise and the possibility that a masking effect specific to skin perception was obtained.

Acknowledgment

This work was supported by JSPS KAKENHI JP18H04183 and JP21H05805, and JSPS Core-to-Core Program (grant number: JPJSCCB20220006).

References

1. Ian D. Stephen, David I. Perrett, Handbook of Color Psychology (A. J. Elliot, Mark D. Fairchild, Anna Franklin), pp. 585-602 (2015).
2. Akane Takahashi, Hiromi Sato, Yoko Mizokami, The 43rd ECVP, Perception, 50, 1S, p.112 (2021).
3. Takaaki Maeda, Naomi Arakawa, Motoji Takahashi, Yoshihisa Aizu, Optical Review, 17, 3, pp. 223-229 (2010).
4. J. Anthony Movshon, Lynne Kiorpes, J. Opt. Soc. Am. A, 5, 12 , 2166-2172(1998).

Prediction of Color Discrimination in Color Vision Deficiency based on the Cone Sensitivity-Shift Model

Yuka Onozaki[a], Hiromi Sato[b], and Yoko Mizokami[b]*

[a]Graduate School of Science and Engineering, Chiba University, Japan.
[b]Graduate School of Engineering, Chiba University, Japan.

[a, b] 1-33, Yayoi-cho, Inage-ku, Chiba-shi, Chiba, 263-8522 Japan

Abstract

Color vision deficiency is a decreased ability to distinguish certain color combinations. It has been considered that anomalous trichromats possess longer or shorter wavelength-shifted photopigments instead of normal L- or M-photopigments. Yaguchi et al. (2018) developed a cone sensitivity-shift model that assumes spectral sensitivity shifts in the L and M cones of the color vision deficiencies. This study investigated how well the cone sensitivity-shift model can predict the perceptual color difference of color vision deficiency. Sixteen protan or deutan observers evaluated the color discrimination of color-patch pairs under white illumination using a grayscale. We tested conditions with bare eyes and with color-correcting glasses. The stimuli consisted of twenty-five color-patch pairs with different degrees of discrimination difficulty. As a result, the discriminability of some color pairs was improved using color-correcting glasses, and others were not. We calculated the chromaticity difference, luminance difference, and color difference for all color pairs predicted by the cone sensitivity-shift model. The observer's color discrimination results showed the highest correlation with the chromaticity difference, whereas it showed little correlation with the luminance difference. Our results suggest that the chromaticity difference based on the color-shift model can considerably predict the color discrimination of color vision deficiency.

Introduction

People with Color vision deficiency (CVD) have difficulty in discriminating specific combinations of colors. The severity of CVD varies largely from dichromacy to weak anomalous trichromacy. It has been considered that anomalous trichromats possess longer or shorter wavelength-shifted photopigments instead of normal L- or M-photopigments. Yaguchi et al. proposed a computational simulation of the color appearance for anomalous trichromats (from now on, referred to as the cone sensitivity-shift model). It assumes spectral sensitivity shifts in the L and M cones of the color vision deficiencies. Cone spectral sensitivity was defined based on the CIE 2006 spectral absorbance of cone pigments [1, 2]. The model employed the low-optical density spectral absorptances of the ocular media and pigments and the peak optical densities of L-, M-, and S-cones defined in the CIE 170-1 [2], assuming a standard adaptation condition, such as an equal-energy white. However, the evaluation of the predictability of the cone sensitivity-shift model has not been sufficient yet. This study investigated whether the cone sensitivity-shift model could predict the perceptual color difference of color vision deficiency.

Color-correcting glasses have been developed to help people with CVD to discriminate colors. However, it has not been well evaluated how effective the glasses are and how color perception changes when wearing them. We also investigated the effectiveness of color-correcting glasses.

Experiment

To quantify the predictability of the cone sensitivity-shift model and verify the effect of color-correcting glasses, we conducted experiments to evaluate the appearance of color-patch pairs by observers with color vision deficiencies. In the experiment, an observer with or without a color-correcting glass judged the discriminability of the color-patch pairs.

The experiments were conducted in an environment illuminated by a white LED light stand (Yamada Shomei Co., Ltd. Z-208PROB) with an illuminance on the working surface of about 500 lx and a correlated color temperature of about 5000 K (R_a = 97). We tested a pair of commercially available color-correcting glasses with a spectral transmittance shown in Fig. 1.

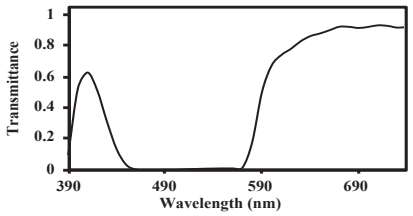

Figure 1. Spectral transmittance of a color-corrective glasse

We made the stimuli consisting of twenty color pairs with different degrees of discrimination difficulty for evaluation as shown in Table 1 (a) PCCS: easily confused color [3], (b)-1 Color Universal Design: easily confused colors [4], (b)-2 Color Universal Design: easily identifiable colors [4], (c) black and red, (d) Japanese Industrial Standard: safety color [5], (e) the three primary colors, (f) easily confused colors for duetan. The chromaticity coordinates of color patches are shown in Fig. 2.

Table 1: Color-patch pairs for evaluation

(a) PCCS: easily confused color		(b)-1 CUD: easily confused colors		(c) black and red	
1-1	6RP 6.5/7.5	9-1	10R3/4	18-1	4R 3.5/11.5
1-2	N7	9-2	10P4/10	18-2	N1
2-1	6RP 6.5/7.5	10-1	2.5R8/6	19-1	6RP 4.0/12.5
2-2	5BG 6/8.5	10-2	2.5G7/4	19-2	N1
3-1	4R 6/12	11-1	7.5Y8.5/12	(d)	JIS:safety color
3-2	3G 6.5/9	11-2	2.5GY8/8	20-1	8.75R5/12
4-1	4R 4.5/6.5	12-1	10B8/4	20-2	5G5.5/10
4-2	5BG 4.5/10	12-2	2.5P7/4	(e)	the three primary colors
5-1	3PB 5/5.5	13-1	10R3/4	21-1	6.8RP 4.6/17.9
5-2	10BG 4/10	13-2	N1.5	21-2	9.4Y 9.1/14.8
6-1	10R 4/11	14-1	5Y9/4	22-1	9.4Y 9.1/14.8
6-2	5Y 4/5.5	14-2	N9.3	22-2	9.6B 5.3/13.9
7-1	4R 4.0/14.0	(b)-2 CUD: easily identifiable colors		23-1	9.6B 5.3/13.9
7-2	9G 4.0/10.5			23-2	6.8RP 4.6/17.9
8-1	4R 2.5/6	15-1	5YR6.5/14	(f)	easily confused colors for Duetan
8-2	3G 3/4.5	15-2	6.25G6/10		
		16-1	7.5Y8.5/12	24-1	N7
		16-2	10B7/8	24-2	10GY6/6
		17-1	10YR7.5/6	25-1	2.5R8/4
		17-2	2.5P7/4	25-2	5G9/2

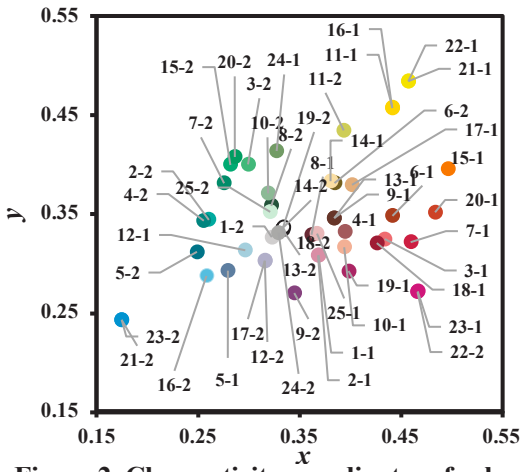

Figure 2. Chromaticity coordinates of color patch on the CIE1931 xy chromaticity diagram (See Table 1 for numbering)

Observers evaluated the discriminability of the color-patch pairs on the desk with the naked eye and a color-correcting glass using a grayscale evaluation chart, as shown in Fig. 3. The color patch pairs were attached to the center of a gray mount. It consisted of a reference color patch (N9) with apertures and seven equally spaced comparison color patches (from N3 to N9). The observer moved the mount with the apertures on the comparison color patches and responded with a number (0-6 in 0.5 steps) corresponding to the difficulty of distinguishing between the reference and comparison color-patch pairs.

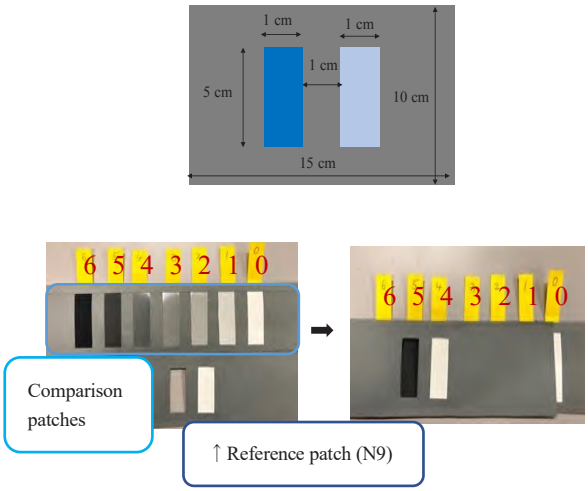

Figure 3. Example of color-patch pairs (top) and grayscale evaluation (bottom)

Sixteen observers (all males) participated. Their color vision type was classified based on several tests, including an Anomaloscope, Ishihara test, SPP, and PANEL D15. They were fourteen deuteranopes and two protanopes.

Results and Discussion

Fig. 4 shows the average scores of fourteen deutan observers (a) and two protan observers (b) for each color-patch pair. The scores were highly variable depending on the color-patch pairs or the type of color vision. Also, the discriminability of some color pairs was improved using color-correcting glasses, while others were not.

We calculated the correlations between the observer's score with no glasses and the model predictions from the simulations of deuteranomaly with M cones shifted by a wavenumber of 500 cm^{-1} (D (M-500)) as the moderate intensity of deutan and from the simulations of protanomaly with L cones shifted by a wavenumber of 500 cm^{-1} (P (L+500)) as the moderate intensity of protan. The model-predicted chromaticity difference, luminance difference, and color differences of the color-patch pairs in CIELUV color space were calculated. The CIELUV values based on the CIE 2006 $X_F Y_F Z_F$ tristimulus values are not defined formally, but we used them for convenience.

The score assigned by the observers showed the highest correlation with chromaticity difference ($R^2_{chromaticity} = 0.23$), suggesting that people with color vision deficiency discriminate colors based on chromaticity differences. The chromaticity differences based on the cone sensitivity-shift model could predict color discrimination of color vision deficiency. The low correlation between the model prediction of luminance differences and the score ($R^2_{luminance} = 0.04$) suggests that the observers were unlikely to discriminate colors based on luminance differences. Additionally, the discriminability of some color pairs

was improved using color-correcting glasses, while others were not, probably because the color-correcting glasses cut some wavelengths of the color-patch pair. However, factors such as the individual difference in the optical density of ocular media and photopigment and the different adaptation states to various illumination colors could also influence the simulation results. They should be considered for a more precise simulation. Furthermore, our present results are consistent with the previous experiment that obtained color discrimination by a subjective evaluation [6], suggesting that the grayscale evaluation chart is useful.

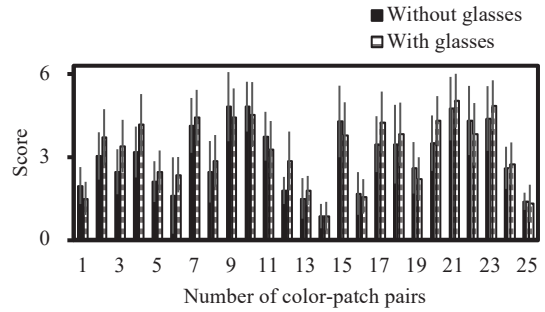

(a) Deutan

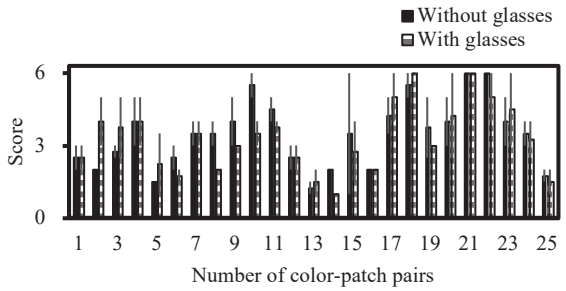

(b) Protan

Figure 4. The average score for each color-patch pair. Error bar shows standard deviations.

Conclusion

This study investigated whether the cone sensitivity-shift model could predict the perceptual color difference of color vision deficiency and the effectiveness of color-correcting glasses. Although we need further investigation, our results suggest that the chromaticity difference based on the color-shift model can considerably predict the color discrimination of color vision deficiency. Also, it is important to consider the reflectance of patches, the transmittance of glasses, and cone sensitivity and their combination for the discriminability of color deficiency.

Acknowledgment

This work was supported by JSPS KAKENHI JP19H04196 and JSPS Core-to-Core Program (grant number: JPJSCCB20220006).

References

1. Hirohisa Yagchi, Junyan Luo, Miharu Kato, and Yoko Mizokami, Computerized simulation of color appearance for anomalous trichromats using the multispectral image. JOSA A, 3, B278-B286. (2018).
2. CIE, CIE 170-1:2006 Fundamental chromaticity diagram with physiological axes–Part 1. CIE Central Bureau: Vienna, Austria. (2006).
3. Japan Color Research Institute (2021). Prototype of mixed color chart for people with color blindness. COLOR No. 154. (In Japanese), Retrieved October 10, 2021, from https://www.jcri.jp/JCRI/hiroba/COLOR/buhou/154/154-5.htm.
4. Kei Ito, Color universal design: Towards barrier-free design for diverse color visions. Journal of Information Processing and Management, 55(5), 307-317. (2012). (In Japanese)
5. Japanese Standards Association (2018). JIS Z 9101:2018. (In Japanese) https://www.jsa.or.jp/
6. Yuka Onozaki, Hiromi Sato, and Yoko Mizokami, Validation of cone sensitivity-shift model for the perceptual color difference of color vision deficiency. Asia Color Association (ACA), Indonesia, online. (2021).

Development of Eco-Friendly Materials from Biomass and Designed Processing Technology

Shalida Rosnan, Megumi Kitamura, Toshiaki Hayashi, Toshiharu Enomae

Biomaterial Engineering, Faculty of Life and Environmental Sciences, University of Tsukuba
Tennodai 1-1-1, Tsukuba, Ibaraki 305-8572, Japan

Abstract

In the laboratory of Paper device and Eco-friendly materials, many types of biomass have been intended to be utilized for paper product (1) During the production of cardboard gift boxes, laser cutting processes were introduced for flexible design of the packaging shape and function. To minimize the carbonization near the kerf edges due to thermal decomposition, the cutting speed and laser power ratio was successfully optimized through the measurement of the area of the heat-affected (blackened) zones (HAZ) using the suitable binarization filtering (Otsu technique) applied to the micrograph images of HAZ. (2) Agricultural wastes like rice and barley straws were tried to be applied to papermaking. Trial paper was successfully produced especially after digestion with sodium hydroxide. Those types of pulps seem to be valuable to replace plastics and even wood pulps for sustainable development. (3) Filamentous algae sometimes grow overly in river and ocean, and they must be removed and treated as waste. From the standpoint of waste utilization, application of them to papermaking was investigated and the algae paper was found to be rigid enough and considered to be a plausible, raw material for papermaking.

1. Imaging technology for Laser cutting of paperboard

1.1. Laser cutting technology

The application of laser cutting has recently become a fascinating element in fabrication of paper-based products. The reason behind this is because the ability of laser to cut, engrave, perforate, and cut complex geometrics [1−3]. However, carbonization (blackening) and its resultant heat-affected zone (HAZ) led to the intriguing discussion on the possibility to reduce the HAZ in the laser cutting process. Through studies and understanding, the optimal parameters can be obtained. The paper materials react to the heat coming from the laser beam irradiation and will evaporate from the surface. The cutting mechanism is decomposition and vaporization [4].

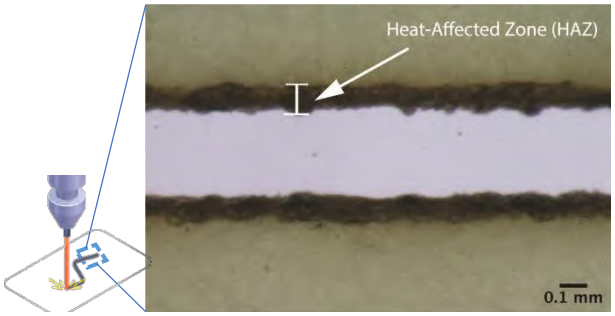

Figure 1: Heat-affected zone by laser cutting.

1.2. Image analysis to extract HAZ

To reduce the HAZ area to improve the packaging appearance, identification of the HAZ area is essential. Then, an image analysis technique was tried to be applied to determine the outline and the area quantitatively.

This study focused on Otsu thresholding technique (OTT) developed by Nobuyuki Otsu [5] and its algorithm is assembled in ImageJ [6], an image processing freeware. The OTT performs extraction of HAZ by detecting its outline following a certain calculation algorithm for thresholding. The algorithm returns a single gray level of the threshold that can separate pixels into foreground and background region [7].

1.3. Experiments of laser cutting

1.3.1. Paper Sheet Preparation

Laboratory-made paper sheets were prepared from hardwood pulp fibers loaded with a sizing agent (alkyl ketene dimer (AKD, AD1608, Seiko PMC Corp., Tokyo, Japan) and cationic polymer (polyamine polyamide epichlorohydrin (PAE, WS4030, Seiko-PMC Corp.) for retaining the size. First, a 1% AKD emulsion and 1% of PAE solution were prepared. Then, 27 g of air-dried hardwood pulp was weighed and disintegrated. Then, dewatered pulp at 10% solids were beaten to 5000 revolutions with a PFI mill for increasing the mechanical strength of the finished sheet [8]. After that, the AKD emulsion and PAE solution were added to the beaten pulp slurry. The pulp slurries were subjected to sheet forming on a standard sheet former (ISO 5269-1:2005), wet-pressing, and restraint drying to obtain laboratory sheets.

1.3.2. Addition of heat resistant agent

Aluminum hydroxide (AH) is known for its property of reinforcing heat resistance [9]. Some pulp slurries were furnished with AH ($Al(OH)_3$, special grade, Fujifilm Wako Chemicals Corp., Kanagawa, Japan). The laboratory AH-loaded paper sheet was classified under the name of AH40 indicating that AH was loaded at 40% on the dry pulp mass.

1.3.2.1. Laser cutting setup

A CO_2 laser cutting machine (PODEA 20W ZERO Corsa, PODEA Co. Ltd, Saitama, Japan) with a maximum output power of 20 W and a spatial resolution of 1000 dpi was applied. One straight cut, each of 5 mm in length was performed for each experimental run as shown by **Figure 2**.

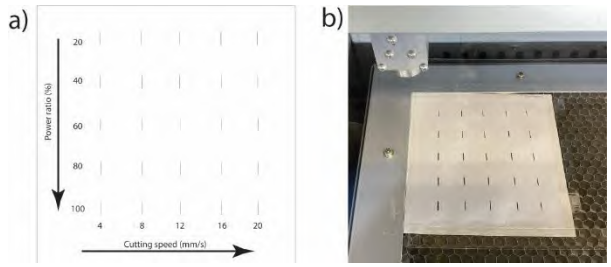

Figure 2: a) Illustration and b) photograph of cuts

The laser power ratio (%) of the maximum output power (20W) was set to 20%, 40%, 60%, 80%, and 100%. The cutting speed (mm/s) was set to 4, 8, 12, 16, and 20 mm/s. The laser cuts of HAZ with the smallest area values were chosen for optimization [10].

1.3.2.2. Scanning Electron Microscopy (SEM) and Optical Microscopy

Scanning Electron Micrographs (SEM) using Hitachi Tabletop Microscopes (TM4000Plus) to identify the surface morphology. Optical micrographs were taken with an industrial stereo microscope OLYMPUS SZX10 (Olympus Corporation, Tokyo, Japan) and digital single-lens reflex camera (EOS Kiss X8i, Canon Inc., Tokyo, Japan) to observe and digitally extract the HAZ.

1.3.2.3. Binarization and HAZ Area Measurement

The HAZ area calculation using ImageJ was based on the procedure in **Table 1**. First, each pixel of HAZ images to the grayscale format from the RGB color coordinates. Then, binarization was performed using the OTT as well as other thresholding techniques.

Which thresholding methods presented the best performance was evaluated using the similarity index defined as the Pearson's correlation coefficient described as equation (1). The correlation coefficient implies that the value of 1 means the relationship between X and Y coordinates lies on a line. The closest values to exactly 1 means that the similarity between the two images is high. The correlation coefficient R is described as equation (1).

Table 1: Image Processing for HAZ area

Image processing	Sequence of ImageJ command
Grayscale conversion	Image > Type > 8 bit
Thresholding	Image > Auto (global) Threshold > Select method (All 16 global threshold methods applied and optimal thresholding selected.)
Particle analysis	Analyze > Analyze particles The total number of the pixels is the HAZ area.

$$R = \frac{\sum_x \sum_y \left\{\left(f(x,y) - \overline{f(x,y)}\right) \times \left(g(x,y) - \overline{g(x,y)}\right)\right\}}{\sqrt{\sum_x \sum_y \left(f(x,y) - \overline{f(x,y)}\right)^2 \times \sum_x \sum_y \left(g(x,y) - \overline{g(x,y)}\right)^2}}, \quad (1)$$

where $f(x, y)$ and $g(x, y)$ are two images compared, x and y are the horizontal and vertical coordinates constituting the images.

1.4. Results and discussion of laser cutting

1.4.1. SEM and Optical Microscopic photographs

Figure 2 shows SEM images of laboratory sheet surfaces with and without AH loaded and clarifies that small AH particles are dispersed well all over the sheet surfaces.

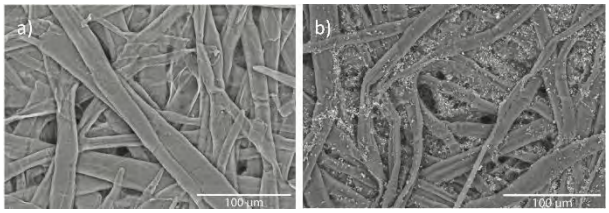

Figure 2. Micrographs of surfaces of a) paper with no additive and b) paper with 40% of AH loaded.

1.4.2. Binarization via thresholding methods

Figure 3 shows binary images created via 17 thresholding techniques including the OTT method from the original micrograph at the top left. When all the binary images are overviewed and compared to the original, the OTT-treated binary image seems to have the most successfully extracted the HAZ.

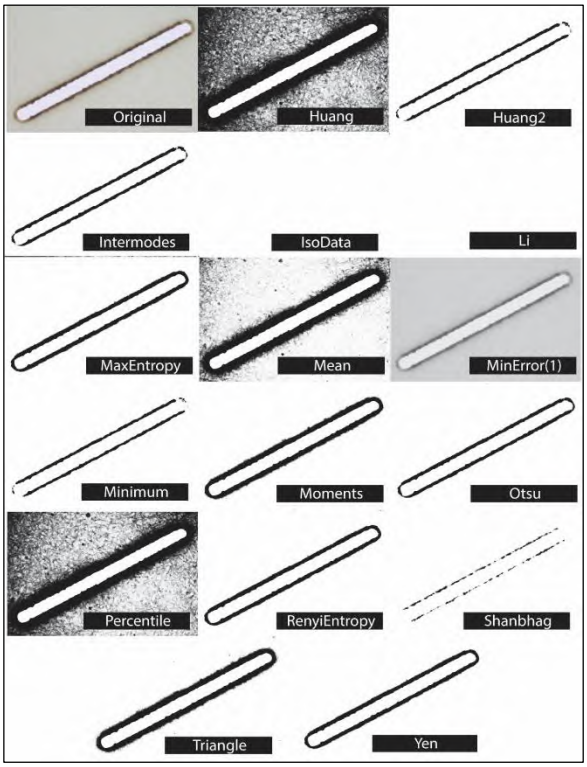

Figure 3: Binary images resulting from 17 thresholding methods applied to the same cut

To identify the threshold performance of the OTT method, the similarity index between a pair of images: original and each binary image was calculated and compared as shown in **Table 2**. Consequently, the OTT method provided the highest *R* value of 0.87, meaning that the OTT method binarized the original image most faithfully.

Table 2: Thresholding methods and its similarity index (*R*)

Threshold method	R	Threshold method	R
Huang	0.84	Minimum	0.84
Huang2	0.85	Moments	0.82
Intermodes	0.85	Otsu	0.87
IsoData	0.85	Percentile	0.42
Li	0.85	RenyiEntropy	0.85
MaxEntropy	0.85	Shanbag	N/A
Mean	0.64	Triangle	0.75
MinError(1)	N/A	Yen	0.74

(N/A: Not available)

1.4.3. Optimum Laser cutting condition

Figure 4 shows the HAZ area at various cutting speeds and laser power ratios for laboratory sheets with no AH loaded. On the whole, the HAZ area decreased with a decrease in the cutting speed; however the highest laser power ratio did not always give the largest HAZ area. The smallest HAZ area, that is, the least blackened area, was obtained at a laser power ratio of 80% and a cutting speed of 20 mm/s. In this optimum condition, the HAZ area was 0.705 mm^2. If the peripheral length is assumed to be 10 mm the HAZ width becomes 70.5 μm and this distance is an influential range of carbonization.

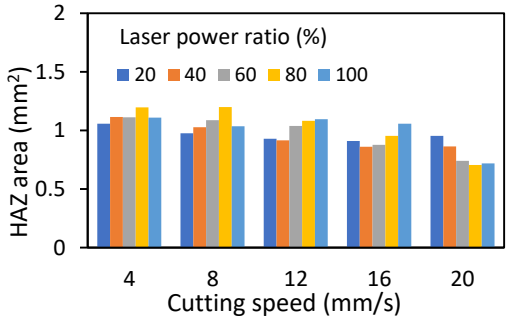

Figure 4: HAZ area vs. laser power ratio and cutting speed for laboratory sheets with no AH.

Figure 5 shows the HAZ area results of sample AH (loaded with AH at 40%). The combination of a 60% power ratio with a cutting speed of 20 mm/s successfully provided the smallest HAZ area of 0.629 mm^2. After the 50 laser cuts had been performed, it demonstrated that the AH-modified paper showed resistance to heat and produced a smaller HAZ area compared to the control sample.

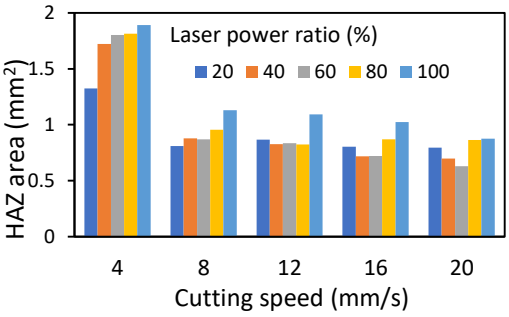

Figure 5: HAZ area vs. laser power ratio and cutting speed for laboratory sheets with 40% AH.

1.5. Conclusion of laser cutting

It is crucial to determine and understand the HAZ in the field of laser process study. Furthermore, it is important to understand the HAZ area and its correlation with the laser process parameters. Through this process, accurate information extraction of HAZ has become possible using the image analysis data. The HAZ area was measured by image processing software ImageJ through OTT. The image binarization based on OTT allowed to accurately measure

the HAZ area based on the similarity evaluation. Also, the optimal setting with combination of the laser power ratio and cutting speed providing a minimum of the HAZ area was pursued. We have found that the laboratory paper sheets loaded with amount of AH produced the smallest area of HAZ by a combination of a laser power ratio of 60% and a laser cutting speed of 20 mm/s.

2. Preparation of rice straw paper for global sustainable development

2.1. Background of RS utilization

Wood has the potential to be a commercial product for trading of carbon credit for the coming generation. Wood fibers are the most popular raw materials to produce paper and paper also can be a target of carbon credit; therefore, a decline of paper production stability due to a lack of raw materials could a concern. A huge amount of rice straws (RS) is wasted in agriculture but has the potential of being a viable alternative fiber source to wood fibers for paper and give a sustainable solution to agricultural waste. To convert RS to pulp fibers, there are several methods of chemical pulping (digesting). In this study, sodium (NaOH) pulping was tested as a trial for its viability.

2.2. Pulp treatment and sheet making

The raw RS pulp (RSP) containing RS and chicken manure ash was supplied by local poultry farmers. Approx. 20 g of the provided RS pulp was disintegrated for 5 min and beaten in a PFI mill to 5000 revolutions followed by redispersion of fibers.

For sizing laboratory sheets, alkyl ketene dimer (AKD) as a size and polyamine-amide epichlorohydrin (PAE) as a retention aid was added into the pulp in a dry mass ratio of 0.2% to the pulp and mixed at 1000 rpm for 5 min to evenly disperse them.

The laboratory sheets were prepared using a standard sheet former (ISO 5269-1:2005), wet pressed for water absorption at 410kPa for 5 min and restraint-dried between steel rings with a weight placed. Weight, tensile strength, and folding endurance were measured after conditioning the paper samples at 23 °C and 50% relative humidity.

2.3. Results and discussion of RS paper

2.3.1. Observation and properties of RS laboratory sheets

Figure 6 shows SEM photographs of surfaces of laboratory sheets prepared from RSP. In (a) parenchyma cells are observed among fibers and in surface pores. In (b), AKD and PAE resulted in a surface to have smaller surface pores presumably with a function of PAE to aggregate parenchyma cells.

Figure 7 shows tensile index which was higher for RSP sheet loaded with AKD and PAE than raw RSP sheet. PAE is supposed to promote aggregation of parenchyma

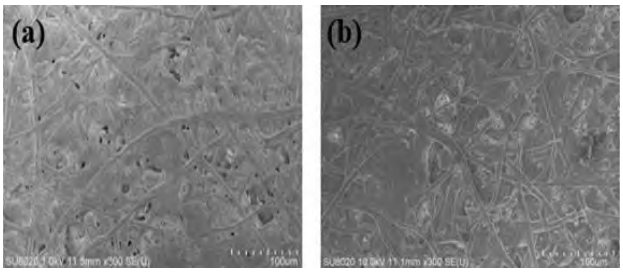

Figure 6: SEM photographs of RSP sheet (a) and RSP sheet with AKD and PAE contained (b).

cells and filled pores among fibers with them to strengthen the intefiber bonding.

2.4. Conclusions of RS paper

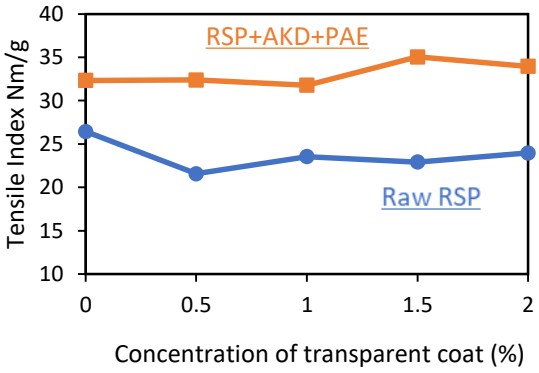

Figure 7: Tensile index of RSP sheet (a) and RSP sheet with AKD and PAE contained (b).

The tensile strength of the RSP sheet was lower than that with AKD and PAE loaded presumably because PAE retain a large amount of parenchyma cells to fill the interfiber pores with them.

3. Papermaking from algae

3.1. Introduction of algae paper

Non-wood plant fibers were one only raw material for papermaking before mechanical and then chemical pulping of wood was invented and industrialized in the 19th century. Since the balance between a huge demand for wood for paper production and its supply have been somehow managed until recently, the emission of carbon dioxide with a greenhouse effect has been net-zero. However, wood biomass storing a quantity of carbons in its large volume is competitively traded and invested in the market. This sudden change may cause lack of supplied wood as a raw material for pulps. Non-wood fibers are expected to compensate this lack.

3.2. Materials and methods of algae paper

3.2.1. Filamentous algae for papermaking

Filamentous algae are a species growing in a fibrous manner with many cells connected straight. These filamentous algae do not contain lignin then the application to paper appears promising but its suitability for papermaking has never been investigated. The genus *Oedogonium* was chosen and tested for suitability for pulping and papermaking.

3.2.2. Papermaking processes

To prepare algae fibers, *Oedogonium* samples were boiled in water for 10 min then soaked in ethanol at room temperature for 24 h to remove chlorophyll. Finally, the treated alga was immersed in a 17.5% aqueous sodium hydroxide (NaOH) solution for 12 h for removing proteins and so on, then weighed to determine the yield.

In preparation to form laboratory paper sheets, the filaments were cut to 1–2 mm long using a blender with a sharp edge to prevent entanglement. Next, shorter filaments were beaten to 5 000–20 000 revolutions in PFI mill so that they swell and make interfiber bonding in a drying process later. Then, laboratory sheets were formed on a standard sheet former, and the wet sheet were sided with two sheets of blotting paper and pressed together for water absorption. Finally, a set of laboratory sheet with blotting paper together was dried in a restraint condition between steel rings. Then, tensile strength was measured at 23 °C and 50% relative humidity for comparison with those prepared from softwood pulp fibers.

3.2.3. Observation and properties of

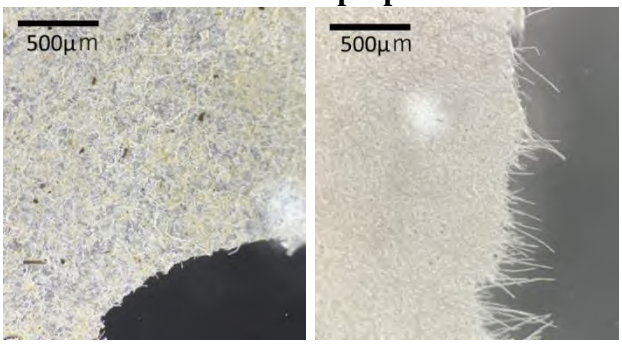

Figure 9: Fracture edges of *Oedogonium* paper (a) and SBKP paper (b) after tensile test.

Oedogonium paper

The shape of *Oedogonium* filaments was observed under an optical microscope.

3.3. Results and discussion of algae paper

3.3.1. Observation of Oedogonium paper

Figure 8 shows an optical micrograph of filaments. *Oedogonium* filaments appeared to have a length of a few hundred mm without branching and a width of 20–30 µm,

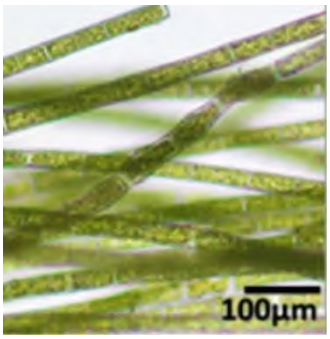

Figure 8: *Oedogonium* filaments consisting of cylindrical cells packed in series.

consisting of a series of short cells connected unlike wood fibers.

3.3.2. Yield of pulp from *Oedogonium* filaments

The yield of *Oedogonium* was approx. 90% after the ethanol extraction, 60% to 65% after NaOHaq extraction, while that of kraft pulping of wood is commonly as low as 50 to 55% because wood contains lignin at 20 to 30%.

3.3.3. Tensile properties of Oedogonium laboratory paper sheet

Table 3 compares tensile index, stretch at break, and Young's modulus of *Oedogonium* sheets compared to that of SBKP sheets. Tensile index of *Oedogonium* was half that of the SBKP paper sheet, but is supposed to be equivalent to that of HBKP (hardwood bleached kraft pulp) more often used for copy paper, book paper and so on. The laboratory sheet obtained from *Oedogonium* in this study was

Table 3: Tensile properties compared between *Oedogonium* and SBKP sheets

Property		*Oedogonium*	SBKP
Tensile index (Nm/g)		27.2	57.3
Stretch at break (%)		7.1	37.5
Young's modulus (GPa)	Beating (Rev)		
	5 000	2.7	2.1
	10 000	3.1	2.5
	20 000	3.3	2.6

SBKP: Softwood bleached kraft pulp
Rev: number of revolutions

demonstrated to be rigid but poorly tough properties compared to those from SBKP.

Figure 9a shows a fracture cross-section of the *Oedogonium* sheet in almost no fibril, while **Figure 9b** shows that of the SBKP sheet has many fibrils occurring from the fracture. Presumably, almost all *Oedogonium* fibers broke at the cross-section, but SBKP fibers slipped

through the network of fibers bonded each other less strongly than fiber strength.

3.4. Conclusions of algae paper

Oedogonium filaments uniquely have a structure consisting of a series of short cells connected unlike wood fibers; however, the laboratory paper sheet from them showed a higher Young's modulus, but lower tensile index and poorly tough properties due to a low stretch at break compared to those from SBKP. The possibility to apply them to papermaking was high enough.

Acknowledgments

JSPS Core-to-Core Program, (grant number: JPJSCCB20220006) Formation of a Strategic Base in Asia Creating and Developing of Global Minded Imaging Science (Base of Asian Global Imaging Science, BAGIS) centered by Department of Imaging Sciences, Faculty of Engineering, Chiba University is greatly thanked for a financial support to travel fee.

Shalida Mohd Rosnan wants to thank the Japanese Government Monbukagakusho (MEXT) Scholarship under the Special Program on Trans-world Professional Human Resources Development Program on Food Security & Natural Resources Management (TPHRD), University of Tsukuba.

References

1. F. Masoud, S. M. Sapuan, M. K. A. Mohd Ariffin, Y. Nukman, and E. Bayraktar, "Cutting processes of natural fiber-reinforced polymer composites," Polymers, vol. 12, no. 6. MDPI AG, Jun. 01, 2020. doi: 10.3390/POLYM12061332.
2. R. T. Mushtaq, Y. Wang, M. Rehman, A. M. Khan, and M. Mia, "State-of-the-art and trends in CO2 laser cutting of polymeric materials-A review," Materials, vol. 13, no. 17. 2020. doi: 10.3390/ma13173839.
3. R. Shalida and T. Enomae, "The art of gift-giving: Laser cutting as a value-added technology for fabricating customized biodegradable packaging," International Conference on Digital Printing Technologies, 2021, vol. 2021-Oct. doi: 10.2352/ISSN.2169-4451.2021.37.69.
4. H. Piili, "A Theory of Interaction Mechanism between Laser Beam and Paper Material," in Physics Procedia, 2015, vol. 78, pp. 163-173. doi: 10.1016/j.phpro.2015.11.029.
5. Nobuyuki Otsu, "A threshold selection method from gray-level histograms," 1979, doi: 10.1109/TSMC.1979.4310076.
6. Schneider, C. A., Rasband, W. S., & Eliceiri, K. W. (2012). NIH Image to ImageJ: 25 years of image analysis. Nature Methods, 9(7), 671?675. doi:10.1038/nmeth.2089.
7. R. C. dos Santos, M. Galo, A. C. Carrilho, and G. G. Pessoa, "The use of Otsu algorithm and multi-temporal airborne LiDAR data to detect building changes in urban space," Applied Geomatics, vol. 13, no. 4, pp. 499-513, Dec. 2021, doi: 10.1007/s12518-021-00371-6.
8. H. R. Motamedian, A. E. Halilovic, and A. Kulachenko, "Mechanisms of strength and stiffness improvement of paper after PFI refining with a focus on the effect of fines," Cellulose, 2019, doi: 10.1007/s10570-019-02349-5.
9. F. Yang, Y. Zhang, and Y. Feng, "Adding Aluminum Hydroxide to Plant Fibers Using In Situ Precipitation to Improve Heat Resistance," 2017, Accessed: Jan. 20, 2022. [Online]. Available: https://bioresources.cnr.ncsu.edu/wp-content/uploads/2017/01/BioRes_12_1_1826_Yang_ZF_Aluminum_Trihydrate_Plant_Fibers_Improved_Heat_Resistance_10943.pdf
10. F. Masoud, S. M. Sapuan, M. K. A. M. Ariffin, Y. Nukman, and E. Bayraktar, "Experimental analysis of heat-affected zone (Haz) in laser cutting of sugar palm fiber reinforced unsaturated polyester composites," Polymers (Basel), vol. 13, no. 5, pp. 1-12, Mar. 2021, doi: 10.3390/polym13050706.

Preparation of antimicrobial microcapsules printable on food packaging paper

Peifu Kong, Toshiharu Enomae

Degree Programs in Life and Earth Sciences, University of Tsukuba
Tennodai 1-1-1, Tsukuba, Ibaraki 305-8572, Japan

Abstract

This study aims to prepare antimicrobial microcapsules that are printable on food packaging paper by inkjet-printing or bar-coating technology. SDGs 2 and 12 highlight that food loss and waste are two big challenges in the stages of a food system. To prevent them, antimicrobial packaging paper is a feasible and promising approach. In this study, essential oils extracted from *Houttuynia cordata* were encapsuled with β-cyclodextrin to form a microcapsule dispersion. With a co-precipitated method at a low temperature, powdered microcapsules from the dispersion were obtained. The formation and antimicrobial activity of microcapsules were confirmed by Fourier transform-infrared spectroscopy and an antimicrobial assay using *Bacillus subtilis*, respectively. We presume that the microcapsule dispersion is well suited to inkjet-printing on food packaging paper, whereas the powdered microcapsules can be loaded onto food packaging paper by bar-coating a mixture of powdered microcapsules and chitosan solution.

Introduction

The SDGs 2 “Zero Hunger” and 12 “Responsible Consumption and Production” highlight that food loss and waste are two big challenges in the stages of a food system. Microbial growth is a major cause of the food spoilage. However, in the field of food packaging paper, the use of antimicrobial agents offers a potential to retard the growth rate of microorganisms. To date, nanoparticles of gold, silver and zinc oxide have been successfully exploited to obtain antimicrobial packaging paper. Nevertheless, these substances in direct contact with food surfaces could place restrictions on their benefits as they may diffuse rapidly into the food mass, triggering some physiological reactions during the consumption[1].

Active substances isolated from botanical sources are promising alternatives[2]. *Houttuynia cordata* (referred to as “HC” hereafter) is a perennial herb native to Asia. This plant has been used as a traditional remedy for the treatment of various diseases or symptoms in local areas of Japan and China. A large number of reports have revealed that the essential oils (EOs) from HC not only can effectively inhibit the growth of numerous bacteria and viruses, but also availably hinder the breeding of molds and yeasts. However, EOs are unstable due to their high volatility, high heat sensitivity, and easy oxidation, which greatly limit their application fields. Microencapsulation using β-cyclodextrin (β-CD) is a viable technology to prevent above problems and achieve a superiority of prolonged release. β-CD, recognized as a non-toxic ingredient, has a hydrophilic outer surface and hydrophobic hollow cavity which can embed EOs by use of their similar physical property.

In this study, EOs of HC were extracted by ethanol with a pre-heating. Then, the obtained extract was applied to form a microcapsule dispersion using β-CD. With a co-precipitated method at a low temperature, powdered microcapsules from the dispersion were obtained. Finally, *Bacillus subtilis* was chosen as an object microorganism to evaluate the antimicrobial activity of the powdered microcapsules.

Materials and Methods

EOs extraction

HC was picked in the campus of Univ. of Tsukuba and stored in a freezer (approx. -20 °C) until just before use. A total of 10 g of frozen HC wrapped in aluminum foil was heated in an electromagnetic cooker at 800 W for 2 min and a paste-like HC product (referred to as “HCP” hereafter) was obtained. After that, an ethanol extract of HCP (referred to as “eHCP”) was prepared in the following way. The HCP was put into 5 mL of 99.5% ethanol, and extracted using a vortex mixer (HS120214, Heathrow Scientific, USA) at 3000 rpm for 10 min, followed by a centrifugation at 1400 g for 5 min. After centrifugation, the supernatant (which is considered as eHCP) was collected via a suction filtration.

Preparation of microcapsules

A total of 2.5 g of β-CD (Wako 1st Grade, FUJIFILM Wako Chemicals, Japan) were dissolved in 50 mL of a co-solvent of ethanol and distilled water (1:2 v/v) mixture at 55 °C and 700 rpm on a hot stirrer plate. After cooling the solution to 45 °C, 2 mL of the eHCP was added dropwise. Subsequently, the mixture was stirred at 45 °C for 2 h to obtain a microcapsule dispersion. With a co-precipitated method at 4 °C overnight, powdered microcapsules from the dispersion were recovered via a suction filtration and then the powdered microcapsules were dried in a desiccator at 23 °C for 72 h.

Physicochemical characterization of microcapsules

The morphological structures of the powdered microcapsules were observed using a scanning electron microscopy (SEM) (TM4000Plus, Hitachi High-Tech Corporation, Japan) in the backscattered electron mode at a low-vacuum condition. The variation in crystal

structure before and after microencapsulation was confirmed with an X-ray diffractometer (XRD) (D8 ADVANCE/TSM, Bruker AXS, USA) using Cu-Kα radiation at an accelerated voltage of 40 kV and a current of 40 mA. The formation of microcapsules was confirmed via a Fourier transform-infrared spectroscopy (FT-IR) (FT/IR-6800, JASCO, Japan). The FT-IR spectra were collected between 4000 and 400 cm^{-1} at a resolution of 4 cm^{-1} with averaging from 16 scans.

Antimicrobial assay of microcapsules

A total of 15 mL sterilized tryptic soy agar with 0.075 g of powdered microcapsules was poured into a Petri dish to achieve a microcapsule content of 5 g/L. A total of 10 µL of 6 ×10^4 CFU/mL *Bacillus subtilis* was inoculated in the center of the Petri dish. After that, the Petri dish was sealed with a Riken wrap and incubated at 37 °C for 48 h to evaluate the antimicrobial activity from the aspect of the growth of *Bacillus subtilis*. The plain β-CD was set as a control.

Results and Discussion

Figure 1 shows the SEM images of plain β-CD (a) and powdered microcapsules (b). Plain β-CD as purchased was characterized as homogeneous massive or lamellar plates with well-grown crystals in varying sizes. However, the powdered microcapsules were more granular and had irregular structures and exhibits clustering.

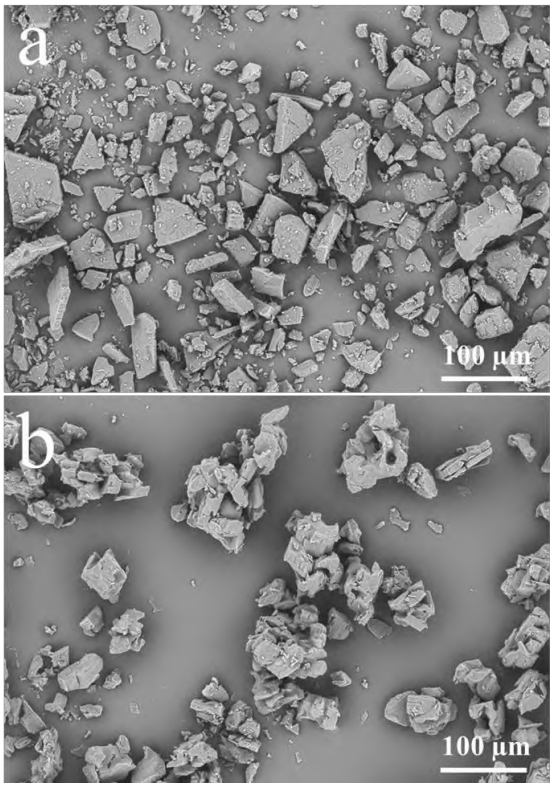

Figure 1. SEM images of plain β-CD (a) and powdered microcapsules (b).

Figure 2 shows the XRD patterns of plain β-CD (a) and powdered microcapsules (b). The XRD pattern of powdered microcapsules was similar to that of plain β-CD in the peak position (2θ) but with different peak intensity mutually. The diffraction angle 2θ of the plain β-CD had intense and sharp peaks at 11.32, 14.47 17.42 and 18.53°. However, in the XRD pattern of powdered microcapsules, these peaks were substantially compressed, despite heightened peaks at 10.43, 12.24 and 19.45°. This indicates that the crystal orientation of β-CD changed after microencapsulation.

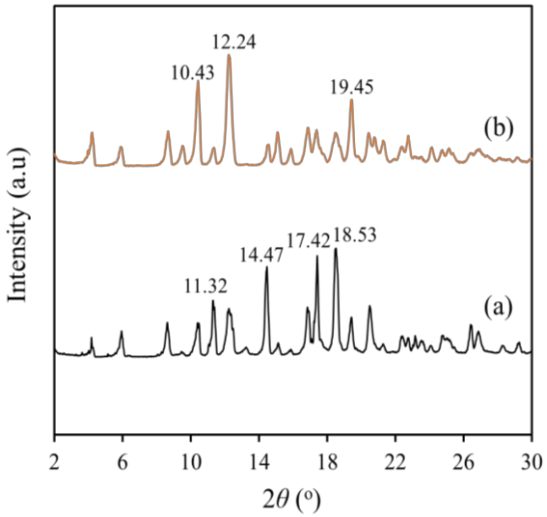

Figure 2. XRD patterns of plain β-CD (a) and powdered microcapsules (b).

Figure 3 shows the FT-IR spectra of eHCP (a), plain β-CD (b) and powdered microcapsules (c). Typically, eHCP exhibited three characteristic peaks at 3356 cm^{-1} (for O-H stretching vibrations), 2923 cm^{-1} (for C-H stretching vibrations), and a prominent absorption peak at 1630 cm^{-1} (for C=O stretching vibration of amides). The absorption bands of plain β-CD were observed at 3369, 2925, 1650, 1157 and 1029 cm^{-1}, corresponding to the vibration of symmetrical and asymmetrical stretching of the O-H, C-H stretching vibrations, H-O-H bending, C-O stretching vibration, and symmetric stretching link C-O-C, respectively. Obviously, the FT-IR spectra of powdered microcapsules revealed a high degree of similarity to the spectra of plain β-CD. Noteworthy, the highly intense peak of eHCP located at 1630cm^{-1} was not detected in the spectra of powdered microcapsules, indicating the successful microencapsulation of the eHCP with β-CD.

Figure 4 shows the growth status of *Bacillus subtilis* in tryptic soy agar medium with the addition of plain β-CD (a) and powdered microcapsules (b). Plain β-CD resulted in rapid breeding of *Bacillus subtilis* due to the fact that β-CD is a polysaccharide that can provide a carbohydrate source. On the contrary, the addition of powdered microcapsules containing eHCP showed a potent inhibitory ability.

Microcapsules prepared in this study are prospective agents to develop an antimicrobial food packaging paper. The outer surface of the microcapsules is hydrophilic, suggesting that they can form strong hydrogen bonds with cellulosic paper. **Figure 5** depicts two probable loading methods: inkjet-printing (a) and

bar-coating (b). The microcapsule dispersion is assumed to be well suited to inkjet-printing, and the powdered microcapsules can be loaded onto food packaging paper by bar-coating a mixture of powdered microcapsules and chitosan solution.

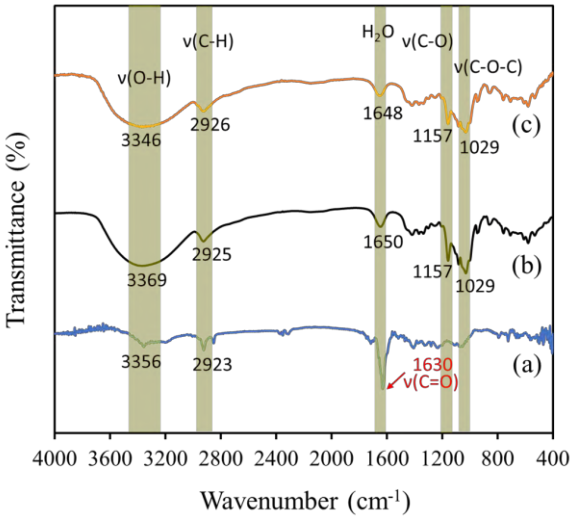

Figure 3. FT-IR spectra of eHCP (a), plain β-CD (b) and powdered microcapsules (c).

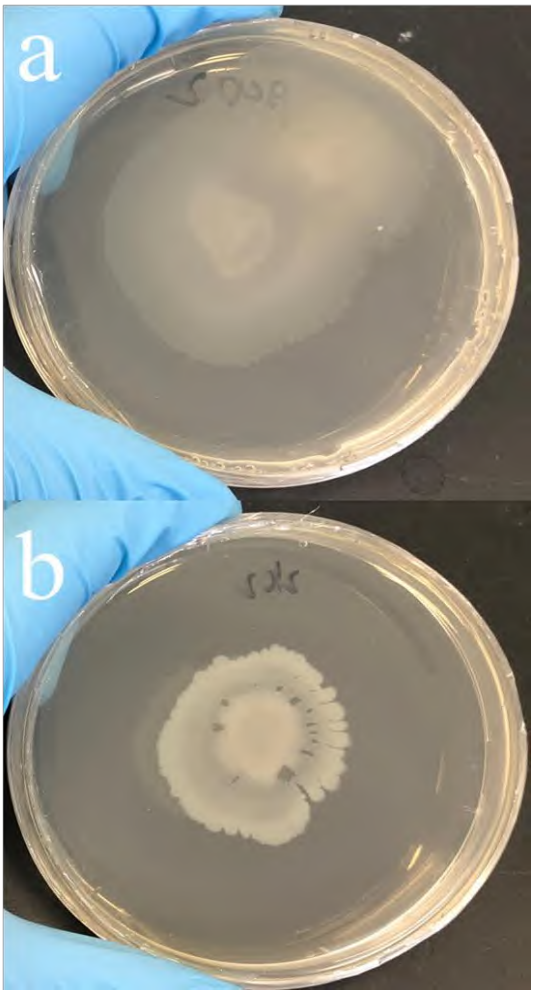

Figure 4. Growth of *Bacillus subtilis* with plain β-CD (a) and powdered microcapsules (b).

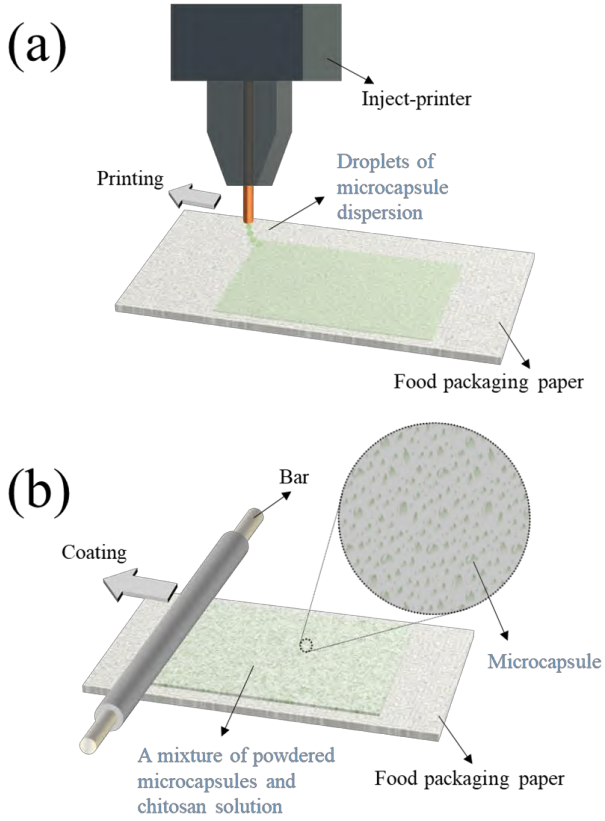

Figure 5. Schematic of inkjet-printing (a) and bar-coating (b) technologies.

Conclusion

This study prepared antimicrobial microcapsules containing an HC extract. The result of FT-IR confirmed that the extract was well embedded within hollow cavities of β-CD. The antimicrobial assay demonstrated a satisfactory antimicrobial activity of the fabricated microcapsules. We presume that the microcapsule dispersion is well suited to inkjet-printing on food packaging paper, whereas the powdered microcapsules can be loaded onto food packaging paper by bar-coating a mixture of powdered microcapsules and chitosan solution.

Acknowledgement

We would like to thank the “Base of Asian Global Imaging Science (BAGIS)” project centered by Department of Imaging Science, Faculty of Engineering, Chiba University for providing travel fee for this presentation.

References

1. Martins et al. Antibacterial paper based on composite coatings of nanofibrillated cellulose and ZnO. Colloids and Surfaces A: Physicochemical and Engineering Aspects, 417, pp. 111-119 (2013).
2. Kong et al. Preparation of an eco-friendly antibacterial agent for food packaging containing *Houttuynia cordata* Thunb. extract. RSC Advances, 12, pp. 16141-16152 (2022).

Fabrication and investigation on optical properties of ZnS quantum dots for application in security ink

Nguyen Thanh Phuong

Printing Material Lab, Faculty of Graphic Arts and Media, HCMC University of Technology and Education, Ho Chi Minh City, Viet Nam

Abstract

ZnS quantum dots (ZnS QDs) were synthesized in the air using thioglycolic acid (TGA) as a stabilizer, and ZnS QDs ink was prepared by dispersing ZnS QDs in PVA solution. X-ray diffraction (XRD) and Transmission electron microscope (TEM) show that the ZnS QDs possessed the zinc-blende structure were spherical in shape with the particle size of about 20 nm, and ZnS QDs were successfully dispersed in the solution of PVA. Furthermore, photoluminescent properties of ZnS QDs were characterized by ultraviolet-visible (UV-vis) absorption and photoluminescence (PL) spectroscopy. The results show that ZnS QDs ink exhibited a strong blue emission at about 430 to 445 nm with an excitation wavelength of 325 nm. The study indicated that the ZnS QDs ink is suitable for security ink application.

Introduction

Luminescent II–VI compound semiconductor quantum dots (QDs) such as CdS, CdSe, CdTe,… have attracted great interest recently due to their characteristic optical properties and potential applications. This group's zinc sulfide quantum dots (ZnS QDs) is relatively a non-toxic material compared to Cd-based QDs. Additionally, ZnS has a wide direct bandgap of 3.6 eV and a small exciton Bohr radius of 2.5 nm [1]. As a result, ZnS is particularly suitable as a host material for many luminescent ions such as Ag^{+}, Cu^{2+}, Mn^{2+}, Eu^{3+}, Sm^{3+}, Tb^{3+}. ZnS can be applied in a variety of fields such as fluorescent labeling agents [2], photocatalyst [3], solar cells [4, 5], AC thin film electroluminescent (EL) devices [6, 7], and printing inks [8]. Recently, many researchers have studied structural and optical properties of ZnS quantum dots synthesized by various methodologies such as the chemical precipitation method [2], sol–gel [6], reverse micelle method [9], the microwave method [10], hydro-thermal process [11], etc. Among these methods, the chemical precipitation method is one of the more widely used methods due to its several advantages, such as low temperature control, easy handling, and requiring inexpensive equipment.

Moreover, most of the previous work on ZnS QDs focuses on different capping agents [8-11], exploring methods to grow highly crystalline nanoparticles, and controlling the particle size of ZnS nanostructure. However, to the best of our knowledge, there are not any reports that thoroughly studied the application of ZnS QDs in security printing ink.

Therefore, in this work, ZnS quantum dots were synthesized in the air using thioglycolic acid (TGA) as a stabilizer. The structure and photoluminescence properties of the quantum dots were investigated, and these ZnS QDs were used as blue luminescent pigments in the security ink formula.

Experiment

Materials

Zinc acetate dihydrate ($Zn(CH_3COO)_2•2H_2O$, 98%), sodium sulfide nonahydrate ($Na_2S•9H_2O$, 98%), and poly(vinyl alcohol) (PVA) were purchased from Aldrich. Thiolglycolic acid (TGA, $HSCH_2COOH$, > 98%) was obtained from Merk. Distilled water was used in all experiments.

Preparation of ZnS quantum dots

This study used the chemical precipitation method to synthesize ZnS QDs. Initially, 0.4 M of $ZnCl_2•2H_2O$ was dissolved under vigorously stirring in 100 ml de-ionized water at 80ºC for 30 min. Then, 1.0 ml of thioglycolic acid (TGA) HSCH2COOH was injected into the solution. After 120 min, 50 ml of 0.4 M $Na_2S•9H_2O$ solution was dropped into the above solution. The clear colloidal solution was formed immediately. This mixture was vigorously stirred for 30 min under air atmosphere at 90ºC. ZnS QDs were prepared in an aqueous solution by following a sample reaction:

$ZnCl_2•2H_2O + HSCH_2COOH$ (TGA) + $Na_2S•9H_2O \rightarrow Zn^{2+}$-$SCH_2COOH + NaCl + H_2O$

The colloidal solution was then isolated by centrifuging at 4000 rpm and washed several times using de-ionized water and ethanol. Finally, the wet precipitate was dried for 24 h at 90oC in an air atmosphere for further analysis.

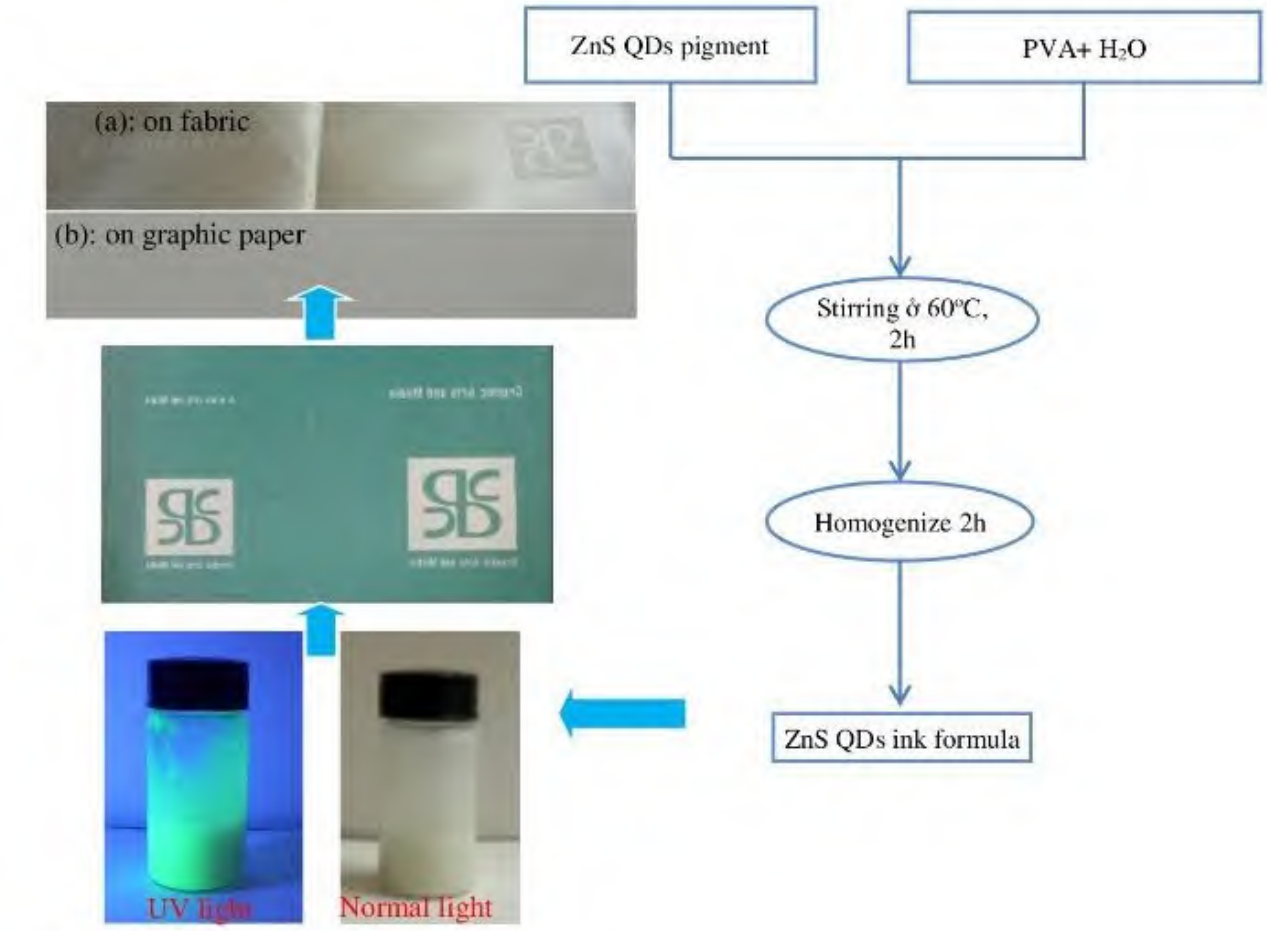

Fig. 1. Schematic diagram of the preparation of ZnS QDs ink and the process of printing ZnS QDs ink on paper and fabric by the screen printing technique

Preparation of ZnS quantum dots ink

The schematic diagram of the preparation of ZnS QDs ink is presented in Fig. 1. First, 6.5 g of PVA and 40 ml of de-ionized water were mixed at 60oC for 1 hour to achieve a clear solution. Second, 1.5 g of the post-preparative ZnS QDs powder was added to the above solution under vigorously stirring at 60oC for 2 h. Finally, the obtained mixture was homogenized in an ultrasonic bath for 2 h. The ZnS QDs ink formula was printed on paper and fabric by screen printing technique as shown in Fig. 1.

Characterization

Powder X-ray diffraction (XRD) [D/max – II Cu Kα radiation] was used to identify the structure of the quantum dots. The particle shape and size were studied using a JEM1010-JEOL transmission electron microscope (TEM). UV-Visible absorption spectra were obtained using a Model PB-10 spectrophotometer. Photoluminescence (PL) spectroscopy was obtained using a Horiba Jobin Yvon Fluorescence Spectrometer with an excitation wavelength 325 nm.

Results and Discussion

Structural and morphological properties of ZnS QDs

The XRD pattern of ZnS quantum dots (QDs) is shown in Fig. 2(a). The three major diffraction peaks are located at 2θ = 28.7°, 47.7°, and 56.4° of the cubic zinc-blende structure, which is very consistent with the values in the JCPDS card no. 005-0566. The broadening of the diffraction peaks is attributed to the nanocrystalline nature of the ZnS QDs. The crystallite sizes were calculated according to the Debye – Scherrer's equation (1) [12].

$$D = \frac{0.9\lambda}{\beta_{hkl}\cos\theta} \quad (1)$$

where D is the crystallite size, λ is the wavelength of X-ray (λ=1.54 Å), θ is the Bragg angle, and β_{hkl} is the full-width at

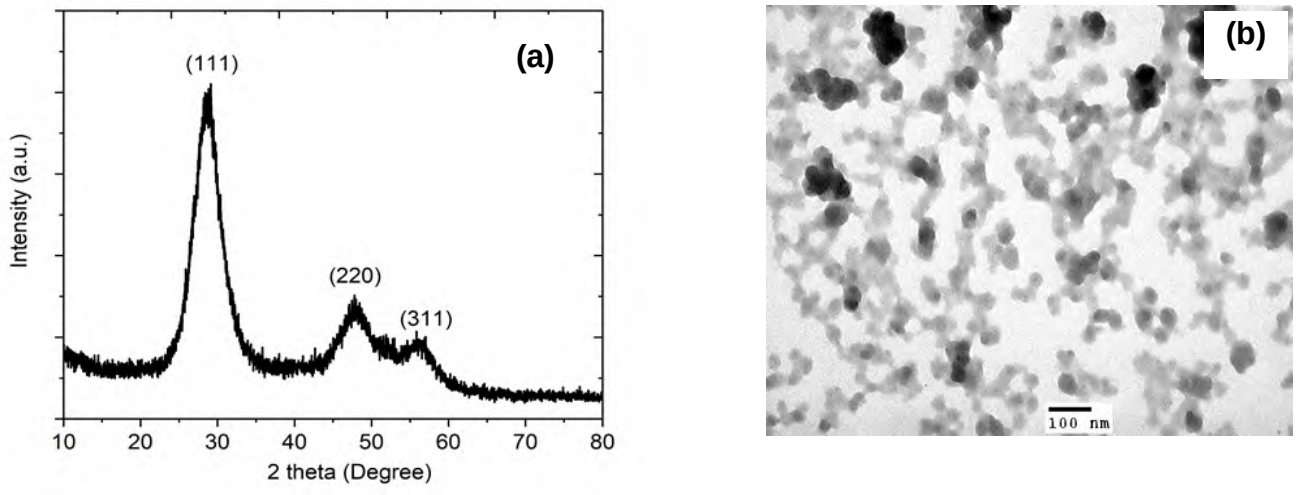

Fig. 2. (a) XRD pattern of ZnS quantum dot powders, (b) TEM image of ZnS quantum dots colloid

half maximum (FWHM) of the diffraction peak (in radians) at 2θ. Based on the FWHM of (111) reflection, the crystallite size of ZnS QDs was estimated to be 2.5 nm.

Fig. 2(b) shows the TEM image of ZnS QDs colloid prepared with TGA capping agent. The TEM image reveals that TGA-capped ZnS QDs are monodispersed and spherical in shape and the size of particles was estimated to be 10 nm. The particle size is larger than the crystallite size, indicating that the particles probably are polycrystalline [13].

Optical properties of ZnS QDs

Fig. 3 reveals the UV – Vis spectra of ZnS QDs colloidal solution synthesized with different $[Zn^{2+}]/[S^{2-}]$ ratios. Absorption peaks were observed at 270 nm, and all absorption peaks are significantly blue-shifted from the bulk ZnS (≈ 3.6 eV) [1]. The result is due to the quantum confinement effect. Moreover, the particle size can be calculated by [15]:

$$d(E) = \frac{0.32 - 2.9\sqrt{E - 3.49}}{3.5 - E} \quad (1)$$

where E is the optical bandgap (E_g^*) in eV and d(E) is the average diameter of the quantum dots in nm. As a result, the average diameters were calculated to be 2.72 nm. The particle sizes are smaller than the exciton Bohr diameter of ZnS (2αB ≈ 5 nm). The result indicates the strong quantum confinement in all ZnS QDs.

Fig. 4(a) shows the PL spectra of ZnS QDs powder prepared with varying the $[Zn^{2+}]/[S^{2-}]$ ratios under the excitation wavelength (λ = 325 nm). For all the QDs, the PL spectra reveal two emission peaks at around 430 – 500 nm. which could be attributed to defect-states in the ZnS host [4]. Moreover, the shoulder edge of PL spectra, extending beyond 500 nm, was attributed to the presence of sulfur vacancies (S^{2-}) in the lattice [9]. The inset in Fig. 4(a) shows the strong blue

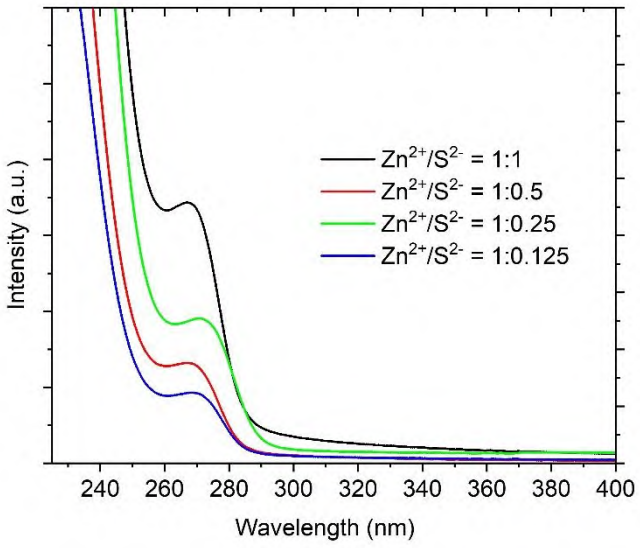

Fig. 3. UV-vis spectra of ZnS quantum dot colloid

emission of ZnS QDs colloid under the 325 nm UV excitation. Besides, Fig. 4(b) displays that the CIE (x, y) coordinates of ZnS QDs were shifted to the bound of the CIE chromaticity diagram with the increase of the $[Zn^{2+}]/[S^{2-}]$ ratios from 1:0.125 to 1:1. The result indicates that the color purity (CP) of ZnS QDs increases, which mean more saturated emission color of ZnS QDs.

Optical properties of ZnS QDs ink

Fig. 5 shows the UV – Vis spectra of ZnS QDs colloidal solution and ZnS QDs ink. Absorption peaks were observed at about 270 nm. The result indicates that ZnS QDs are in good dispersion in PVA solution.

The PL spectra of PVA solution, ZnS QDs, and ZnS QDs ink are displayed in Fig. 6(a), respectively. For PVA solution, the emission peaks observed at about 340 and 408 nm

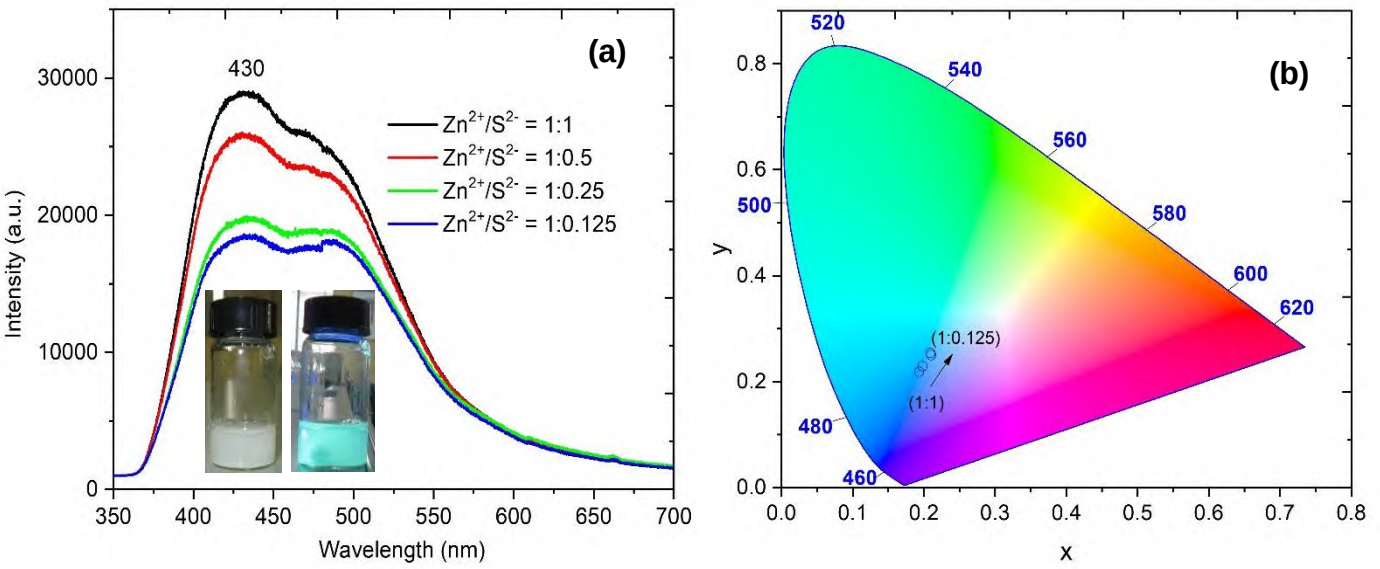

Fig. 4. (a) PL emission spectra of ZnS QDs, and (b) CIE 1931 chromaticity diagram of ZnS QDs

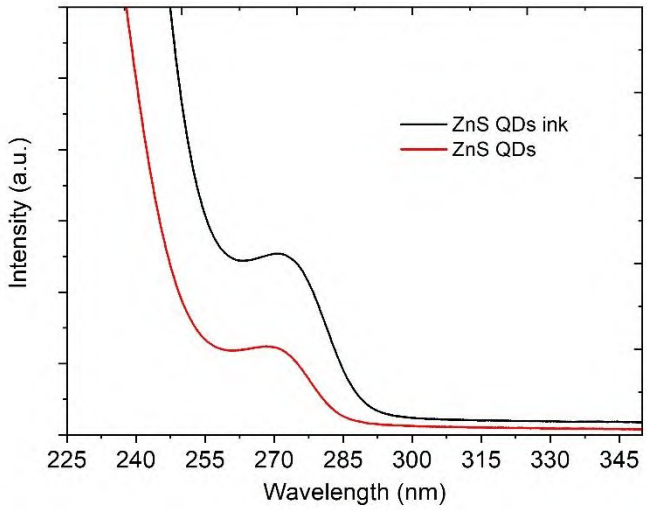

Fig. 5. UV-vis spectra of ZnS QDS and ZnS QDs ink

attributed to the n ← π* transition of the OH groups in PVA polymer molecules [16]. For ZnS QDs ink, the blue emission was observed at about 445 nm, while this emission was displayed at about 430 nm for pure ZnS QDs. The result may be due to the interaction between ZnS QDs and PVA molecules in the ink formula. The CIE (x, y) coordinates of PVA solution, ZnS QDs, and ZnS QDs ink are shown in Fig. 6(b), respectively. The result shows that the CIE (x, y) coordinates of ZnS QDs ink are slightly shifted in the blue emission, which is consistent with the PL analysis.

Furthermore, the application of the ZnS QDs ink for anti-counterfeiting is displayed in Fig. 6(c). The security printing demonstration of the word "Graphic Arts and Media" and the symbol were printed on fabric and graphic paper and then excited by normal light and UV light excitation, respectively, which emitted blue color with the UV light excitation as Fig. 6(c).

Conclusion

In summary, we have successfully synthesized ZnS QDs by the chemical precipitation method in air. The studied results show that the ZnS QDs have the zinc-blende structure, and the TEM analysis shows spherical in shape with the particle size of about 20 nm. The ZnS QDs have a strong blue emission at about 430 – 445 nm. Especially, ZnS QDs were successfully applied for anti-counterfeiting ink.

Acknowledgment

The authors would like to acknowledge the financial support for this study from Ho Chi Minh City University of Technology and Education (HCMUTE).

References

[1] Abdul Kareem Thottoli, Anu Kaliani Achuthanunni, Effect of polyvinyl alcohol concentration on the ZnS nanoparticles and wet chemical synthesis of wurtzite ZnS nanoparticles, Journal Nanostruct. Chem. 4 (2013) 1. doi.org/10.1186/2193-8865-3-31.

[2] Malgorzata Geszkea, Marek Murias, Lavinia Balan, Ghouti Medjahdi, Jaroslaw Korczynski, Michal Moritzb, Janina Lulek, Raphaël Schneider, Folic acidconjugated core/shell ZnS:Mn/ZnS quantum dots as targeted probes for two photon fluorescence imaging of cancer cells, Acta Biomater. 7 (2011) 1327.

doi: 10.1016/j.actbio.2010.10.012

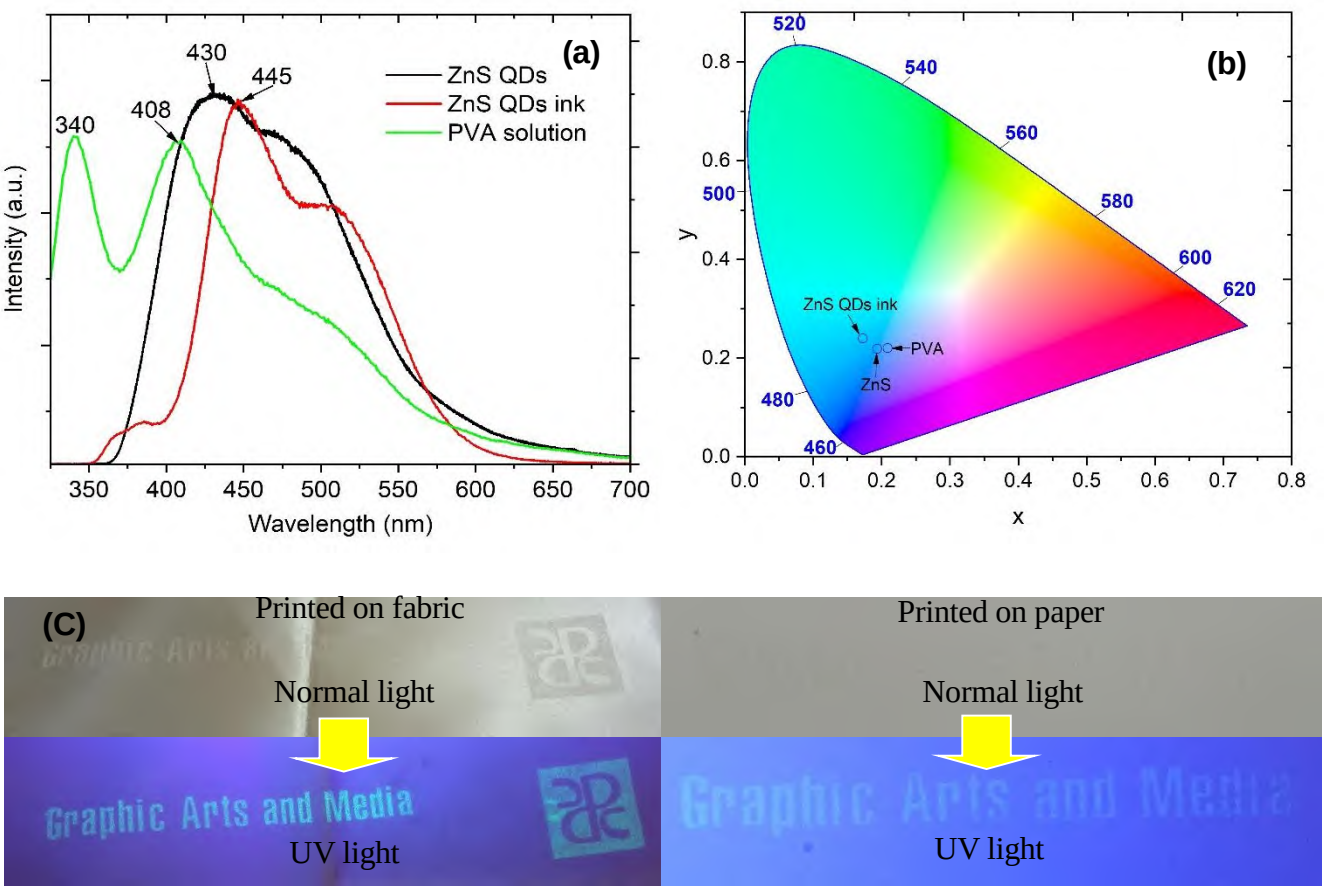

Fig. 6. (a) PL emission spectra of ZnS QDs, PVA solution and ZnS QDs ink, (b) CIE chromaticity diagram of ZnS QDs, PVA solution and ZnS QDs ink, (c) Experimental digital images of ZnS QDs ink on paper and fabric under normal light and UV light

[3] Fatemeh Karimi, Hamid Reza Rajabi, Leila Kavoshi, Rapid sonochemical water-based synthesis of functionalized zinc sulfide quantum dots: study of capping agent effect on photocatalytic activity, Ultrason. Sonochem. 57 (2019) 139.

[4] Alessia Le Donne, Sourav Kanti Jana, Sangam Banerjee, Sukumar Basu, Simona Binetti, Optimized luminescence properties of Mn doped ZnS nanoparticles for photovoltaic applications", J. Appl. Phys. 113 (2013) 1. doi: 10.1063/1.4772668

[5] K.T. Vadiraj, Shiddappa L. Belagali, Synthesis and characterization of Mn:ZnS quantum dots for photovoltaic applications, Nano-Struct. Nano Objects 14 (2018) 118. doi: 10.1016/j.nanoso.2018.02.001

[6] P.K. Shon, J.H. Shin, G.C. Kim, S.N. Lee, Enhanced luminescence related to transparent conductive oxide in ZnS-based EL device fabricated by screen printing method, J. Lumin. 132 (2012) 1764. doi: 10.1016/j.jlumin.2012.01.012

[7] T.W. Kanga, K.W. Parkb, G. Deressac, J.S. Kim, Drastic enhancement of blue-to-orange color conversion efficiency in heavily-doped ZnS:Mn2+ phosphor and its application in white LEDs, J. Lumin. 194 (2018) 551. doi: 10.1016/j.jlumin.2017.07.036

[8] Fatemeh Esmaeili, Mehdi Ghahari, Mahdi Shafiee Afarani, Atasheh Soleimani, Synthesis of ZnS–Mn nano-luminescent pigment for ink applications, J. Coating Technol. Res. 15 (2018) 1325. Doi: 10.1007/s11998-018-0081-4

[9] R.M. KrsmanovićWhiffena, D.J. Jovanović, Ž. Antić, B. Bártová, D. Milivojević, M.D. Dramićanin, M.G. Brik, Structural, optical and crystalfield analyses of undoped and Mn2+-doped ZnS nanoparticles synthesized via reverse micelle route, J. Lumin. 146 (2014) 133. Doi 10.1016/j.jlumin.2013.09.032

[10] S. Joicy, R. Saravanan, D. Prabhu, N. Ponpandian, P. Thangadurai, Mn2+ Ion Influenced Optical and Photocatalytic Behaviour of Mn–ZnS Quantum Dots

Prepared by a Microwave Assisted Technique The Royal Society of Chemistry, 2014, p. 44592. DOI: 10.1039/C4RA08757G

[11] Yun Hu, Bin Hu, Bo Wu, Zhaorong Wei, Jitao Li, Hydrothermal preparation of ZnS:Mn quantum dots and the effects of reaction temperature on its structural and optical properties, J. Mater. Sci. Mater. Electron. 29 (2018) 16715 DOI: 10.1007/s10854-018-9764-y

[12] Yongbo Wanga, Xuhua Liang, Xuan Maa, Yahong Hua, Xiaoyun Hub, Xinghua Li, Jun Fan, Simple and greener synthesis of highly photoluminescence Mn2+ –doped ZnS quantum dots and its surface passivation mechanism, Appl. Surf. Sci. 316 (2014) 54. DOI: 10.1016/j.apsusc.2014.07.135

[13] B. Qadri, E.F. Skelton, D. Hsu, A.D. Dinsmore, J. Yang, H.F. Gray, B.R. Ratna, Size induced transition-temperature reduction in nanoparticles of ZnS, Phys. Rev. B 60 (1999) 9191. Doi 10.1103/PhysRevB.60.9191

[14] R. Viswanath, H.S. Bhojya Naika, G.S. Yashavanth Kumar, P.N. Prashanth Kumar, K.N. Harisha, M.C. Prabhakara, R. Praveen, Synthesis and photoluminescence enhancement of PVA capped Mn2+ doped ZnS nanoparticles and observation of tunable dual emission: a new approach, Appl. Surf. Sci. 301 (2014) 126. doi: 10.1016/j.apsusc.2014.02.013

[15] ShankerRam, T.K. Mandal, Photoluminescence in small isotactic, atactic and syndiotactic PVA polymer molecules in water, Chem. Phys. 303 (2004) 121. doi: 10.1016/j.chemphys.2004.05.006

Applying the G7 method to color calibration for Offset printing machines

Tra Do Thi Thu[1], Vu Do Anh[2], Cuong Nguyen Viet[1]

1.Department of Printing Technology, Chemical Engineering, Hanoi University of Science and Technology

2.Thu Do Packaging JSC.

Address:1. No 1, Dai Co Viet road, Hai Ba Trung, Hanoi, Vietnam

2. Quang Minh Industry zone, Me Linh, Hanoi, Vietnam

Email: cuong.nguyenviet@hust.edu.vn

Abstract

Calibration of offset printing machines is an important work in maintaining the color of printing products. Which standard for calibration is currently being discussed by scientists. Applying the G7 method to calibrate offset printing machines to maintain the desired colors is a way forward in color standardization. The G7 controls and calibrates the offset printing machine using colorimetric values instead of negative increments.

Using gray balance and NPDC curve to evaluate is a direction in the study. The first printing provides the data to create a control curve known as the Neutral Print Density Curve (NPDC). Second print with gray balance assessment makes alignment more efficient, curves are visually rendered especially in neutral colors.

1.Introduction

G7 is a method created by Don Hutcheson in 2005. It builds on the success of photography and applies the convenience and simplicity of RGB space to CMYK correction. RGB controls color values according to four general principles:

• White with R = 255; G = 255; B = 255
• Gray R = G = B
• Black R = G = B = 0
• Contrast 2.2

The primary purpose of G7 calibration is to provide grayscale reproduction across a variety of devices, processes, and using a variety of printing methods. Calibration to G7 is to get a Neutral Print Density Curves (NPDC) over the entire tonal range from 0 to 100 with gray balance instead of the ISO tone value increase curve (TVI).

a. The essence of G7

To assess whether a color printed sheet is correctly restored, it is evaluated through two principles.

The first rule: restore the correct level, ie the tone value on the file is equal to the tone value on the printed sheet. The value of the layer to care about: the value of the layer of each color channel, the difference between the lightest and darkest areas.

The second rule is to ensure color balance. Color balance is assessed through gray balance. Since color balance is judged by the eye's color perception, the eye is most sensitive to gray. Gray balance is a measure of color balance.

For that reason, the G7 aims to guide the work towards achieving the international standard for color, ISO 12647. Delivering grayscale reproduction across a variety of devices, processes, and methods different printing methods.

The G7 interferes with both principles to ensure color accuracy:

• Find out the imbalance ratio between C- M- Y of the system to ensure gray balance.
• Interfere with each color's scale value C- M- Y- C

b. G7's gray balance principle [1]

The principle of gray balance according to G7 is determined based on the color adaptability of the human eye. As we know the values of a*, b* do not always give the correct perception of gray and usually we always want the gray color to be compatible with the print media but not all materials are neutral because the paper a*= b*= 0. Therefore, grayscale rendering is relative to the color of the media, meaning that images printed on different colored substrates look slightly different when viewed side by side. However, when viewed individually, it is thanks to a process known as "visual adaptation," whereby the eye uses the surrounding white paper as a neutral reference

The resulting formula depends on the whiteness of the paper, which means that the CMYK gray tones will shift to a gray balance according to the paper color. The G7 gray balance is rated by the value "ΔCh".

In order to obtain gray-balanced sheets on a wide range of papers, the G7 specification must solve the problem by defining gray balance as a function of the paper color expressed in CIE, where the values a* and b * ideal for each gray scale level is reduced to zero then gray scale is at its best. So to obtain the desired a* and b* values for any step in the CMY grayscale by multiplying the a*/b* value of the paper by the inverse percentage of the Cyan color of that step (i.e. percentage value on the gray scale). Where Cyan color is the approximate index of the grayscale value.

The formula for calculating gray balance according to G7:

a* = paper_a* x gray factor
b* = paper_b* x gray factor
gray factor = 1 – C/100

c. Neutral Print Density Curve [1]

G7 defines tone through the neutral print density curve (NPDC). The G7 NPDC is the relationship between the measured neutral density value and the value on the scale. G7 defines two standards for NPDC, one for grayscale CMY combined and the other for K black

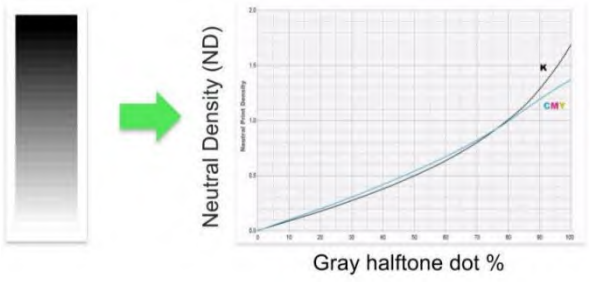

Figure 1. Neutral Print Density Curve (NPDC)

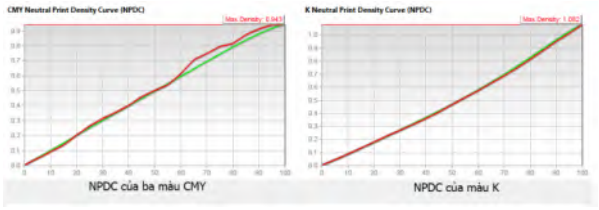

Figure 2. Description of CMY and K color curves on Curve 4 software (green curve is desired value, red is measured value)

d. SCCA Calculator- Substrate Corrected Color Aim Calculator

Different types of paper, will differ in the white point (or color of the paper). In the case, the paper selected for production does not exactly match the reference and in these cases some adjustment of the print color values may be necessary.

SCCA- is a tuning tool based on the principles defined in ISO 15339, using the Tristimulus linear equation [2]

$$X_2 = X_1(1 + C) - X_{\min}C$$

$$C = \frac{X_{w2} - X_{w1}}{X_{w1} - X_{\min}}$$

In there:

• X1: One of the three CIE XYZ values of the original paper
• X2: One of the three CIE XYZ values of the paper after adjustment
• C: is a constant
• XS1: One of the three CIE XYZ values of the original paper
• XS2: One of the three CIE XYZ values of the destination paper
• Xmin: The minimum CIE value at the maximum TAC position of the original paper (usually determined at the 4-color stacked cardboard box)

SCCA is a standard math formula based on color adaptation of the human eye, simulating what the target CIE Lab color value would look like. That is, compared to the linear equation Tristimulus, the SCCA tool has added features to convert XYZ values to Lab or vice versa. [3]

After the data is modified against the new CIELab values, the user will know in advance how the final print color will be affected by the background color. The recalculated data can be used to create profiles for more accurate inspection/transformation, and the reported CMYK, RGB, and grayscale tones can be used for new process control purposes. when printing on new substrates.

The purpose of the study is to find a method to apply G7 in color calibration on industrial offset printing systems that are popular in the market.

2.Materials and methods

- Using Duplex Seha 250 g/m^2 paper, DIC Apex G plus ink

- Printing was carried out on a Heidelberg CD 102-6L Industrial Offset Printer [4]
- Measurement is performed on the eXact Colorimeter
- i1iO+ i1Pro Color Scanner [5]
- Using Software Curve 4

The experimental procedure is summarized in the following diagram:

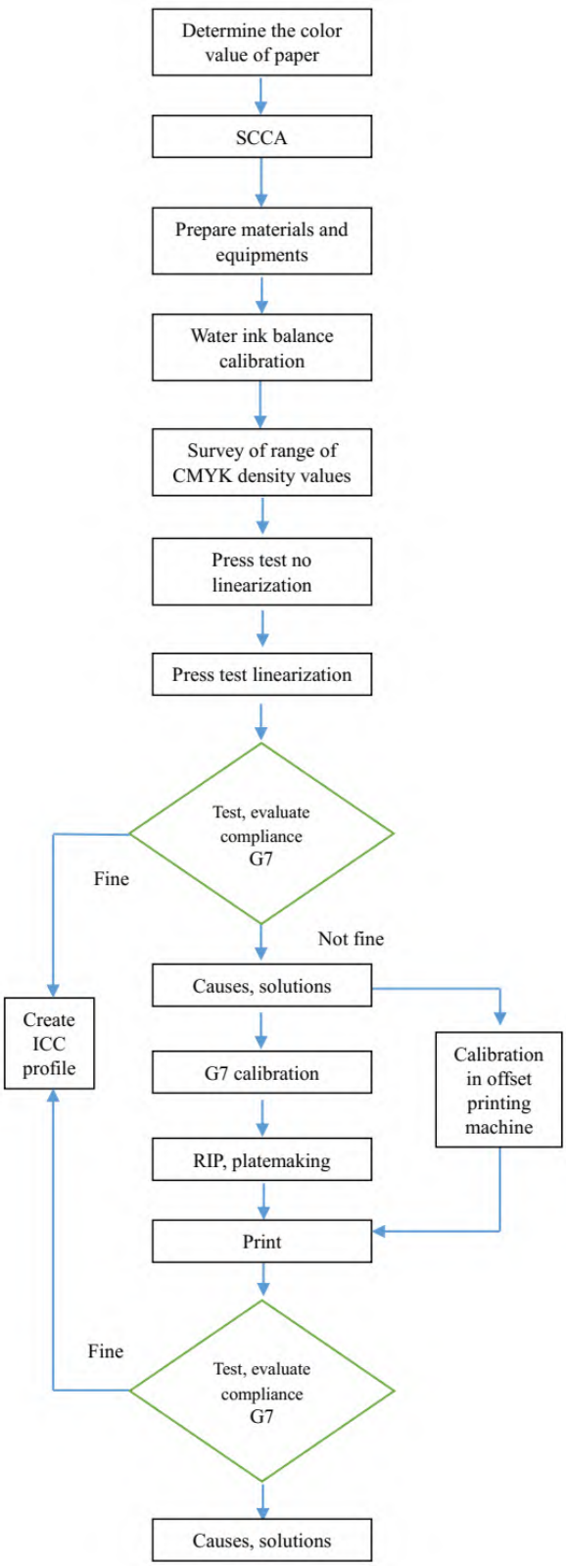

Figure 3. The experimental procedure of G7 calibration

3.Results and Discussions

3.1. Target color value correction results with SCCA

The results table returns the target value of CMYK raw tones, RGB colors corrected to the new Duplex Seha 250 g/m^2 substrate

Table 1. Target value corrected results by SCCA

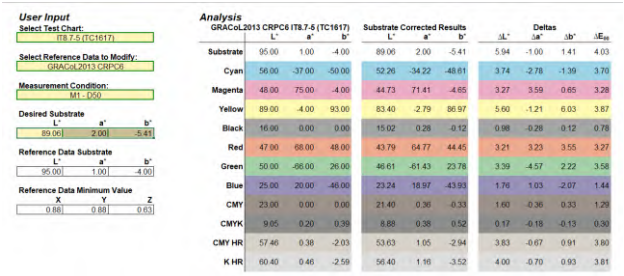

This results, with the next reference will be adjust the tone value density to stick to the target value color, so that the results obtained by dEoo are the best.

Data on color value of column 4 and column 5 on the P2P51 scale are extracted from the corresponding TC1617 scale with new quality to serve for gray balance assessment in the next steps.

3.2. Results of 1st linear printed sheets

a G7 Targeted results

Table 2. Colorimetric results between SCCA and 1st linear printed sheets

Color	SCCA			1st linear printed sheets			dEoo
	L	a	b	L	a	b	
C	52.26	-34.22	-48.61	53.96	-30.00	-48.61	2.36
M	44.73	71.41	-4.65	46.48	68.28	-5.76	1.91
Y	83.40	-2.79	86.97	82.69	-4.50	83.37	1.35
K	15.02	0.28	-0.12	16.59	0.68	2.11	2.44
R	43.79	64.77	44.45	46.14	61.97	47.08	3.00
G	46.61	-61.43	23.78	47.86	-59.31	29.15	2.79
B	23.24	18.97	-43.93	24.41	22.05	-45.05	1.78

Currently all colors are within the tolerances of the G7 Targeted level. But the dEoo range is very high, for example for color C the dEoo value is 2.36 while the tolerance is 3.5, for the color R the dEoo value is 3.00 while the allowable tolerance is 4.2, it is dangerous when applied in mass production, because fluctuations in the printing process can also cause very large errors and the system is no longer up to the mark.

b. Gray balance test results

Evaluate K NPDC and CMY NPDC:

+ If the system achieves gray balance, then ideally two curves: the green curve - the target curve of G7 and the red curve - the actual curve of the printing system will overlap.

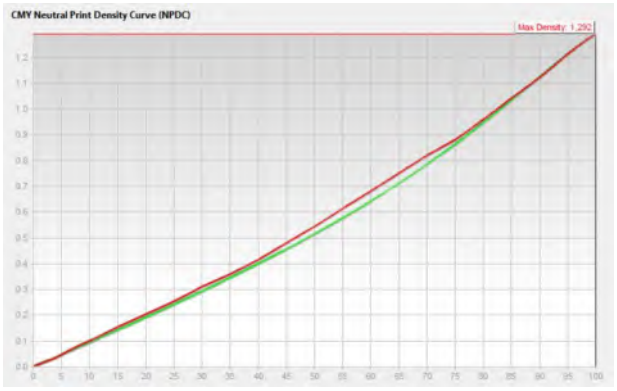

Figure 4. CMY NPDC of 1st linear printed sheet

+ With CMY NPDC, it is found that from 0-5% the two curves almost completely coincide, starting from 5%-40% the two curves begin to separate. And the most obvious difference is from the region of 40%-75%, from the region of 75% onwards the two curves start to meet and from 85%-100%, the two curves almost coincide. Thus, gray imbalance is occurring in the 5% to 85% region, and is most pronounced in the 40%-75% region

Figure 5. K NPDC of 1st linear printed sheets

• Look at the figure above: The K NPDC, the green and red curves are completely separate from 15% to 100%

• The system is out of gray balance

c. Results of tone value increase test

Table 3. Results of tone value increase on 1st linear printed sheets

% File	Tone value increase on the 1st linear printed sheets (%)			
	K	C	M	Y
0	0.20	0.00	-0.37	-0.20
5	5.67	0.50	4.20	4.73
10	8.60	3.20	6.23	7.70
20	11.67	6.50	7.07	11.33
30	13.20	8.80	8.93	13.83
40	14.00	10.60	10.37	15.57

50	16.00	11.50	10.97	17.80
60	15.97	10.80	11.57	18.07
70	13.13	9.00	9.83	15.97
80	9.97	6.80	7.33	12.37
90	6.10	4.20	4.03	7.40
95	3.70	2.20	2.67	4.30
100	0.03	0.00	0.00	0.00

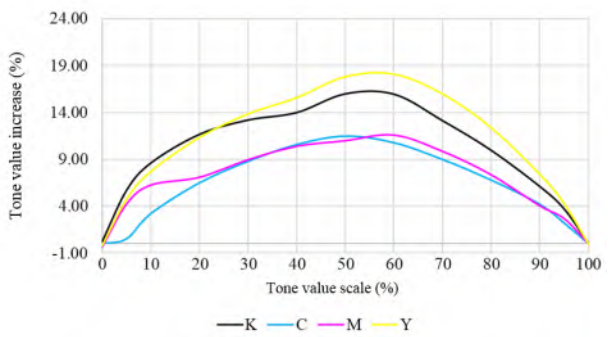

Figure 6. Tone value increase of 1st linear printed sheets

Refer to the regulation on the level of increment in the ISO 12647-2 standard as follows

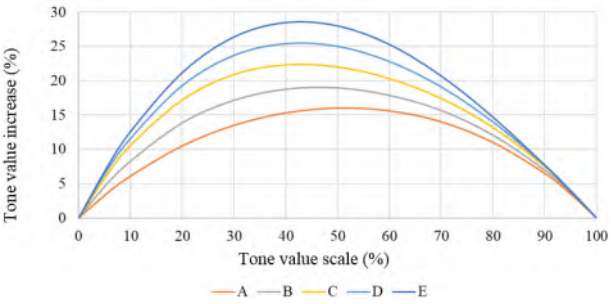

Figure 7. Tone value increase according to ISO 12647-2

• The growth rate of Y is very high, the strongest increase is in the 40%-70% region, in the 50% region the increase is up to 17.8%. Exceeded the allowable limit in ISO 12647-2 by 16%. This proves that it is absolutely correct to observe the results on column 5, of the P2P51 scale being yellowed.
• The increase of K is highest in the range of 50%-60% with an increase of about 16% but still within the requirements of ISO 12647-2.
• For C and M, the TVI is relatively low. Color C increased the most in the 50% region at 11.5%, in the 40% and 60% region, the increase in the range was 10.6% - 10.8%. Color M has the highest increase in the area of 60% increase of 11.57%, and increase of 10.97% in the region of 50%.

d. Discussion

• From the results reported above, the system has not yet achieved gray balance and the target result also gives a rather high dEoo value. With the above target value results, when applied in mass production with very large fluctuations in printing conditions, then the results of the calibration process are no longer accurate.
• Ignoring the gray balance result of the system in this first calibration, the first thing to solve is to adjust the density value of the CMYK colors to give a better target G7 result, ie. is the dEoo result of the CMYK and RGB colors compared to the smaller target, so that when applied in mass production, the tolerance range will be wider and then the application and implementation will be easier.
Currently, in the results of testing the density value compared with the results of the no linear printed sheets, the density value has not reached the same result as the survey value of the no linear print. Based on the results of the layer increment analysis presented above, it is possible to adjust the density value to allow for better target G7 results. Thus, in order to achieve better target results, it is necessary to adjust the density value of the solid tones to the density value of the no linear print. For all CMYK colors need to increase the density value. The adjustment is made by increasing the amount of ink supplied to the print, not choosing to increase the density by increasing the printing pressure because observing the result of the K color increase, the current increase in the Kth layer is of K color was quite high in the 50%-60% tone area the increase went up to 16%. With colors C and M also adjust the ink level, because the increment of these colors is also relatively high, if the pressure increase can be increased, the level will exceed the specified standard.
For Y, currently the density result of color Y is lower than the value selected from the no linear print, although the gradation of the Y color is quite high, but still decided to adjust the ink level up to make sure the R and G color combinations get the best results.

3.3. Results of 2nd linear printed sheets

a. Result of G7 Targeted test

Table 4. Colorimetric results between SCCA and the 2nd linear printed sheets

Color	SCCA			2nd linear printed sheets			dEoo
	L	a	b	L	a	b	
C	52.26	-34.22	-48.61	52.90	-30.69	-50.25	1.75
M	44.73	71.41	-4.65	45.35	70.19	-4.44	0.66
Y	83.4	-2.79	86.97	82.96	-4.34	86.52	0.91
K	15.02	0.28	-0.12	15.51	0.71	2.18	2.30
R	43.79	64.77	44.45	44.74	64.02	47.52	1.81
G	46.61	-61.43	23.78	46.33	-61.42	27.37	1.51
B	23.24	18.97	-43.93	22.63	22.10	-44.48	1.86

The results of the 2nd linear printed sheets are better than the first, with all targets having dEoo values less than 2. Especially with color Y and color M giving dEoo results less than 1.

b. Gray balance test results

Evaluate K NPDC and CMY NPDC: if the system achieves gray balance, then ideally two curves: the green curve - the target curve of G7 and the red curve - the actual curve of the printing system will overlap.

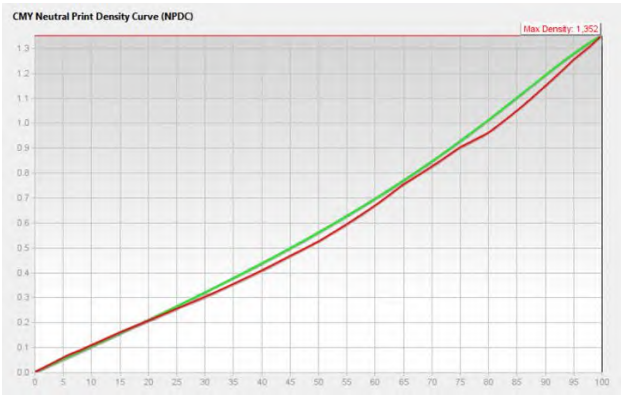

Figure 8. CMY NPDC of 2nd linear printed sheets

Compared to the target curve of G7, the actual CMY NPDC is much different. The difference is most evident in the region from 25% to 65% and from 70% to 100%.

Figure 9. K NPDC of 2nd linear printed sheets

Compared to the target curve of G7, the actual CMY NPDC is completely different. With color K almost no points overlap. The system is out of gray balance.

c. Results of tone value increase test

Table 5. Results of tone value increase on 2nd linear printed sheets

% File	Tone value increase on 2nd linear printed sheet (%)			
	K	C	M	Y
0	0.00	0.47	0.00	0.00
5	6.70	4.67	2.30	-0.50
10	10.30	6.60	5.40	4.70
20	18.30	9.00	8.90	11.80
30	22.10	9.73	11.50	15.20
40	24.20	11.70	14.10	18.30
50	25.60	13.10	15.60	21.00
60	24.50	14.13	14.80	20.80
70	20.00	11.23	12.40	17.80
80	14.90	8.30	9.30	13.70
90	8.30	4.83	5.60	7.80
95	4.30	2.90	3.10	4.20
100	0.00	0.00	0.00	0.00

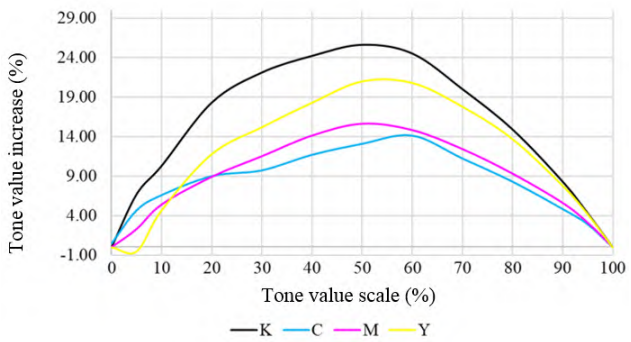

Figure 10. Tone value increase of 2nd linear printed sheets

Refer to the regulation on the level of increment in the ISO 12647-2 standard as figure 7, it can be said that

• The growth rate of is very high from 10% to 80%, especially in the 50% area, the increase is 25.6%.

• Compared with the results of the first linear printing, the TVI of the Y color is increased quite a bit. Currently, in the 50%-60% region, the increase is approximately 16%, the 40% and 70% regions are approximately 18%.

• The increments of color M and color C are not too high and are still within the tolerances of the standard.

d. Discussion

With color K, comparing the density value of the 2nd linear print which is 1.71 with the reference density value from the no linear print of 1.77, the density value currently does not meet the reference, otherwise. Observe that the Kth color gradation is very high, if the K color density value is adjusted up, the increase can be even higher and will cause problems with the water level balance on the printed sheet. . On the other hand, the G7 Targeted result with K color is getting a dEoo of 2.30 compared to the G7 Targeted tolerance for K color of 5, which is also a good result. So accept the color result K with a density value of 1.71. The G7 grayscale result, although it has reached the specified tolerances, but the current maximum value compared to the tolerance is only 0.07 difference. To ensure G7 Targeted results and increase tolerance range for G7 Grayscale. Thus, for color K will adjust the value of the layer to achieve a better G7 Grayscale level.

For colors C, M, and Y, the density values of all colors are obtained from the reference value from the no linear print and the G7 Targeted results of each color are 1.75, 0.66

and 0.91 respectively compared to the allowed tolerances. is 3.5 these are very good results. But now the system is gray unbalanced, because the overlapping CMY combination is exceeding the specified tolerance of the G7 Grayscale (result shown above). The main cause of this imbalance is that the value of b is very high, the printed sheet is yellowed, this is also proven with the result of increasing the yellow layer being at a very high and high level. than the rest of the colors. Looking back at the results of the first linear printing, the yellow density is being adjusted from 1.04 up to 1.08 for the second linear printing, giving dEoo less than 1, and this is also the best value of color density Y. when combined with colors C and M to produce good color combinations R, G, dEoo is 1.81 and 1.51 respectively.

With the value of Δa in column 5 from the 17th to the 25th cell, the result of Δa is negative, that is, it is moving to the green (G) direction and the maximum deviation has exceeded the value 2 not only The strong impact of color as analyzed above causes gray balance, but here is also the effect of color C. If the density of yellow and color C is reduced at the same time, gray balance can be achieved in this region, but cells from 9th to 17th are showing a positive shift a ie redder in This is also the effect of color M, the result of the increase in the color layer of the M color in these cells is quite high and higher than the increase in the C color layer, if the C color density is reduced, then in the area from the second cell 9 through 17 the effect of color M will be stronger, and gray balance results are also difficult to achieve

3.4. Results of G7 calibration using Curve 4

Table 6. Colorimetric results between SCCA and the after G7 calibrated sheets

Color	SCCA			After G7 calibrated sheets			dEoo
	L	a	b	L	a	b	
C	52.26	-34.22	-48.61	52.84	-30.77	-50.11	1.68
M	44.73	71.41	-4.65	45.45	70.29	-4.57	0.73
Y	83.4	-2.79	86.97	82.81	-4.15	86.12	0.87
K	15.02	0.28	-0.12	14.34	0.15	0.94	1.15
R	43.79	64.77	44.45	43.95	64.52	48.72	1.98
G	46.61	-61.43	23.78	45.42	-61.74	27.9	2.02
B	23.24	18.97	-43.93	22.03	22.34	-44.63	2.09

All colors achieve target values within tolerance

3.5. Test of G7 compliance

Test results by Curve 4 as follow:

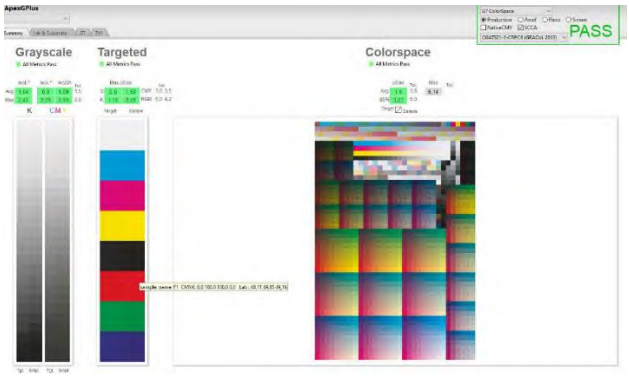

Figure 12. Test results by Curve 4 [6]

After calibrated sheets have achieved G7 Colorspace, such as the internal system and processes have been maintained stably.

The result of machine adjustment in Offset achieved the highest level of G7 is G7 Colorspace with GRACoL 2013 and has been completed the create ICC profile for host in offset information through the G7 calibration

4. Conclusion

G7 calibration can generally be used to calibrate industrial offset printing machine, using it under production conditions in Vietnam is completely feasible. Through calibration, the ICC profile of the offset printer was created. G7 calibration has properties that are very suitable for application in offset printing machine, also Flexo printing, screen printing, gravure printing [7] and other printing methods. In experimental conditions, G7 calibration is selected as interfering with master, ie interfering with the value of CMY colors according to G7 method to find new combinations to help the system achieve gray balance. Besides, fluctuations in the printing process are very large. If the best possible target value is not achieved, then when applied to mass production, the same fluctuations will cause the system to no longer reach the target value. Therefore, the density value of the CMYK colors will be preserved to achieve the best target value. Therefore, G7 calibration is completely suitable for industrial printing, convenient and promises to help printing facilities manage colors during the printing process.

References

1. IDEAlliance ®, IDEAlliance Guide to print production best practices and specifications for printing.
2. ISO, ISO/PAS 15339-2:2015- Part 2: Characterized reference printing conditions, CRPC1-CRPC7.
3. IDEAlliance®, *SCCA Calculator*, https://idealliance.org/idealliance-releases-new-scca-calculator/ [online]
4. Heidelberg ®, Technical information Speedmaster CD 102- 6L- UV.
5. https://www.xrite.com/categories/calibration-profiling/i1io-for-i1pro-3-plus, 20 04 2022. [online].

6. Chromix®, "http://www.chromix.com/curve4/," 01 04 2022. [online].
7. Robert Chung et al., Gravure Press Calibration by G7 Simulation, RIT, 2014

The study of the characteristics and printing quality of offset inks based on palm oil

Wannarat Wirachkul, Suchapa Netpradit and Juntira Komasatith

Department of Printing and Packaging Technology, Faculty of Industrial Education and Technology, King Mongkut's University of Technology Thonburi
126 Pracha Uthit Rd., Bang Mod, Thung Khru, Bangkok 10140, Thailand

Abstract

The objectives of this project were 1) to study the properties of varnish using palm oil as a solvent and 2) to compare the printing ink properties and qualities between palm-oil-based offset ink and soybean-oil-based offset ink. The varnish in the experiment was produced using palm oil (crude palm oil and crude palm kernel oil) as the same method as soybean oil varnish. Unfortunately, the crude palm oil could not be used due to the coagulation of varnish that was too sticky to mix in the printing ink component. Then the properties of varnish using crude palm kernel oil were tested. The result showed that the palm-oil-based varnish had more tack and viscosity than the soybean-oil-based varnish, resulting in a slower flow and dispersion rate. After that, the varnishes obtained from both oil types are mixed to produce oil-based printing ink using the ratio of each component by weight; colorant 18-20%, linseed oil 30-35%, palm kernel oil or soybean oil 30%, additive 5% and solvent 10-17%, as the formulation of an ink manufacturer. The properties of printing inks; cyan, magenta, and yellow colors, were compared between palm-kernel-oil-based ink and soybean-oil-based ink. It was found that both printing inks have the same fineness, but the palm-kernel-oil-based ink had more tack and viscosity than the soybean-oil-based ink, resulting in less flow rate and dispersion rate. Most palm-kernel-oil-based inks had less ink-water balance, faster setting time, longer drying time, and skinning time than soybean-oil-based ink. Both ink types were then printed on 2 types of paper; uncoated paper and coated paper, to determine the qualities of the ink film. The results showed that the palm-kernel-oil-based ink has higher gloss values and more rub resistance than the soybean-based inks. The color shade comparison between the two ink types showed a slight color difference on the uncoated paper ($\Delta E<3$) while the greatest color difference for magenta color ($\Delta E>6$) on the coated paper and a significant color difference for cyan color ($\Delta E>3$). However, the color density of the two printing ink types printed on both paper types was not significantly different. Therefore, crude palm oil could replace the soybean oil for varnish production and offset printing ink mixing with some near properties but need to be further improved in some different properties.

Keywords: Crude Palm Kernel Oil / Crude Palm Oil / Offset Ink / Palm Oil / Soybean Oil / Vegetable Oil-Based Ink

Background

The offset printing technology uses solvent-based inks that are oil-based, and historically, petroleum was the oil that was most commonly utilized in these inks. However, the property of petroleum oil is that it contains odorous, environmentally hazardous volatile compounds. Nowadays, people pay more attention to the environment, so petroleum-based ink does not meet consumer demand because of the environmental unfriendliness of petroleum solvents. Environmental issues are an important issue along with print quality. Therefore, vegetable oil-based ink was invented and developed by using soybean oil to replace and had been accepted. In addition to soybean oil-based inks, other types of vegetable oils are also used to improve the properties of printing inks. In the printing process, they can be used for offset printing systems and can also produce beautiful print quality with bright, high color intensity, and with shiny texture. In addition to the environmental friendliness of soybean oil-based ink, this ink extends the life of the printer and reduces printing costs in the long run [1]. But soybean oil used as a solvent in printing inks to replace petroleum oil is quite expensive because soybean oil is not produced in Thailand, so soybean oil must be imported into the country.

In this regard, the study anticipated the issue of somewhat expensive soybean oil-based ink and considered testing out palm oil-based ink. Based on a survey, there is a large quantity because it is a Thai economic crop with high production capacity [2] to be mixed into an eco-friendly vegetable oil base ink as another alternative. Palm oil is a less expensive vegetable oil than other vegetable oils and in Thailand, the palm is mainly cultivated. Since more than 70% of

the ink composition is solvent, if the cost of the solvent in the ink can be reduced, the ink price will be lower, and most importantly, the palm-oil-based ink is also environmentally friendly that does not cause pollution as well.

Objectives

To study the properties of varnish using palm oil as a solvent

To compare the printing ink properties and qualities between palm-oil-based offset ink and soybean-oil-based offset ink.

Method

The processes in comparing the printing ink properties and qualities between palm-oil-based offset ink and soybean-oil-based offset ink were as follows:

1. Varnish production process. Two types of palm oil were weighed, consisting of 390 g each of crude palm oil from palm husks and palm kernel oil and 210 g of resin to produce varnish for C M Y paint.
   a. Weighed palm oil is boiled to a temperature of 140 degrees Celsius.
   b. When it reached a temperature of 140 °C, the weighed resin were mixed into it.
   c. The resin was stirred until it was dissolved homogeneously.
   d. The homogeneous varnish was taken out to let the varnish cool.
2. Varnish property test; Tack value, Viscosity, Flow rate, Spread flow
3. Ink production process
   a. Applied palm-oil-based varnish that has been mixed with coloring agents, additives and other solvents according to the ratio of each ink formulation. The formula of each color used was the same as that of soybean-oil based ink.
   b. The ink was mixed according to the ink formula of each color. Then it was stirred well, and grinded with a three-roll mill method.
   c. When the ink resolution was less than 5 microns, the toughness was measured. The range of toughness should be in the range of 9.0 – 12.0 GM. But if the toughness was not within the acceptable toughness value, the ink woukd be grinded again. In this respect, the toughness value of 9.0 – 12.0 GM was the toughness of soybean oil-based ink. Structurally, palm kernel oil-based ink has more toughness value than soybean oil-based ink.
4. Ink property test; Fineness of grind, Tack value, Spread flow, Flow rate, Viscosity, Water pickup, Setting time, Drying time, Skinning time
5. The layer of Ink property. The properties of printing ink layer were measured using uncoated paper 100 gsm. and glossy coated paper 130 gsm with a size of 26*27 cm. The sample was printed with a printability tester, and then the sample was taken to measure the properties of the ink layer as follows: gloss test, rub resistance, color different and density.

Result

1. Varnish property test

a. Tack value of varnish

Type of varnish	**tack value (GM.)**
Soy	9.7
Palm	10.9

b. Viscosity of varnish

Type of varnish	**viscosity (Pa.s.)**
Soy	23.42
Palm	62.49

c. The flow rate of varnish

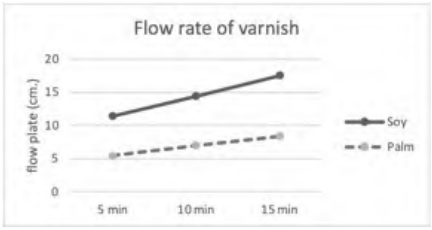

d. Spread flow of varnish

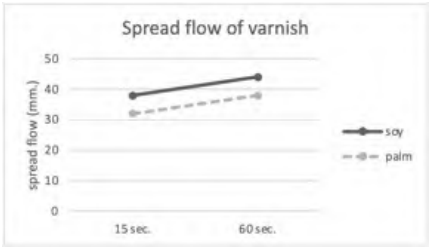

2. Ink property test

a. Fineness of grind
   Soybean oil-based inks and palm kernel oil-based ink showed that the resolution of soybean oil-based inks and palm kernel oil-based ink were the same at 3 micrometers.
b. Tack value of ink
   Palm kernel oil-based ink had more toughness value than soybean oil-based ink.
c. Viscosity of ink
   Palm kernel oil-based ink was more viscous than soybean oil-based ink, especially Magenta which was more viscous than soybean oil-based ink the most due to the structure of palm kernel oil ink contained a lot of saturated fat, so it resulted in high viscosity.
d. Flow rate of ink
   Palm-oil-based ink had a slower flow rate of ink than soybean-oil-based ink due to the flow

correlation with viscosity. If the viscosity is high, the flow will be slow.

e. Spread flow of ink
Palm kernel oil-based ink had a slower dispersion than soybean oil-based ink. The dispersion was influenced by the structure of both types of oils. Palm kernel oil had a high saturated fatty acid content, which resulted in high viscosity, where the viscosity was related to the dispersion. If the viscosity was high, the dispersion would be slow.

f. Water pickup
Palm kernel oil-based ink with Magenta color and Cyan color had less ink-water balance than soybean oil-based ink, especially Magenta. Except for Yellow color where palm kernel oil-based ink had slightly more ink balance than soybean oil-based ink, ink-water balance was related to viscosity. If the viscosity was high, the ink-water balance would be low.

g. Setting time
Palm kernel oil-based ink had a faster setting time than soybean oil-based ink, and Yellow had the slowest setting time of both inks, while Cyan had the fastest setting time of the both types of ink.

h. Drying time
Palm kernel oil-based ink had a much slower drying time than soybean oil-based ink compared to other oil-based inks. The structure of the palm kernel oil-based ink was high in saturated fatty acids, where saturated fatty acids are composed of single bonds that did not react with oxygen. At the same time, soybean oil had a high content of polyunsaturated acids, where polyunsaturated fatty acids had multiple double bonds, thus reacting with more oxygen in the air, thus allowing for faster drying.

i. Skinning time
Palm kernel oil-based ink had a much slower skinning time than soybean oil-based ink. The skinning time was based on the structure of both oils as well as the drying time.

3. The Layer of ink property test

a. Gloss test
Palm kernel oil-based ink had a higher gloss value than soybean oil-based ink because the gloss value was related to the drying of the printing ink. The drying time of palm kernel oil-based ink had a faster setting time and therefore higher gloss values.

b. Rub resistance
Palm kernel oil-based ink had a higher degree of rub resistance than soybean oil-based ink because the color of palm kernel oil-based ink had less shedding, while palm kernel oil-based ink with Yellow color had less rub resistance. than soybean oil-based ink.

c. Color different
The color difference of soybean oil-based inks and palm kernel oil-based inks on coated and uncoated paper showed that the color difference of ink on coated paper was higher than that of uncoated paper. Yellow had the lowest ink color difference on both types of paper, and Magenta on coated paper had the greatest ink color difference.

d. Density
Soybean oil-based ink and palm kernel oil-based ink in all color have similar density values.

Conclusion and discussion

The soybean-oil-based varnish had better varnish properties than palm-oil-based varnish in terms of toughness, viscosity, flow rate and dispersion because soybean oil is a high polyunsaturated fat, in which this type of fat was a liquid at room temperature and would become solid at lower temperatures. While palm kernel oil was a higher saturated fat, it was solid at room temperature, so the ink properties in terms of toughness, viscosity, flow rate and dispersion were consistent with the properties of the varnish. In terms of ink and water pick up properties, there was a correlation with viscosity. If the viscosity was low, ink and water pick up value would be high. If the viscosity was high, ink and water pick up value would be low. Moreover, palm kernel oil-based ink had better setting, drying and skinning properties than soybean oil-based ink because of the chemical structure of polyunsaturated fat of palm kernel oil, and palm kernel oil-based ink had a higher gloss than soybean oil-based ink which was related to the setting of the ink. For the rub resistance level of palm kernel oil-based ink, most had better rub resistance, better adhesion than soybean oil-based ink. For the color difference of prints printed with both types of ink, Yellow had the lowest ink color difference on both paper types, and Magenta on coated paper had the largest difference in ink color. And the density value on coated paper has similar blackness values for prints printed with both inks. For uncoated paper in Magenta and Cyan color, the density value of palm kernel oil-based ink was lower than that of soybean oil-based ink.

Acknowledment

We would like to express my sincere thanks to Patum Vegetable Oil Co.,Ltd. for providing the palm oils. Many appreciations to Chalerm Chaichan Co., Ltd. for the suggestion and preparing the raw materials and facilities for printing ink mixing.

References

1. Smile Siam Printing Service, **Smile-Siam.com** [Online], Available : https://www.smile-siam.com/printing_content-soy_ink/. [14 May 2021].
2. The Agricultural Research Development Agency (Public Organization), **arda.or.th** [Online], Available : https :// www.arda.or.th/kasetinfo/south/. [14 May 2021].
3. Ploysri, W.and Charoensopa, K., The production of processed color of offset printing ink from used vegetable oil, **Journal of industrial technology Ubon Ratchathani Rajabhat University**, vol.10, No. 2, pp. 89-98. (2020)
4. Cem Aydemir, Semiha Yenidoğan, Arif Karademir and Emine Arman Kandirmaz, "The examination of vegetable and mineral oil-based inks' effects on print quality: Green printing effects with different oils", **Journal of Applied Biomaterials & Functional Materials**, Vol.16, No.3, pp. 137-143. (2018)

Improvement of electrical property of printed TiO_2 thin film by the mixture of small and large particle size using LDM 3D-printing system

Korkit Saejiw, Krairop Charoensopa**, Intach Hongrattanavichit* and Aran Hansuebsai**

**Department of Imaging and Printing Technology, Faculty of Science, Chulalongkorn University, Bangkok Thailand 10330*

*** Department of Industrial Arts and Science, Faculty of Industrial Technology, Suan Sunandha Rajabhat University, Bangkok, Thailand 10300*

Abstract

. Our research is to study the optimizing materials integration process for dye-sensitized solar cell electrode by using a LDM 3D-printing system. The 3D-printer will play an important role in adjusting the TiO_2-deposition on an electrode depending on the TiO_2 structures and their rheological property. This method also allows us to create multilayer design when different TiO_2 types are used which will be beneficial for electrical property improvement. It appears that the double layers TiO_2 electrode comprising of small and large particles lead to the improvement of sheet resistance. The light-scattering effect of the large particle most likely contributes to the performance improvement. Available commercial nano-TiO_2, P25 (30 nm) and ST-41 (160 nm), were used. Results showed the achievement of sheet resistance of printed TiO_2 was 1.12E+4 Ω/sq at thickness 16.67 µm and roughness (Ra) 257 nm. While single layer TiO2 of small and large particle size gave the sheet resistance values at 3.77E+6 Ω /sq and 6.20E+5 Ω /sq respectively.

Introduction

Titanium oxide (TiO_2) thin films have emerged as one of the most promising oxide materials owing to their optical, electrical and photo electrochemical properties [1-2]. There are several methods have been employed to fabricate TiO_2 thin films including reactive sputtering, chemical vapor deposition, sol–gel process and printing [3-5]. 3D printing system offers many advantages over other deposition and printing techniques due to the use of simple and inexpensive equipment and quick process. The application of liquid deposition modeling (LDM) 3D printing has become more and more widespread. Novel morphologies and physical properties can be obtained depending on the 3D printing technique such as multi-layer coating, the mixture of TiO_2 with different particle size - layer by layer and variable printed pattern. The rheological property of TiO_2 paste can give rise to the formation of thin films.

3D printing technology has evolved very rapidly in recent years and has shifted apart from its traditional application field. The difference among printer types is based on cost, spatial resolution and materials used. LDM technique (Liquid Deposition Method) of 3D printing system using an extruded syringe could be one of the proper fabrication method by controlling the nozzle size, printing pressure and printing speed. With proper pressure force and moving speed, it is possible to accurately control the flow of materials and also the retraction to interrupt deposition. By this method, the production of freeform structure could be achieved by using a computer-controlled extruder moving along the x,y and z axes. The system allows the use of functional, end-use materials such as TiO_2 and other conductive pastes in order to fabricate thin films for optoelectronic applications. In addition, nano-particle TiO_2 material is now available in a variety of applications in the environmental and energy fields. By this recommendation, it is expected that multilayer TiO_2 electrodes comprising of the mixture of small and large nano-particles can lead to the improvement of the photocurrents. The efficient light-scattering effect in multilayers of mixed particles most likely contributes to the performance improvement.

Experiment

Two commercially available nano-TiO_2 paste types were employed to prepare the proper paste samples for the LDM 3D-printer by diluting with ethanol 99.5% in order to be able to flow through the nozzle.

- P25 [av 30 nm size, 80% anatase (d = 21 nm) and 20% rutile (d = 50 nm)]
- ST-41 [av 160 nm size, 100% anatase]

The diluted paste was printed directly on a fluorine doped tin oxide (FTO) glass (4 mm thickness with sheet resistance 11 Ω/square) with an effective area of 5 by 5 mm2, representing as the photo-electrode of DSSC.

Printing parameters such as printing speed, pressure and nozzle size were defined by the guideline of earlier study to obtain the uniform thin film without crack [6,7]. Dilutes paste preparation was designated as x-TiO_2 where x is the weight ratio of ethanol:TiO_2. It was suggested that the 0.1-TiO_2 paste for 0.42 mm nozzle size be suitable for fabricating the TiO_2 thin films as the printer's parameters setting fell in the moderate values with larger

tolerance. Air pressure setting at 4 bar gave the crack-free and uniform TiO2 layer in the range of printing speeds from 25 to 35 mm/min. Four printed samples were done as followings :

S1: 1 layer using P25 type paste
S2: 1 layer using ST-41 type paste
S3: 2 layers using ST-41/P25 paste
S4: 2 layers using P25/ST-41 paste

After printing, the printed samples were kept in a closed chamber for a while in order to let the wet thin film relax and to reduce the surface irregularity and then heat treated on a hot plate at 150 °C for 5 min. Later, the samples were gradually sintered in an oven up to 500 °C for 4 hrs. The surface characteristics of TiO_2 thin films such as surface morphology, thickness and roughness were observed and measured by Scanning Electron Microscopy (SEM) and surface roughness tester (Profilometer). Sheet resistance property was also considered by using a Keithley SourceMeter model 2410 with a Four-Point Probe. We expect the improvement of TiO_2 thin film based on the assumption that the properties of TiO_2 films appear to strongly depend on the process conditions and starting materials used in the processes

Results and Discussion

Surface morphology, roughness and film thickness

It was reported by previous study that the thickness of TiO_2 thin films and relevant sheet resistance by 3D printing system were achieved at 6.25 µm and 6.10E+6 Ω/sq - 6.80E+6 Ω/sq respectively based on 20nm TiO_2 particle size (PST-18NR)[6].

Figure 1 shows the surface morphology of printed TiO_2 thin film of different TiO_2 paste samples (S1-S4).It was found that nano-particle TiO_2 could lead to the change in the microstructure and porosity of the thins film forming on top of electrode. Their surfaces show a tetragonal structure representing an anatase phase. It is due to the existing of larger grain size nanostructured of TiO_2 thin film which can be observed to increase roughness after the sintering process. The measured roughness (Ra) was 25 nm, 187 nm, 44 nm and 257 nm of printed samples S1-S4 respectively as given in Table 1. The measurement was done by Profilometer The larger particle size gave higher surface roughness. It was found that the mixture of small and large particle size of TiO_2 gave higher roughness values (S3, S4) than the thin film with single particle size. Note that the sample S4 shows the highest roughness as the TiO_2 ST-41 type was on the top surface. The profile measurement was done by the standard stylus with the angle 60˚ using the surface roughness tester Mitutoyo SV-3000 as shown in Figure 2.

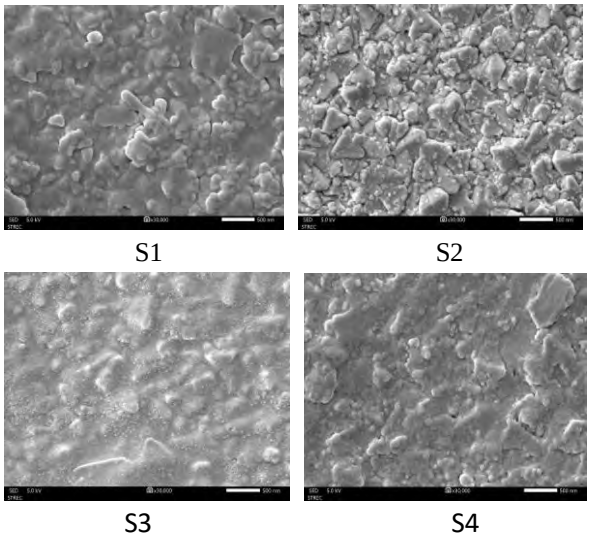

Figure 1 SEM surface images of TiO_2 thin film samples (x30,000)

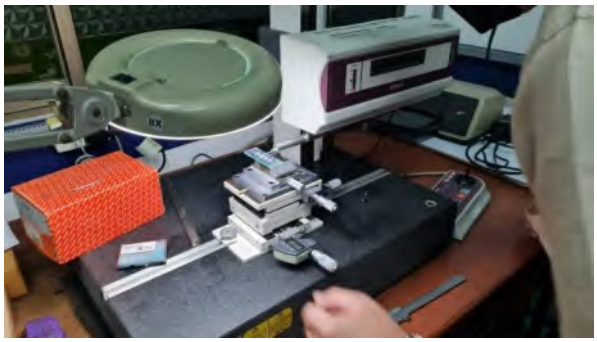

Figure 2 Profilometer – Mitutoyo SV3000

Table 1 Surface roughness (Ra) of printed TiO_2 thin films.

Sample no.	TiO_2 type	Surface roughness / Ra (nm)
S1	P25	25
S2	ST-41	187
S3	ST-41/P25	44
S4	P25/ST-41	257

To consider the thickness of printed thin films, SEM images in Figure 3 show the trend of the increase of their thickness by double layer printing, using the mixture of small and large particle size TiO_2 (P25 + ST-41). The values obtained are given in Table 2. The highest thickness, 16.67 µm, was achieved when printing the large particle size TiO_2 on the top surface (P25/ST-41). While single printing (1 layer) with small (P25) and large (ST-41) particle size gave the averaged thickness at 2.02 µm and 8.65 µm respectively. Note that the film thickness values could be varied by changing the printing parameters such

as printing pressure and nozzle size. However, there is a limitation to set these parameters as the crack on printed films could be occurred.

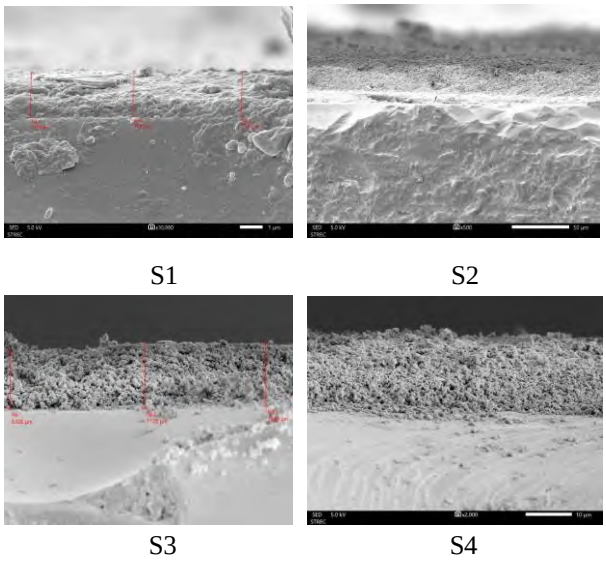

S1 S2

S3 S4

Figure 3 Cross section of SEM images of printed TiO2 thin films showing the film thickness.

Table 2 Averaged Thickness values of printed TiO2 thin film samples (S1-S4)

Sample	TiO_2 type	Thickness (μm)
S1	P25	2.02
S2	ST-41	8.15
S3	ST-41/P25	10.68
S4	P25/ST-41	16.67

Sheet resistance

Sheet resistance (also known as surface resistance or surface resistivity) is a common electrical property used to characterize thin films of conducting and semiconducting materials such as TiO_2. It represents for any thin film of material in which electrical charges are intended to travel along. The measurement is based on the lateral resistance through a thin square of material, i.e. the resistance between opposite sides of a square. The key advantage of sheet resistance over other resistance measurements is that it is independent of the size of the square; and it can be measured directly using a four-point probe. This consists of four electrical probes in a line, with equal spacing between each of the probes as shown in Figure 4. As the thin film thickness is very low compared to the probe spacing, an additional correction factor is not required.

The experiment used the Keithley 2410 as a Source Meter unit (SMU) instrument (1000V, 1A, 20W). It was designed specifically for test applications that demand tightly coupled sourcing and Measurement (Figure 5).

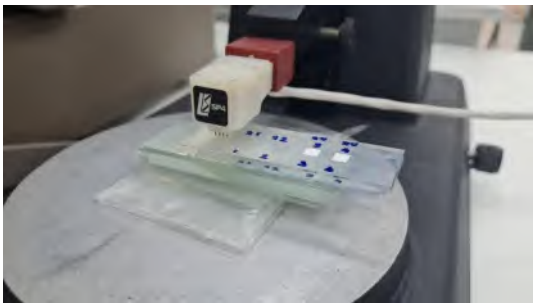

Figure 4 A four-point probe to measure sheet resistance

Figure 5 Source meter unit instrument (Keithley 2410) with a Linear 4-Point Probe

Sheet resistance (Rs) is defined as the resistivity (ρ) of a printed TiO_2 divided by its thickness (t):

$$Rs = \rho / t$$

Normally, the dye sensitized solar cells (DSSC) requires its thickness of printed TiO_2 on conducting electrodes in the nanometer to micrometer range. The electrodes will transport electrical charge laterally and need low sheet resistances to reduce losses before they can be extracted. The resistivity and conductivity can be calculated if the sheet resistance and its thickness are known.

Crystallinity and nanostructure surface area were obtained after the sintering and it gives much surface for electron passes through from one grain to another grain within the TiO_2 thin film. However, its electrical resistivity possibly depends on several factors such as deposition process, thickness, temperature and purity. The sheet resistance of the film calculated from the four-probe method was found to be in a range of 1.12E+4 Ω/sq – 3.77E+6 Ω/sq as given in Table 3. The low value of sheet resistance fell in the sample S3 and S4 which represented the mixture of the particle size of TiO_2. Not only the mixed nanostructure surface, but also the achievable high thickness could reduce the sheet resistance value. Therefore, S4 sample gave the lowest sheet resistance.

Table 3 Sheet resistance of printed TiO2 samples (S1 -S4)

Sample no.	TiO_2 type	Particle size (nm)	Printed layers	Sheet resistance (Ω/sq)
S1	P25	av. 30	1	3.77E+6
S2	ST-41	av. 160	1	6.20E+5
S3	ST-41/P25	160/30	2	4.21E+4
S4	P25/ST-41	30/160	2	1.12E+4

Conclusions

It appears that the double layers TiO_2 electrode comprising of small and large particles lead to the improvement of the electrical property. The light-scattering effect of the large particle most likely contributes to the performance improvement. The introduction of new printing technology such as LDM 3D printing system could establish a cost-effective production process as well as the efficient electrodes. It was found that P25/ST-41 pattern (Sample 4) gave the best results by the achievement of sheet resistance at 1.12E+4, thickness at 16.67 µm and roughness (Ra) at 257 nm. However, the obtained data still depends on the viscosity of the TiO_2 paste and the adjustment of printing parameters of the LDM 3D printer.

Acknowledgement

Authors would like to thank the Department of Imaging and Printing Technology, Faculty of Science, Chulalongkorn University for supporting the research budget. We also appreciate the Foundation of Printing Exhibition Fund of Thailand for her support to send one of us to present this work in the ASPT 2022 Symposium in Vietnam.

References

[1] I. Senain, N. Nayan and H. Saim, Structural and Electrical Properties of TiO_2 Thin Film Derived from Sol-gel Method using Titanium (IV) Butoxide, J of Integrated Engineering, July: 29-35 (2011).

[2] A.A. Daniyan, L.E. Umoru, A.Y. Fasasi, J.O. Borode, K.M. Oluwasegun and S.O. Olugbenga, J of Minerals and Materials Characterization and Engineering, 2:15-20 (2014)

[3] T.K. Gupta, L.J. Cirignano, K.S. Shah, L.P. Moy, D.J. Kelly, M.R. Squillante, G. Entine and G.P.Smestad, Screen-printed dye-sensitized large area nanocrystalline solar cell, Proc. Material ResearchSociety Symposium, 581: 653–658 (2000).

[4] W.Y. Padrón-Hernándeza, M.C. Ceballos-Chuca, D. Pourjafaria, G. Oskama, J.C. Tinocob, A.G. Martínez-Lópezb and G.Rodríguez-Gattornoa, Stable inks for inkjet printing of TiO_2 thin films, Proc. Materials Science in Semiconductor, 81: 75-81 (2018)

[5] S. Amirtharajan, P. Jeyaprakash, J. Natarajan and P. Natarajan, Electrical investigation of TiO_2 thin films coated on glass and silicon substrates—effect of UV and visible light illumination, J. of Appl Nanosci, 6:591–598 (2018).

[6] A. Hansuebsai, K. Chareonsopa and K. Maseki, O ptimization of LDM 3D printing parameters for TiO_2 thin film fabrication, Int. J. Thin. Fil. Sci. Tec. 9, No. 3:163-169 (2020).

[7] K. Charoensopa, A. Hansuebsai and K. Manseki, 3D Printed Titanium Dioxide Thin Films for Optoelectronic . Applications, J. of Key Engineering Materials, 843:79-83 (2020).

Optimization of Printing Conditions to Achieve Effective Ink Transfer in Flexographic Printing.

Phornanan Keawkul*, Pakamas Pachonklaew and Boonchai Waleetorncheepsawat
School of Science and Technology, Sukhothai Thammathirat Open University
9/9 Moo 9, Chaengwattana road, Bangpood, Pakkret, Nonthaburi, Thailand 11100

Abstract

This research aimed to study the factors affecting the ink transfer in flexographic printing, including ink temperature, and anilox roll. The research was experimental research by studying the ink transfer from anilox roller to plate and from plate to print substrate. The independent variables in the experiment were (1) the ink temperature with 5 levels: 25°C, 30°C, 35°C, 40°C, 45 °C, and (2) the anilox roller that used to transfer the ink to the plate having 3 resolutions: 1,000 lpi (volume of 1.7 cm^3m^2, 700 lpi, (volume of 3.5 cm^3m^2), 500 lpi (volume of 5 cm^3m^2). The print image were 7 screen tint of 100%, 90%, 70%, 50%, 30%, 10% and 5%. The dependent variables were the amount of printing ink and the tone value transferred from the anilox roller to the plate and from the plate to the printing substrates. From the experimental results, it was found that the ink temperatures of 25 °C and 30 °C was suitable for flexographic printing whereas the printing speed and anilox roll resolution did not affect the ink transfer from the anilox roller to plate and from plate to printing substrates.

Keywords: Ink Transfer, Printing Conditions, Flexographic Printing

Introduction

Flexography is a printing process derived from aniline printing as relief printing using flexible printing plate as the image carrier and low viscosity inks which make it suitable for use on almost any substrate. Over the past ten years, the role of flexographic printing technology has continuously concerned over quality printing for packaging industries. One of the reasons for the advantages of this printing system is the development of water-based inks to support the food and beverage packaging industry, being environmentally friendly printing. The method of applying ink to the flexographic plate is through engraved roller with a uniform etched cells (size, shape and depth) called 'anilox roll'. The anilox resolution determines the volume of ink transferred to the plate and the plate transfers the ink film to the substrate by impression. [1] The cell count per inch or anilox resolution (lpi) should be 4-5 times greater than dot resolution on the plate to print a dot of as small as 4 % [2]. By examining the flexographic printing process, lots of variable parameters affect the ink transfer to print substrates to achieve good print quality. These includes ink temperature and anilox resolution.
This research aimed to study the printing factors affecting the ink transfer from the ink supply unit to the print substrates including ink temperature, anilox roll resolution to find out optimal printing conditions and enable to reduce printing problems and wastes.

Experimental Method

The experimental study was conducted by 1) studying problems on ink transfer and printed color at solid area and percent dot area 2) finding out possible factors on print image quality that actual encountered by flexographic printing houses 3) examining ink transfer at the laboratories by Flexi Proof Printer and printing samples by Rhyguan rotary flexography printing machine with varying anilox roller resolutions and ink temperature 4) evaluating the printed samples on ink transfer, print qualities affected by varied printing factors; the research framework shown in figure 1.

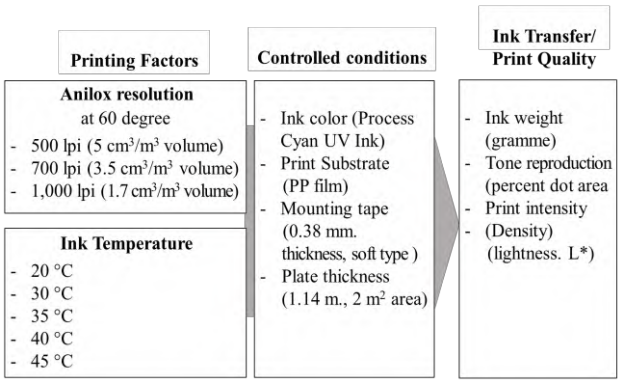

Figure 1. Research Framework

Ink Transfer Study
Three anilox rolls with the resolution of 500 lpi (5 cm^3/m^2 volume), 700 lpi (3.5 cm^3/m^2 volume) and 1,000 lpi (3.5 cm^3/m^2 volume) and flexographic plate with 1.14 mm. thickness and 2 m^2 print area were weighed by weighing scale before and after applying ink from ink supply unit to anilox rolls and from anilox rolls to printing plates. Those practices was done five times on Flexi Proof Printer under controlling ink temperature at five levels of 20°C, 30°C, 35°C, 40°C, 45°C.
Flexographic printing of the samples was carried out by

Rhyguan rotary printing machine on bi-axially oriented, glossy white polypropylene film of 50 µm. thickness (TAPPI T411) using Cyan UV ink with varied printing conditions of anilox resolutions and ink temperatures. Then the printing plates and the printed substrates (PP white film) were weighed before and after printing and calculated percent ink transfer in each printing conditions.

Print Quality Study

The Printed Samples of 100%, 90%, 70%, 50%, 30%, 10% and 5% dot area (figure 2) under studied printing conditions of anilox resolutions and ink temperatures were examined. The percent dot area, print density and Light value (CIELAB) were measured by X-rite e-Xact Portable Spectrophotometer.

Figure 2. Printed samples of dot area on PP white film

Results

Ink Transfer from Ink Supply to Anilox Roll

Experiment for ink transfer from ink supply to anilox roll was carried out with Flexi Proof Printer in the laboratory. The ink transfer from each resolution of anilox rolls showed different results. Different anilox resolution gave different ink transfer from ink supply onto anilox roll, as shown in Figure 3. The lower anilox resolution (500 lpi) gave the higher ink transfer while the higher anilox resolution gave the lower ink transfer. Ink temperature also affected the ink transfer, especially when the ink temperature was higher than 30°C. The ink transfer was gradually increase with the increase of ink temperature, which applied to all anilox resolutions.

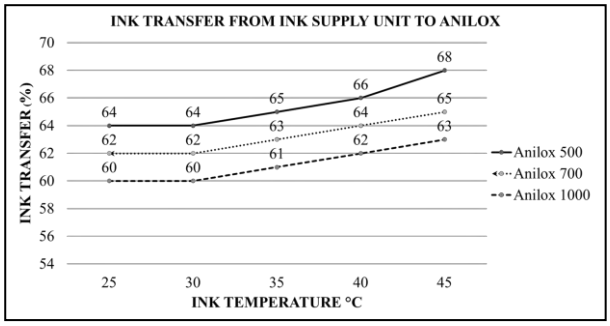

Figure 3. Ink transfer from ink supply unit to anilox roll

The ink viscosity measurement at each ink temperatures was examined by the average ink flow time (sec.) from Zahn cup no. 4 as shown in Table 1. As ink temperature got higher, the shorter time ink flow out of the Zahn cup. From standard conversion table, the measured flow times of ink were converted into ink viscosity. The data showed ink viscosity became lower when ink temperature got higher. However, the flow time of the ink in this study were between 18 – 35 second using Zahn cup no.4 which be suggested for flexographic printing. [3]

Table 1 Ink temperature affected ink viscosity

Ink temperature (°C)	Average time (sec.) Zahn cup no.4	Viscosity* (cP.)
25	35	444
30	34	429
35	30	370
40	26	311
45	23	266

The experiment for sample printing was carried out on Rhyguan rotary flexography printing machine in the printing factory. Samples of dot area on PP white film as shown in Fig 2. was cut from the printing roll and weight for the ink transfer. The ink transfer from anilox to plate and from plate to print substrate was normal transfer with the temperature of 25-30°C either using 1000 lpi, 700 lpi, and 500 lpi anilox roll. However, the ink transfer was increased when the ink temperature increase (more than 30°C), especially at the smaller dot area image. (5% - 50%) as shown in Fig 4 - 6.

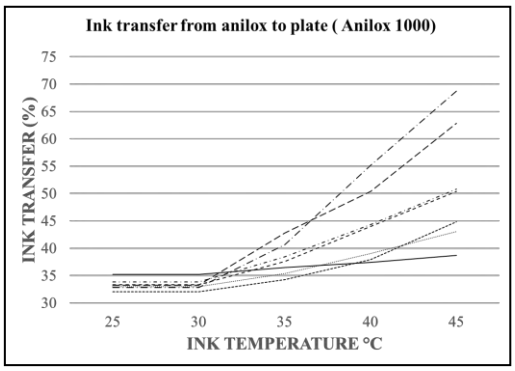

(a) from anilox roll to plate

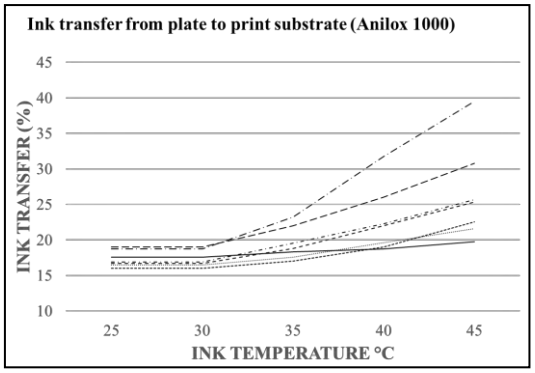

(b) from plate to print substrates

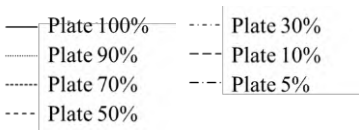

Figure 4. Ink transfer from anilox roll 1000 lpi to print substrates

The higher anilox resolution (1000 lpi) cause more ink transfer in the small dot area (ie. 5%). However the medium anilox resolution (700 lpi) and low anilox resolution (500 lpi) cause lower ink transfer increment in the small dot area. The dot quality of small dot from the printing can be less affected with the increase of ink temperature, as shown in Fig 5. and Fig 6.

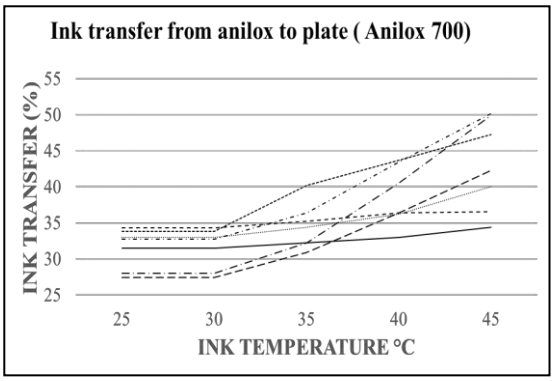

(a) from anilox roll to plate

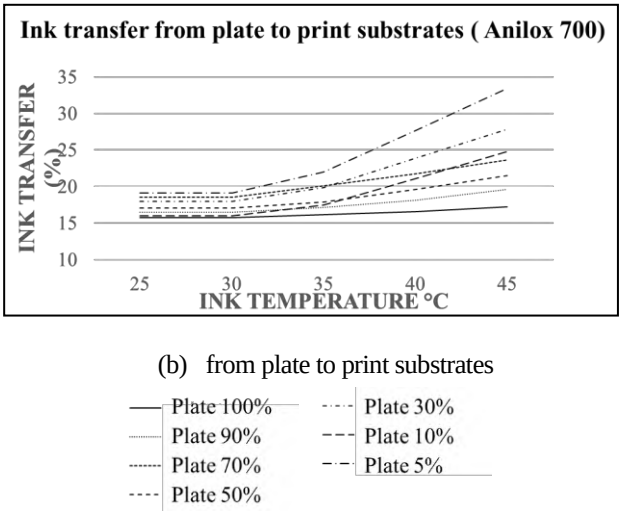

(b) from plate to print substrates

Figure 5. Ink transfer from anilox roll 700 lpi to print substrates

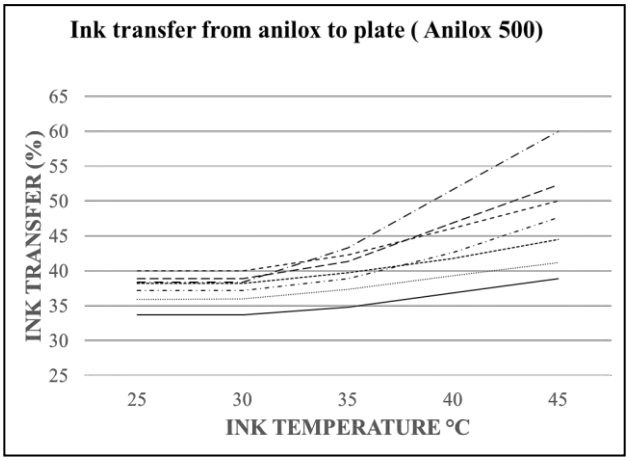

(a) from anilox roll to plate

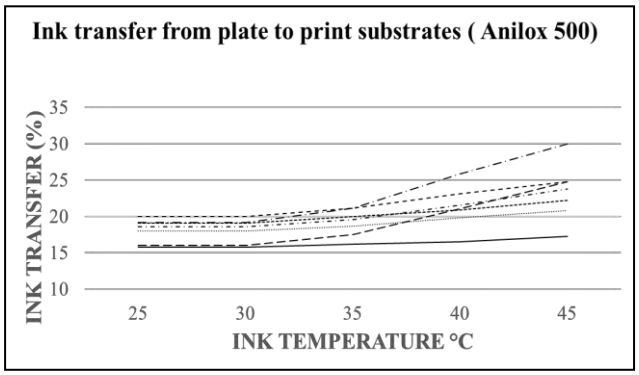

(b) from plate to print substrates

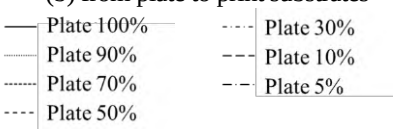

Figure 6. Ink transfer from anilox roll 500 lpi to print substrates

Print Quality of Printed Samples

The print samples of dot area from 5% to 90% representing highlight, midtone and shadow of print image were measured the percent dot area to find out the printing conditions providing less dot gain and good print quality as shown in Fig 7.

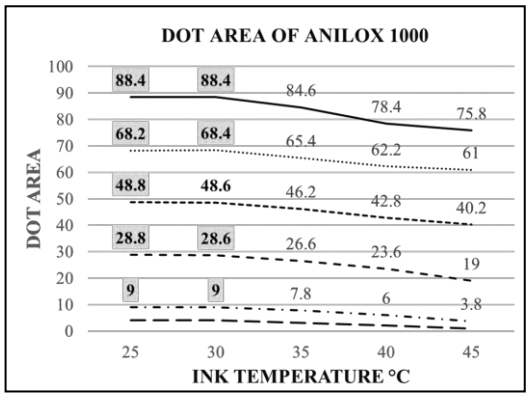

(a) anilox 1000 lpi

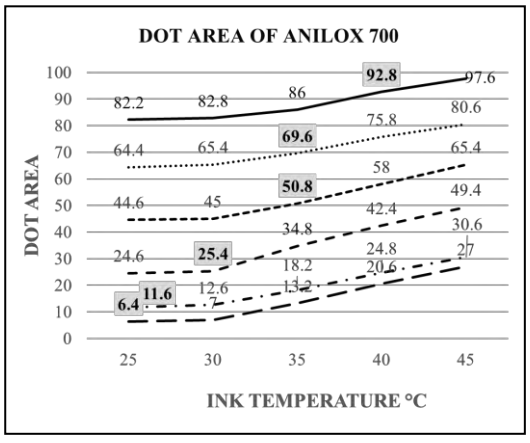

(b) anilox 700 lpi

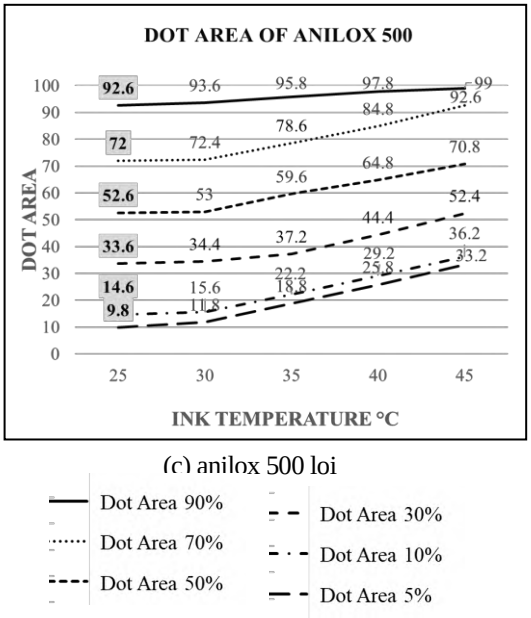

(c) anilox 500 loi

Figure 7. Dot area of printed samples

It is found that ink temperature should be controlled between 25 °C - 30°C either using anilox roll at high resolution (1000 lpi), medium resolion (700 lpi) and low resolution (500 lpi) in order to assure print quality during printing process.

The increased ink temperature more than 30°C also affected print density being higher and lower lightness of print color at solid area as shown in Fig 8.

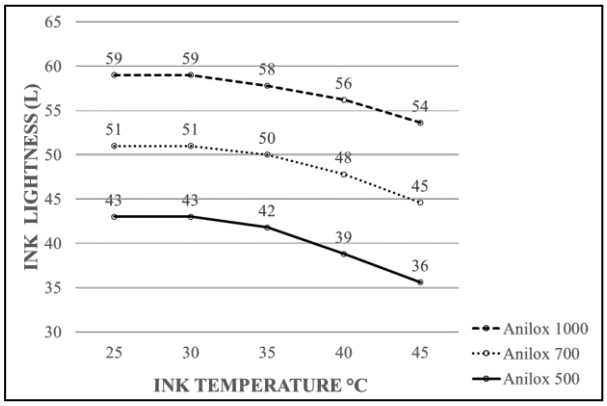

(a) Ink Lightness

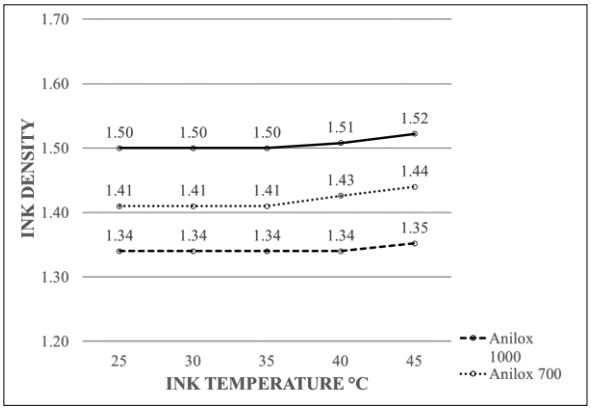

(b) Ink Density

Figure 8. Print Intensity of Print samples

Discussion and Conclusion

The print quality of flexographic printing was largely depended on the ink transfer properties. The ink temperature affected ink viscosity and ink flow onto anilox rollers. From this research, the temperature of 25-30°C was suitable for normal flexographic printing. The resolution of anilox roll also cause the variation of ink transfer. Other than that, the ink temperature variation also cause the ink transfer of different dot size images to reproduce differently, in this case, higher temperature cause higher ink transfer in the small dot area. However, as the suggested ink temperature range of 25-30°C, the printing speed and anilox roll resolution did not affect the ink transfer from the anilox roller to plate and from plate to printing substrates.

Acknowledgement

This research study has been carried out as part of my Master Degree of Industrial Technology at the School of Science and Technology, Sukhothai Thammathirat Open University. I would like to thank reseach advisors for support my research project and also appreciate the Foundation of Printing Exhibition Fund of Thailand for granting the budget for me to present this research paper in ASPT 2022 Symposium at Ho Chi Minh City University of Technology and Education, Vietnam.

References

1. Mumby, R. Printing for Packaging, Packaging Technology, 2012, p. 173.
2. Johanna Johnson, Aspects of Flexographic Print Quality and Relationship to some Printing Parameters, Dissertation Karlstad University Studies, 2008, p. 8.
3. Zuzanna Żołek-Tryznowska, Rheology of Printing Inks, Printing on Polymers, Faculty of Production Engineering, Mechanics and Printing Institute, Warsaw University of Technology,2016, p. 87-99

Digital transformation on business operation and internal administration of printing houses focusing on the problem of adjustable work processes of employees

Koravit Sriwongsa, Banchar Arnonkijpanich and Aran Hansuebsai

Department of Imaging and Printing Technology, Faculty of Science, Chulalongkorn University, Bangkok, Thailand 10330.

Abstract

Nowadays, the print media business is in a recession due to an increased quantity of marketing competitors, an increase of specialized entrepreneurs, and a change in consumer behavior from paper-based publications to electronic format. These factors directly affect the business operation of entrepreneurs. We studied a working system of Chulalongkorn University Press relying on conventional and digital printing technologies. To minimize production costs in the printing house, the parameters derived from the constrained optimization problem need to be computed explicitly according to existing employees. The set of parameters corresponds to the number of jobs assigned to conventional and digital systems were observed, including the work efficiency in both systems. An average of the work efficiency levels was needed to define a constraint in an optimization modeling approach. In the experiments, the simulated annealing algorithm based on evolutionary computation was applied for identifying the parameters of the cost balance model.

Introduction

For years there has been much talk about the power and impact of digital transformation, the publishing industry is included. Book is not dead! But it does not mean that the publishing industry as we know it today will survive. If a printer invests in a new press, this automatically means that he must increase the job volume in order to operate the press economically. It is not only this case. Labor trends, along with the supply chain issue, will also affect the business greatly. Shortages on labor and raw materials will level out. Unfortunately, we think it is going to continue for several years. Publishing houses should rethink their inventory management. With the uncertainty in the markets, publishers are trying to cut back their initial printing quantities. They are going to reprint more frequently in smaller quantities, so instead of doing long run printing, they might do several short runs through the course of the year, moving to a stock replenishment mode.

Another issue to encounter the publishers today is that conventional process like offset printing may be not the proper process any more in book printing as the customers requires short run or on-demand printing, quick delivery and environmentally friendly process. Of course, such process still needs long lead time and many labors to work. This is not the competitive price in the printing market.

Digital production and automation is becoming a good choice. It is because of the stresses of finding labor and high cost of working process, automation is imperative. For those that can't invest in automation, it's going to be more and more difficult. Note that digital is not new to the publishing market, but inkjet advancements are shaking things up, allowing publishers to capitalize on evolving demand, boost productivity, and add value with additional services.

As Chulalongkorn University Press (CUpress) recently invested the web inkjet press in-line with sheet cutting and stacking machines for book printing service while the old offset machines are used for medium and long run printing and cover printing (Figure 1-2). It showed that the inkjet press system used the operators only 2 workers while the conventional system was still run by 12 workers. (pre-press + press + post-press). The question is that how to manage these workers in the conventional system that the CU press should not let them vacant from work. We therefore studied the digital transformation on business operation and internal administration of printing houses focusing on the problem of adjustable work processes of employees in the case of Chulalongkorn University Press. A working system relying on conventional and digital printing technologies were observed. A model relating to the existing employees was proposed to minimize production costs in the printing house. A set of parameters corresponds to the number of tasks was assigned to both systems to estimate the work efficiency level of each position. An average of the work efficiency levels was needed to define a constraint in an optimization modeling approach. In the experiment, the simulated annealing algorithm based on evolutionary computation was applied for identifying the parameters of the cost balance model.


Pre-press (imposition / platemaking) Press (printing)


Cutting machine Folding machine


Gathering machine Glue binding machine

Figure 1 Workers involved in each step in conventional system (Offset printing)


Figure 2 Workers involved in digital web inkjet press + inline sheet cutting and stacking

Experiment

I. We collected the data of working environment from CU press as follows:

- number of workers involved in production process (conventional and digital system)
- salary of workers
- machine payment (ex: inkjet press total click charge minimum 650,000 Baht/month)
- fixed cost and variable cost for each system

II. Mathematical models were proposed to simulate the costing for each system and combined systems between conventional and digital systems. In real situation, the planning division of CU press must arrange the job orders day by day and to define which printing system should be used for each job order.

Heuristic approach was designated as it is a computational procedure that determines an optimal solution by iteratively trying to improve a candidate solution with regard to a given measure of quality. The main advantage of adopting a heuristic approach is that it offers a quick solution, which is easy to understand and implement [1-2]. Heuristic algorithms are practical, serving as fast and feasible short-term solutions to planning and scheduling problems. We proposed the Simulated Annealing (SA) technique to find the most reliable values. This technique is a popular algorithm used to optimize a multi-parameter model that can be implemented relatively quick -

Step 1: Initialize – Start with a random initial placement. Initialize a very high "temperature".

Step 2: Move – Perturb the placement through a defined move.

Step 3: Calculate score – calculate the change in the score due to the move made

To determine the cost when both systems were simultaneously used, we defined the parameters in the model based on staff working in the two processes as they have obligations with the CU press. The proposed costing models could be summarized in linear equation as followings [3]:

$$C^s_o = w_a a_s a_o + w_b b_s b_o + w_c c_{fp} c_o + w_d d_s d_o + w_e e_s e_o + w_f f_s f_o + w_g g_s g_o + w_h h_s h_o \quad \ldots\ldots\ldots\ldots\ldots\ldots (1)$$

$$C^s_n = w_a a_s a_n + w_b b_s b_n + w_c c_s c_n + w_d d_s d_n + w_e e_s e_n + w_f f_s f_n + w_g g_s g_n + w_h h_s h_n \quad \ldots\ldots\ldots\ldots\ldots\ldots (2)$$

where C^s_o : cost of staff in conventional system
C^s_n : cost of staff in digital system
a_o / a_n : number of editorial staff in conventional and digital systems
b_o / b_n : number of designer in conventional and digital systems
c_o / c_n : number of prepress staff in conventional and digital systems
d_o / d_n : number of printer in conventional and digital systems
e_o / e_n : number of folding machine staff in conventional system
f_o / f_n : number of cutting machine staff in conventional system
g_o / g_n : number of gathering machine staff in conventional system
h_o / h_n : number of binding machine staff in conventional and digital systems
$a_s/b_s/c_s/d_s/e_s/g_s/h_s$: salary for each staff
$w_a/w_b/w_c/w_d/w_e/w_f/w_g/w_h$: workload of each staff

Note that the w values fell in the range of $0 \le w_a, w_b, \ldots, w_h \le 1$. For example $w_a = 0.95$, this means that the editorial staff has a workload in this job 95% compared to the maximum 100%. w values were co-variable in both equations as these staff can work in both systems. Accordingly, the cost based on working staff would be:

$$C^s = \alpha C^s_o + \beta C^s_n \quad \ldots\ldots\ldots\ldots\ldots\ldots (3)$$

where α and β were the ratio of job allocation between two systems. Therefore

$$\alpha + \beta = 1.0 \quad \ldots\ldots\ldots\ldots\ldots\ldots (4)$$

In case of variable cost, we could explain it in a linear equation as given in Equation 5.

$$C^p = \alpha C^p_o + \beta C^p_n \quad \ldots\ldots\ldots\ldots\ldots\ldots (5)$$

The total cost would be:

$$C^T = C^s + C^p \quad \text{.....(6)}$$

As C^T was a function of α, β, w_a, w_b, ... , w_h, we thus proposed $P = [\alpha, \beta, w_a, w_b, \dots, w_h]$ as a vector of parameters. This research was to find the optimal solution of these parameters to achieve the lowest total cost (C^T). MATLAB was used as a tool to calculate. In addition, the cost estimation should be determined under the condition that working efficiency of CUpress (ϖ) should not less than that of defined criteria (γ).

$$\varpi > \gamma \quad \text{.....(7)}$$

Where $\varpi = (w_a + w_b + \cdots + w_h)/8$

Finally, constrained optimization was applied as follows:

$$\min_P T(P)$$
$$\text{s.t. } 0 < \propto, \beta < 1$$
$$\propto + \beta = 1$$

Results and discussion

The number of staff working in the conventional and web inkjet printing systems, including their salary are given in Table 1. The parameters obtained from the SA analysis under the present situation were as follows:

- job allocation in conventional system ($\propto$) = 0.599984 (60%)
- job allocation in digital system (β) = 0.400016 (40%)
- average working efficiency (ϖ) 0.95015979
- Total cost (C^T) 2,072,845 THB/month (C^s = 452,845 THB, C^p = 1,620,000 THB)
- C^s calculated from full workload of working staff
- C^p_o 975,000 THB / C^p_n 650,000 THB

Note that if we knew the sale volume of all jobs from the sale department, we could estimate the profit based on the obtained total cost.

Table 1 Number of staff working in the conventional and digital printing systems.

Staff (position)	Conventional printing system	Digital printing system	Salary (THB)
editorial	x	x	28,500/28,500
Designer1	x	x	30,500/27,650
Designer 2	x		26,000
Press operator 1	x	x	36,650/16,500
Press operator 2	x	x	20,000/21,500
Press operator 3	x		21,650
Pre-press 1	x		25,745
Pre-press 2	x		24,650
Cutting machine operator	x		19,500
Folding machine operator 1	x		19,500
Folding machine operator 2	x		21,000
Gathering machine operator 1	x		24,000
Gathering machine operator 2	x		18,500
Binding machine operator 1	x	x	24,000
Binding machine operator 2	x	x	18,500

Digital transformation and costing in the next five years

It should be noted that 1-2 staff of the conventional production will be retired year by year. It is interesting to know how digital transformation can cope with this situation in the next five years, particularly costing. Our model can predict this phenomenon. The job allocation will be moved more to the web inkjet press to fulfill the minimum click charge per month. In addition, the inkjet press gives many advantages such as a few operators usage, reduced cost of paper roll, less waste and quick process.

Our survey showed the reduction of variable cost (C^p_n) of the digital system 15% , compared to the conventional system (C^p_o). While the cost of staff depended on the ratio of job allocation and work load of each staff. To find the optimal solution of parameters in the next five years from the model by SA, evolutional computing by random technique was applied step by step in order to observe the improvement of these parameters and total cost (C^T) [4-5]. Final result is given in Table 2. Job allocation for digital system will be up to 60%. This will help increasing the efficiency of the web inkjet press to reach the minimum click charge per month. Workload of staff in conventional system will decrease 50% as the CUpress will recruit the workers from other departments instead. The total cost (C^T) will reduce down to 20.78% per month. This help increasing the profit of the CUpress and the potential to get more jobs by price competition.

Table 2 Prediction of optimal solution of book production at the CUpress using the combination of conventional and digital systems.

iteration = 89,104,677
total cost (C^T) = 1,642,172.50 THB/Month (C^s: 273,497.50 THB, C^p : 1,430,000 THB)
α = 0.4000 (40%)

$\beta = 0.5999$ (60%)
working efficiency (ϖ) = 95.030141 %

Conclusions

It was shown that digital transformation with the web inkjet press allowed publishing houses to repurpose their business by combining with conventional production, depending on the adjustable work processes of employees. Its benefit was to be able to reduce the total cost which is important to get more jobs. To approve the assumption, the simulated annealing algorithm based on evolutionary computation was applied for identifying the parameters of the cost balance model. Optimal solution showed that the total cost could decrease to the level of CUpress be able to compete in the book printing market. Interestingly, the success of digital transformation will be seen concretely when the CUpress stops using conventional production in the future after the retirement

Acknowledgement

Authors would like to thank the Department of Imaging and Printing Technology, Faculty of Science, Chulalongkorn University for supporting the research budget. We also appreciate the Foundation of Printing Exhibition Fund of Thailand for her support to send one of us to present this work in the ASPT 2022 Symposium in Vietnam.

References

[1] E. Birgin, J. Ferreirab, and D. Ronconib, "List scheduling and beam search methods for the flexible job shop scheduling problem with sequencing flexibility," European Journal of Operational Research, 247:421–440 (2015)

[2] K. Gao, P. Suganthan, Q. Pan, T. Chua, T. Cai, and C. Chong, "Pareto-based grouping discrete harmony search algorithm for multi-objective flexible job shop scheduling," Information Sciences, 289:76–90 (2014)

[3] Q. Liu, Q. Pan, L. Gao, and X. Li, "Multi-objective flexible job shop scheduling problem considering machine switching off-on operation," Procedia Manufacturing, 39:1167–1176 (2019)

[4] E. Ahmadi, M. Zandieh, M. Farrokh, and S. Emami, "A multi objective optimization approach for flexible job shop scheduling problem under random machine breakdown by evolutionary algorithms," Computers & Operations Research, 73:56–66 (2016)

[5] N. Xie and N. Chen, "Flexible job shop scheduling problem with interval grey processing time," Applied Soft Computing, 70:513–524 (2018)

The 12th Asian Symposium on Printing Technology (ASPT 2022)

APPLICATION OF ZNO-POLYCAPROLACTONE (PCL) NANO-COMPOSITE MATERIALS ON COATED OFFSET PAPER PRINTS

Vo Thi Ngoc Chau, Mai Thi Thanh Diem, Nguyen Thi Thuy Trang, Nguyen Thanh Phuong*

FACULTY OF GRAPHIC ARTS AND MEDIA
HO CHI MINH CITY UNIVERSITY OF TECHNOLOGY AND EDUCATION

INTRODUCTION

For the purpose of researching how to fabricate ZnO nanopowder applied as a coating material on printing paper at the graphic arts and media faculty, the team conducted experiments to fabricate ZnO nanopowder dispersed into the coating solution, then coated onto the printed sheet. Survey and analyze the results before and after drying to compare the color fastness, gloss, flatness of the printed surface, tensile strength, and related color parameters.

GOAL

Fabricated ZnO nanoparticles and dispersed them into the coating solution.

Investigation of density, color, and surface properties on coated and uncoated paper.

Determination of the influence of nanoparticles on print quality and changes in print color.

EXPERIMENTAL PROCESS

FABRICATION OF ZNO NANOPARTICLES

Weigh $ZnCl_2$ and NaOH

Put ethanol in 2 bottles $ZnCl_2$ and NaOH

Stirring dissolves ethanol with $ZnCl_2$ và NaOH

Dry the dissolved solution

Allow the dried solution to settle for 48 hours

Dry until a white powder is obtained

ZnO nanopowder

ZNO NANOPARTICLE DISPERSION AND COATING PERFORMANCE

Weigh Ethyl acetate and PCL

Stirring dissolves Ethyl acetate and PCL at a temperature of 60°C

Put ZnO into the solution Ethyl acetate+PCL and ultrasound

Coating solution

Pull the coating solution over the printed sheet

The printed sheet has been coated

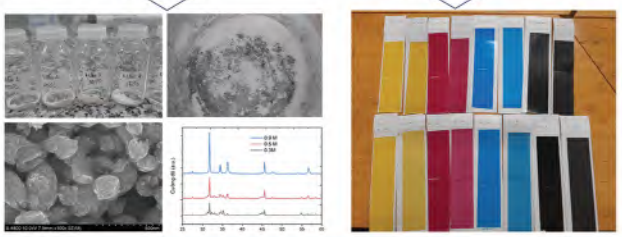

EXPERIMENTAL RESULTS

FLATNESS OF THE PRINTED SURFACE

TENSILE STRENGTH

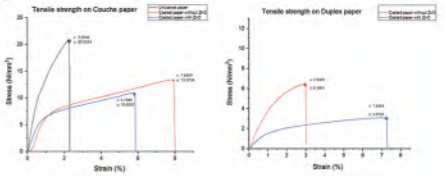

DENSITY

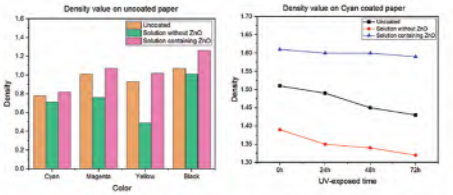

GLOSS

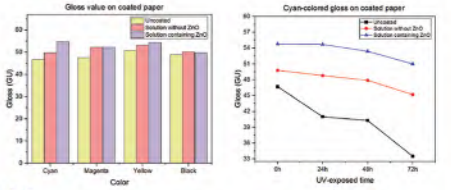

COLOR DIFFERENCE

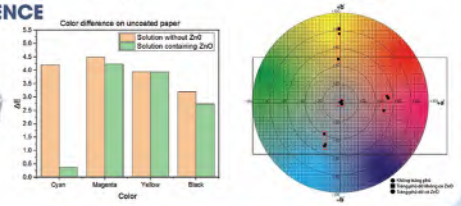

CONCLUSION

- Successfully fabricated ZnO powder dispersed into a coating solution
- The presence of ZnO increases the gloss value of the printed samples without much influence on the density value of the printed samples.
- Investigating the physical and mechanical properties of the coating layer showed that when ZnO nano was added to the coating solution, the tensile strength of the coated printed sheets helped to enhance the physical and mechanical properties of the printed sheets.
- The presence of ZnO helps to reduce the gloss loss and the increase in color difference under UV light.

REFERENCE LIST

VIETNAMESE

(1) Tran Thanh Ha (2013), "Giao trinh Vat Lieu In", VietNam National university Ho Chi Minh city, Ho Chi Minh city, Viet Nam.

(2) La Phan Phuong Ha (2013), "Che tao va nghien cuu tinh chat vat lieu ZnO cau truc nano", VietNam National university Ho Chi Minh city, Ho Chi Minh city, Viet Nam.

ENGLISH

(3) Tomislav Hudika, Tomislav Cigula, (2020), PLC - TiO2 nanocomposite to improve ageing of offset prints, University of Zagreb, Faculty of Graphic Arts, Zagreb, Croatia

(4) Tomislav Cigula, Tomislav Hudika, Mihael Katana, Marina Golik Krizmanić, Tamara Tomašegović (2020), The influence of PCL - ZnO coating composition on coated offset cardboard prints, University of Zagreb, Faculty of Graphic Arts, Zagreb, Croatia.

The 12th Asian Symposium on Printing Technology (ASPT 2022)

Study and fabrication of ZnO/PVA nano-composite film for food packing application

Trieu Thi Thu Huong, Nguyen Thi Nhu Quynh, Ngo Yen Linh, Nguyen Thanh Phuong*

Faculty of Graphic Arts & Media

Ho Chi Minh City University of Technology and Education

INTRODUCTION

Food is an essential part of our daily lives. To protect food from bacteria and oxidation, it is essential to apply the right packaging techniques. One of the films used in food packaging is ZnO - polyvinyl alcohol nanocomposite. Perform XRD, FTIR, SEM measurements and some mechanical properties of materials (color measurement, thickness, turbidity, tensile strength, ...) to select the most optimal material for application in food packaging.

TARGET

- Successfully fabricated ZnO nanoparticles by chemical method.
- Successfully fabricated ZnO/PVA nano composite films.
- Application of the ZnO/PVA film in food packing.

EXPERIMENT

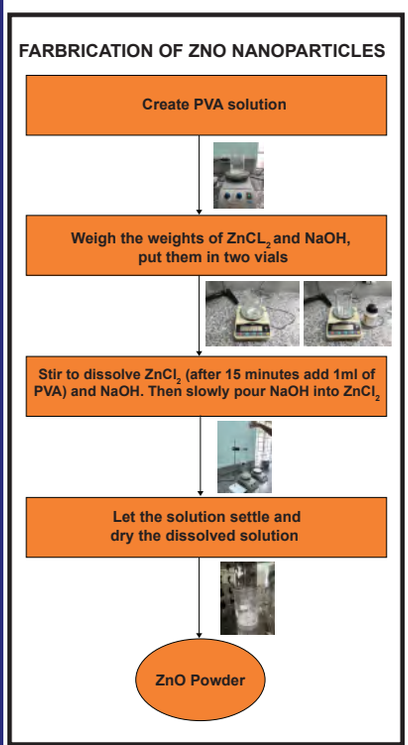

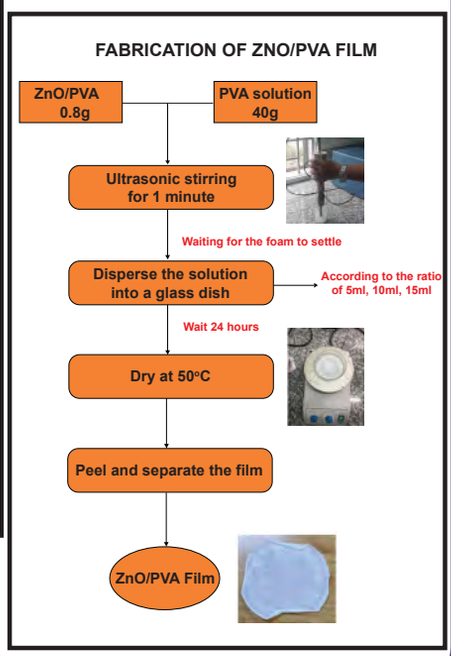

RESULTS

Successfully fabricated nanopowder and ZnO/PVA film

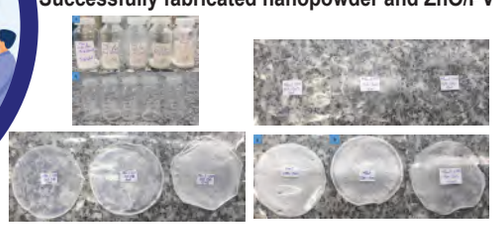

XRD FTIR SEM

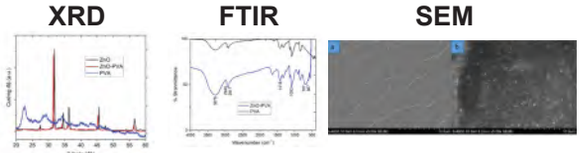

THICKNESS TENSILE STRENGTH

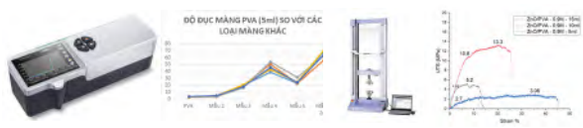

Application in food packaging: TOMATOES

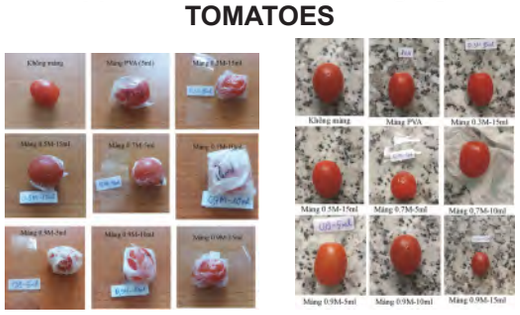

CONCLUSION

1. Successfully fabricating ZnO/PVA films.
2. The best tensile strength of the 5 ZnO/PVA samples.
3. Use 5ml ZnO/PVA sample film to wrap the fruit tomatoes for the best results.

REFERENCES

[1] Ayesha Naveed Ul Haq (2017), "Synthesis Approaches of Zinc Oxide Nanoparticles: The Dilemma of Ecotoxicity, Review articles".

[2] Marina Bandeła (2020), "Green synthesis of zinc oxide nanoparticle: A review of synthesis methodology and mechanism of formation"

[3] Santosh Kumar (2019), "Bionanocomposite films of agar incorporated with ZnO nanoparticles as an active packaging material for shelf life extension of green grape"

The 12th Asian Symposium on Pringting Technology (ASPT 2022)

"EFFECT OF PAPER INK INTERACTION ON THE INK TRANSFER PROCESS IN OFFSET PRINTING"

Lam Thi Huynh Nhu, Tran Thi Bang Nhu, Le Thi Thu Huyen, Nguyen Thanh Phuong*
Faculty Of Graphic Arts & Media
Ho Chi Minh City University Of Technology And Education

1 INTRODUCTION

Analysis of the influence of the surface properties of some papers on the ink transfer process.

Determine ink transfer, optical density, and color difference between prints to assess ink-paper interaction.

Determine the optimal ink transfer, ink layer thickness and color parameters for printing for each type of paper.

2 EXPERIMENTAL METHOD

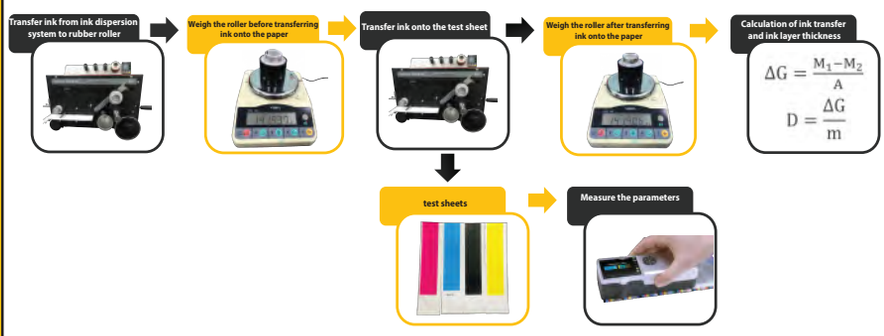

3 RESULTS

Relationship between ink transfer amount (ΔG) and density (D)

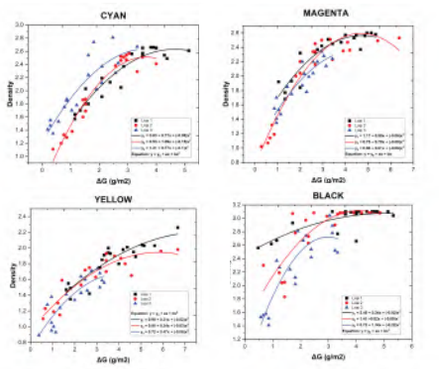

Relationship between ink layer thickness and density (D)

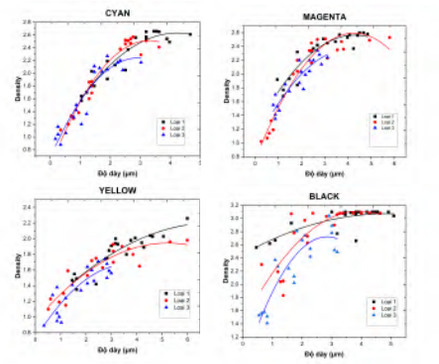

Relationship between ink transfer and color parameters Lab

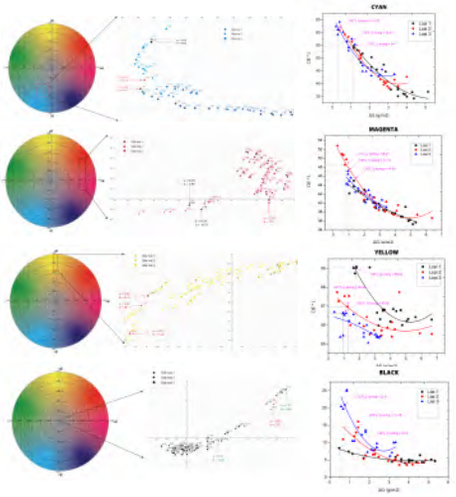

The relationship between (ΔE) and (ΔG)

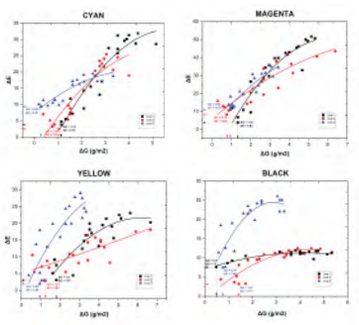

Relationship between ΔE and density (D)

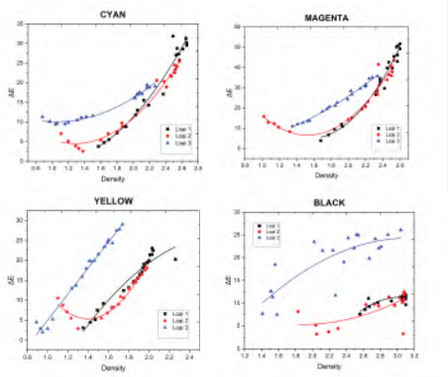

Develop a process to determine optimal parameters for each type of paper

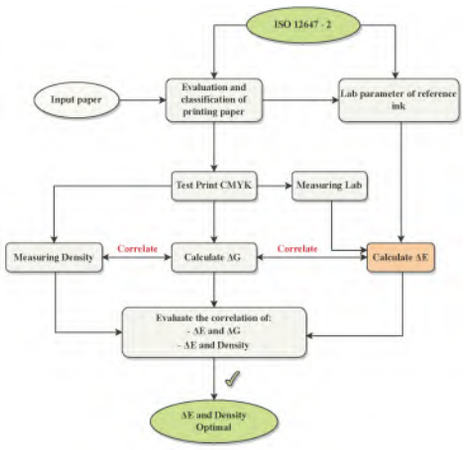

CONCLUSION

Apply the built-in process on the actual output printing device.

If chemicals and measuring equipment are available, the team will conduct experiments and evaluate how the surface energy of the paper affects the ink transfer more clearly and specifically.

The 12th Asian Symposium on Printing Technology (ASPT 2022)

Research on building a database to calculate the amount of CMY ink to apply the SPOT color formula

Nguyen Tran Phuong Duy, Huynh Huu Huy, Ly Thao Huyen, Nguyen Long Giang*

Faculty of Graphic Arts & Media
Ho Chi Minh City University of Technology and Education

INTRODUCTION

When the customer gives the sample to the printer to do, how can we recover and know color composition and proportions to make it color as close to the sample as possible. To meet get the requirements on the printer must have the opportunity Ink database based on local inks production combined with ink metering software to calculate calculate and get the required ink ratio bridge. It is for the above reasons selected topic. **"Research on building a database to calculate the amount of CMY ink to apply the SPOT color formula."**

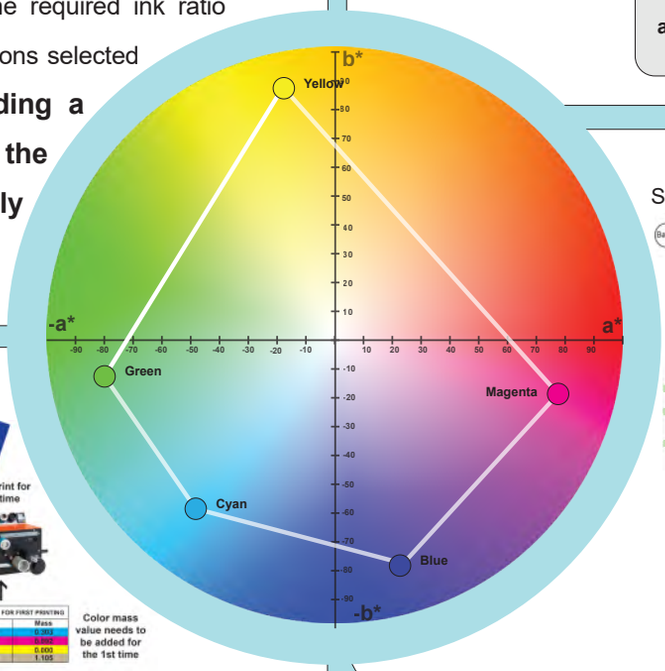

SUMARY

- Theoretical basis
- Working principle of the software Ink Formulation
- Build a data collection process
- Determine the color ratio of ingredients to build formulas
- Experiment and formula correction
- Conclusion and development direction

EXPERIMENT

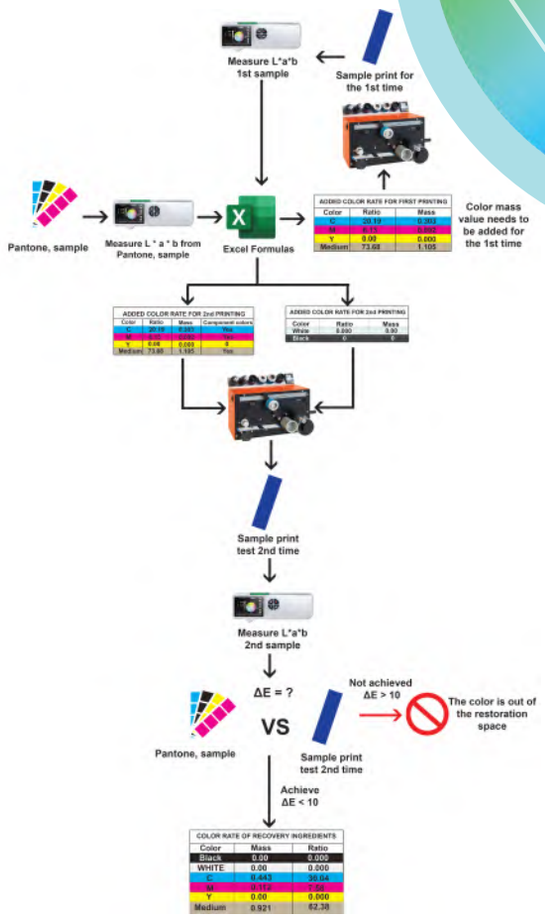

PRODUCT

Steps to build a database

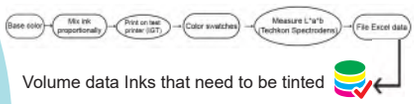

Volume data Inks that need to be tinted

Excel formulas

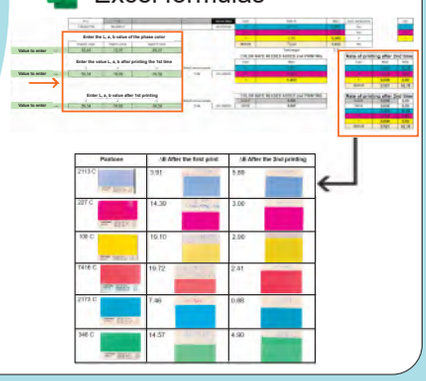

CONCLUSION

During the course of the study, the following objectives were achieved:

- Collect database and Lab values when tinting Cyan, Magenta, Yellow, Black, White, Medium.
- Predict the component inks Cyan, Magenta, Yellow, Medium, Black, White for color mixing.
- Software application combined with the database to calculate and give the amount of ink components required for a particular ink color.
- The obtained results E at the allowable level (ΔE<10) found that this topic is feasible and reliable, can be further developed for practical application.

DEVELOPMENT DIRECTION

- The group expects that when increasing the number of primary colors from 6 colors to 16 colors, it will be possible to reduce the value of ΔE (compared to the sample color).
- The group recommends using a spectrogram to determine the relationship between the sample color and the ratio of the component colors to be mixed. In order to give the correct color ratio to be mixed, suitable for printing industry conditions (ΔE < 2).
- As well as integrated development using software to support such as Machine Learning, AI, ... for the built software.

The 12th Asian Symposium on Printing Technology (ASPT 2022)

Preparation of antimicrobial microcapsules printable on food packaging paper

Peifu Kong[1], Toshiharu Enomae[2]

[1]Degree Programs in Life and Earth Sciences, University of Tsukuba

[2]Faculty of Life and Environmental Sciences, University of Tsukuba

筑波大学 University of Tsukuba

Introduction

- SDGs 2 and 12 highlight food loss and waste are two big challenges in the stages of a food system.
- To prevent them, packaging paper using **antimicrobial agents** is a feasible approach.

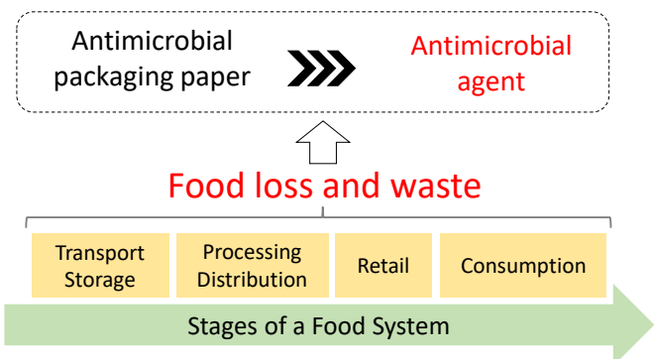

Materials and Methods

- **Essential oils** from ***Houttuynia cordata*** possess excellent antimicrobial property.
- Essential oils are **unstable** due to their high volatility, high heat sensitivity and easy oxidation, which greatly limit their application fields.
- **Microencapsulation** using β-cyclodextrin is a viable technology to prevent above problems and achieve a superiority of **prolonged release**.

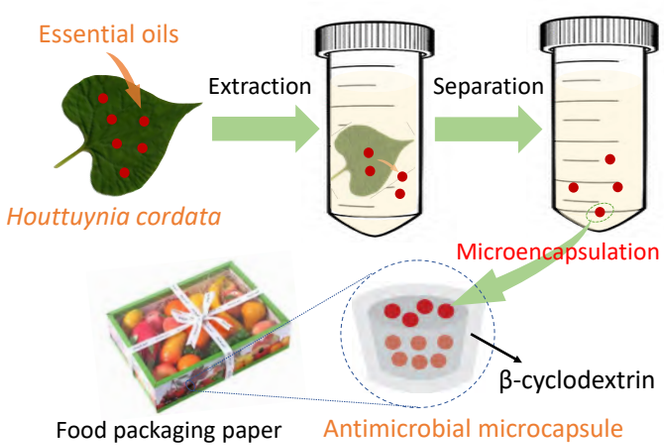

Results and Discussion

Morphological analysis

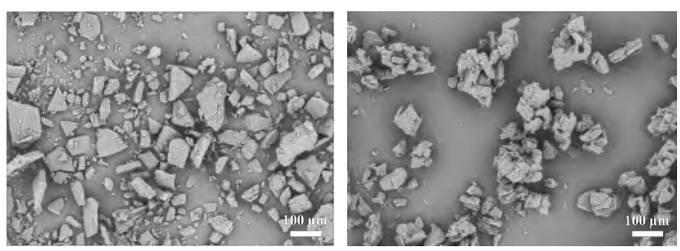

β-cyclodextrin | Microcapsules

Antimicrobial analysis (Incubation time: 48 h)

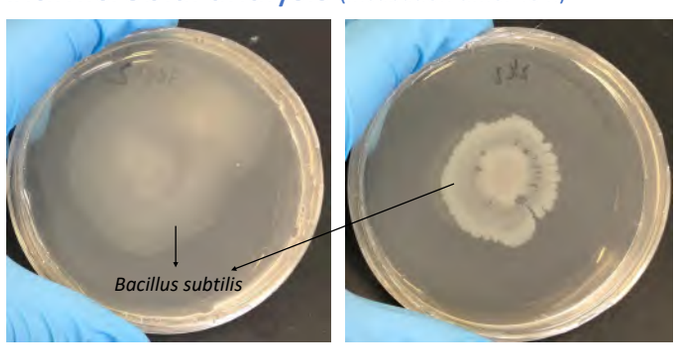

Media with β-cyclodextrin | Media with microcapsules

Printing proposals

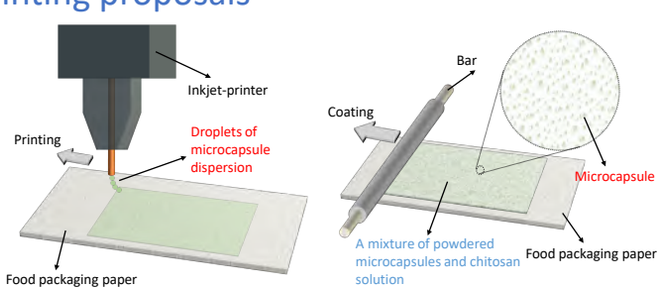

Inkjet-printing | **Bar-coating**

Conclusions

- This study prepared antimicrobial microcapsules containing essential oils of *Houttuynia cordata*.
- Microcapsules are printable on food packaging paper by inkjet-printing or bar-coating technology.

E-mail: peifukong@gmail.com

Identification of DNA from Japanese Traditional Paper, *Washi*, to Trace Diversity of Paper Mulberry Species

Min Soo Shin[1], Toshiharu Enomae[2]

[1]Master program in Agro-Bioresources Science and Technology, Univ. of Tsukuba
[2]Faculty of Life and Environmental Sciences, Univ. of Tsukuba
University of Tsukuba, Tennodai 1-1-1, Tsukuba, Ibaraki, 305-8572, Japan

筑波大学

Introduction

Broussonetia species (Paper Mulberry) is an important bioresource wood species consisting of long fiber and highly versatile for humans to produce a useful tool, such as paper, or bark cloth. Being efficient bioresource wood to produce traditional papers, the *Broussonetia* species varies over Asian countries and pacific islands. To trace the diversity of *Broussonetia* species, the traditional paper is an acceptable source to trace the origins of *Broussonetia* species. Since traditional papers are cooked in mild digestion with weak alkaline ashes and low digesting temperature compared to the western papermaking technique, some tissues or cells may survive and remains DNA.

Materials & Methods

➢ Optimization of DNA Extraction Method

1. Surfactant Method

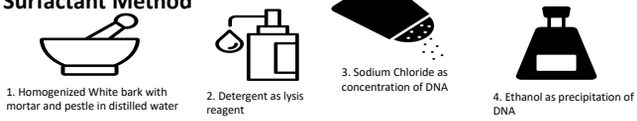

2. DNeasey Plant Pro Kit (Commercial Kit from Qiagen)

- Strictly followed the protocol of kit.
- Use of Micro-spin column to filtrate the purified DNA.

3. CTAB (Cetyl trimethylammonium bromide) Method

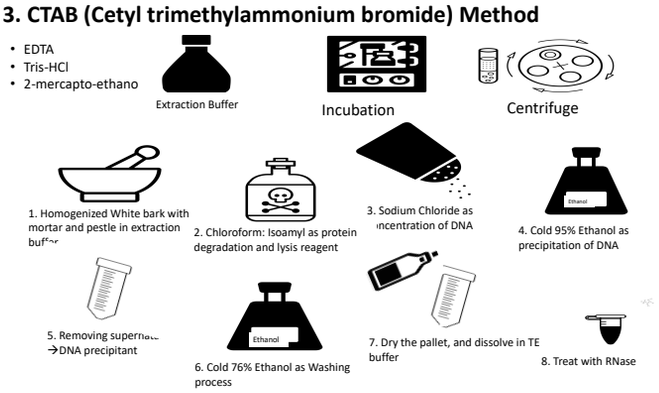

➢ UV-Vis. Spectroscopy → Evaluate DNA Yield and Purity

➢ Evaluation of DNA

1. Thermal Cycler (PCR; Polymerase Chain Reaction)

- Primer of ITS-1 region (Internal Transcribed Spacer-1)

2. Agarose-Gel Electrophoresis

- 2% Agarose

Results and discussion

➢ DNA Yield and Purity Result

Surfactant Method	Digested B.papyrifera bark	Non-treated B.papyrifera bark
Concentration (μg/ml)	6.41	3.03
Yield (μg)	4.49	2.12
Purity (A260/A280)	1.36	0.513
Kit Method	**Digested B.papyrifera bark**	**Non-treated B.papyrifera bark**
Concentration (μg/ml)	0.242	0.226
Yield (μg)	0.169	0.158
Purity (A260/A280)	1.64	1.69

CTAB Method	Digested B.papyrifera bark	Non-treated B.papyrifera bark
Concentration (μg/ml)	24.6	2.73
Yield (μg)	17.2	2.18
Purity (A260/A280)	1.11	1.9
	B.papyrifera Leaf	**Washi**
Concentration (μg/ml)	15.7	0.415
Yield (μg)	12.6	0.332
Purity (A260/A280)	1.82	1.84

Based on the calculation of UV-Vis. Spectroscopy on extracted DNA, the Surfactant method is not appropriate in DNA purity level and DNeasy Plant Pro kit are suitable for purity but not enough yield. However, the extracted DNA from the CTAB method secured DNA yield and appropriate DNA purity for evaluation by PCR.

➢ UV-Vis. Spectroscopy Result: CTAB Method

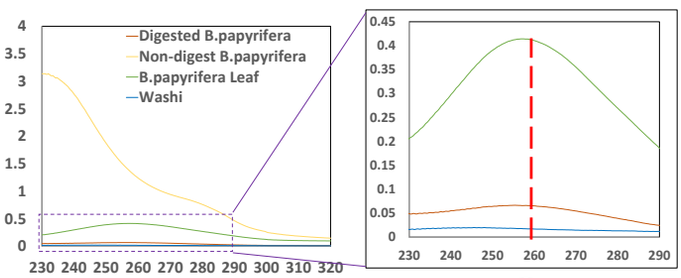

➢ Agarose-Gel Electrophoresis

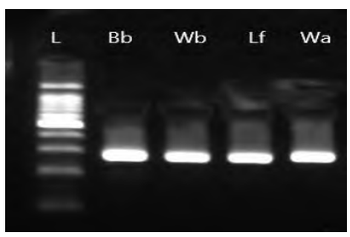

The most suitable DNA extraction from the CTAB method demonstrated clear peaks at wavelengths of 260 nm. Additionally, the DNA yield from Washi is relatively low. However, it proved the DNA remains throughout the traditional papermaking process.

ITS-1 Region of Washi matches with the original *B.papyrifera* bark and leaf sample. Due to the similarity of base-pair size, the Washi may originate from the corresponding source of *Broussonetia* species.

Conclusion

- ❖ **DNA is successfully extracted from Japanese Traditional Paper, *Washi***
- ❖ **CTAB DNA extraction method is the most appropriate extraction method** for *B.papyrifera* bark samples and Japanese Traditional Paper, *Washi*
- ❖ *B.papyrifera* species from a local farm (*Nasu Kozo*) and Japanese Traditional Paper, *washi*, demonstrated a successful match in base-pair size.
- ❖ By finding biomarkers (Primers) between different species of *B.papyrifera* or other *Broussonetia* Species, it is **possible** to trace the **origin of paper production**, and **how *Broussonetia* species propagated** over different countries.
- ❖ Furthermore, **historical paper propagation** may be defined more clearly with specific origins or traditional paper production.

The 12th Asian Symposium on Printing Technology (ASPT 2022)

RESEARCH TO BUILD COLOR MEASUREMENT SOFTWARE FROM DIGITAL PHOTOS

Nguyen Du Nhat Duyen, Nguyen Hoang Thien, Nguyen Van Thuan, Nguyen Long Giang*

FACULTY OF GRAPHIC ARTS AND MEDIA
HO CHI MINH CITY UNIVERSITY OF TECHNOLOGY AND EDUCATION

TOPIC GOALS

- Through TechKon's ColorCatcher, to analyze the status, evaluate and restore the ColorCatcher card.
- Building a database is a premise for researching and developing color measurement software from digital images, applicable in practice.
- Classify and collect databases to serve the construction of color measurement software through images taken with digital cameras.
- Through the process of experimentation to draw objective conclusions, comment by the collected data.

PRODUCT

1 

ColorCatcher Card

2 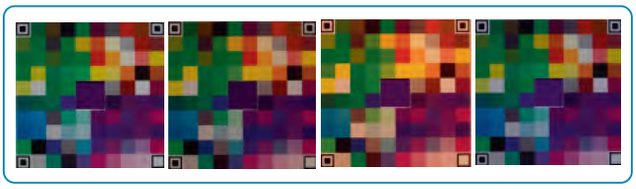

Database (4 lighting conditions)

3 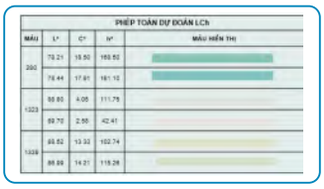

LCH value prediction formula

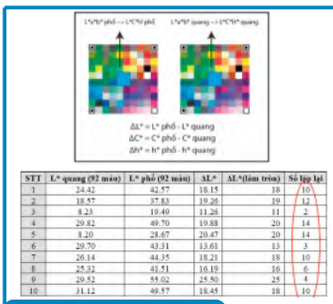

Option 1

- This option can simultaneously and quickly calculate all 1617 colors in testchart IT8.
- With the results predicting all colors, we have an overview and accurate assessment.
- With this embodiment, we accurately predict the colors in the central region around the coordinate angle O(0,0). And those colors are neutral colors.

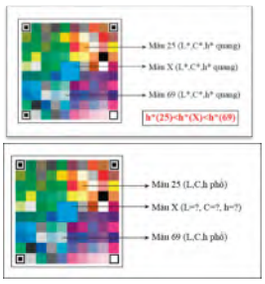

Option 2

Due to this option, selective calculations with conditions are limited to the fact that it is not possible to predict all 1617 colors in TestChart IT8. Since then, it has not been possible to give the most accurate and convincing view.

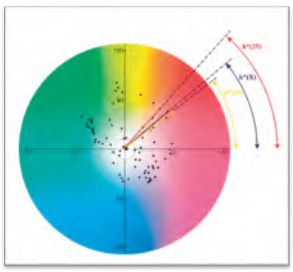

Option 3

- This method can completely predict 1617 colored cells in TestChart IT8. From there, we can comment and evaluate the plan more objectively.
- After evaluating and comparing the LCh prediction results with the standard LCh. We determine the region with the smallest AE in this embodiment. However, the optimal AE zone in option 3 is different from the optimal zone in option 1.

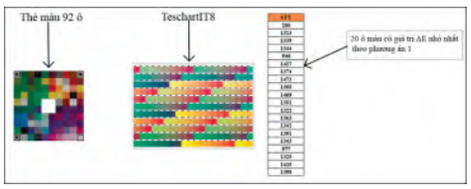

Option 4

Selecting the colors from the best area of option 1, we apply to option 4, the result is a big difference. The largest is ΔE = 71.92 (color no. 977) and the smallest ΔE = 6.60 (color number 1374). Due to this embodiment, selective calculations with conditions are limited to the fact that it is not possible to predict all 1617 colors in TestChart IT8. Since then, it has not been possible to give the most accurate and convincing view.

CONCLUSION

- Collecting databases is an important foundation for later development directions to become faster.
- Read photos from sRGB color space to Lab
- Experimentally demonstrating the correlation of measured Lab color space and LCh based on image extraction
- Determine color value, 2D Lab space color distribution

SUGGESTION

Apply algorithms and programming languages to integrate software using standalone cameras. From there, develop towards integrating the camera into the software (Similar to TechKon's Color Catcher product). Apply an algorithm to calibrate photos automatically according to Photoshop's mechanism. When adjusting H, S, B values, all values also automatically change according to the selection change and enter parameters as in Photoshop software

The 12th Asian Symbosium on Printing Technology ASPT 2022

APPLICATION OF ZnO NANOPARTICLES TO ENHANCE CURING OF UV PRINTING INK

Pham Quoc Huy, Tran Thi Hong Phuong, Duong Thu Trang, Nguyen Thanh Phuong*

Faculty of Graphic Arts & Media

Ho Chi Minh City University of Technology and Education

SUMMARY

In this study, we present the process of making ZnO nanomaterials by two methods, Sol-gel and hydrothermal, and then applying them to UV printing ink to enhance curing ability. Specifically, we use chemicals and experimental equipment available at the Prining Materials Laboratory of Faculty of Graphic Arts and Media of HCMC University of Technology and Education to create ZnO nanopowder at different concentrations. Then, disperse the powder samples into UV ink and test print on PET film using IGT Orange Proofer test printer. After printing, dry the printed sheet through the UV dryer IGT Aktiprint Mini 12-1. To test the curing ability after dispersing ZnO powder into UV ink, FTIR spectroscopy was taken from the FTIR spectrum evaluated through absorption peaks with links affecting ink drying. Besides, we test the colorfastness, ink adhesion as well as related parameters of color and density on the printed sheet. Finally, we will compare these values between the ZnO-dispersed inks fabricaed by Sol-gel and hydrothermal methods with pure ink, thereby giving the most optimal concentrations of ZnO and ZnO nanopartcles. It is manufactured from any method to limit the phenomenon of excessive color deviation as well as ensure the smoothest printing surface while increasing the ability to cure UV ink.

METHOD

PRODUCTION METHODS NANO ZNO

The process of making ZnO nano by Sol-Gel method

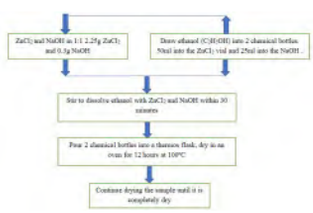

Process for fabrication of ZnO nano by hydrothermal method

Process of dispersing ZnO nano into UV Ink

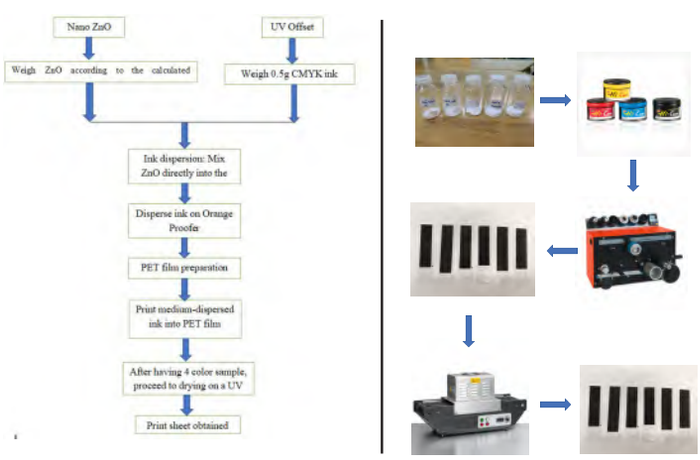

RESULT

UV ink FTIR spectrum

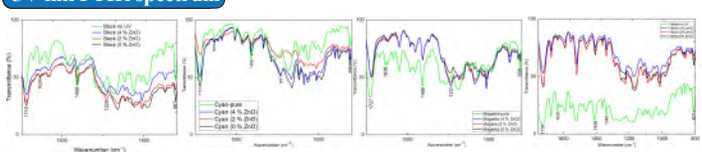

Adhesion Test

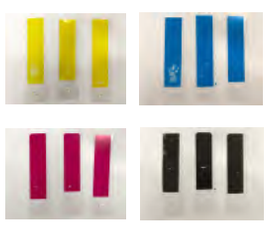

Surface Image

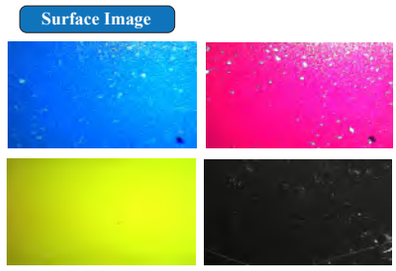

Density & Delta E Chart

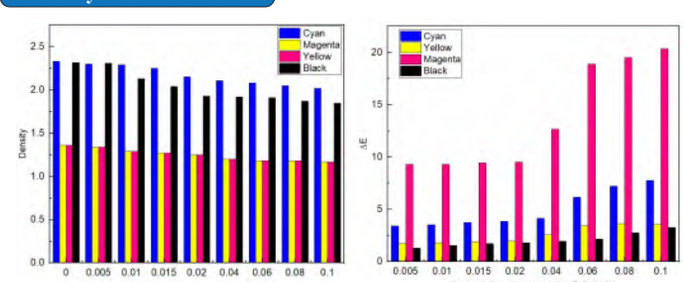

Color fastness chart

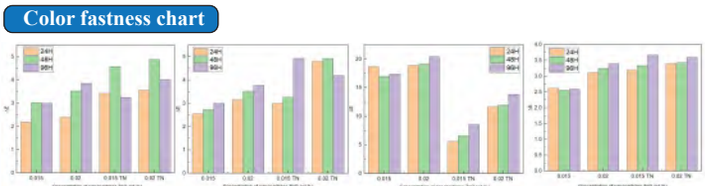

CONCLUSION

We dispersed ZnO nanoparticles with a concentration from 0.5% to 10% and obtained the result that ZnO concentration from 2% onwards, the adhesion ability is sfactory, however, the surface morphology is ZnO concentration. From 4% onwards, many white spots appear and are almost not smooth. In terms of color fastness, Yellow color in Sol-Gel method is the best of all 3 colors. Moreover, the value for color density is almost unchanged, inversely proportional to the amount of ZnO added (the more ZnO, the lower the density) and directly proportional to the color difference interval (the more ZnO, the greater the E). great). ΔE has the change and the color difference is within the allowable range (ΔE is less than 5). Thus, the concentration of ZnO=2% when added to UV ink is optimal because it meets the requirements of enhancing the ink drying process, achieving adhesion, relatively smooth material surface as well as density and ΔE values are within the allowable range..

REFERENCES

[1] Nong Ngoc Hoi (2015), "Study on the properties of Eu3+ doped ZnO materials", Master of Science Thesis, Specialization in Solid State Physics, University of Science, Vietnam National University, Hanoi, page 4 - 8.

[2] Keomany Inthavong (2018), "Fabrication of ZnO materials by ultrasonic chemistry, research on Cr (VI) absorption, photocatalysis of green methylene treatment in aqueous environment", Master thesis in chemistry, University Thai Nguyen, University of Education, pages 4 – 7.

[3] Nguyen Quynh Anh (2018), "Synthesis and optical properties of ZnO: Eu3+ by thermal diffusion method", Graduate thesis, major in Analytical Chemistry, Hanoi National University of Education 2, page 18 – 23…

[4] Chin Boon Ong, Law Yong Ng, Abdul Wahab Mohammad (2018), "A review of ZnO nanoparticles as solar photocatalysts: Synthesis, mechanisms and applications". Renewable and Sustainable Energy Reviews. pp.540.

[5] Snehal Yedurkar, Chandra Maurya, Prakash Mahanwar (2016), "Biosynthesis of Zinc Oxide Nanoparticles Using Ixora Coccinea Leaf Extract – A Green Approach", Open Journal of Synthesis Theory and Application. pp. 6.

[6] Ashraf Abd El-Rahman (2021), "Drying methods of the printing inks", Joural of Graphic Engineering and Design, Vol 12, 2021. pp 2 – 7...

HO CHI MINH CITY UNIVERSITY OF TECHNOLOGY AND EDUCATION
FACULTY OF GRAPHIC ART AND MEDIA

TOPIC OF THE PROJECT

BUILDING THE STANDARD CONTROL FOR THE FLUTE-LAMINATING CARTON PACKAGING STAGE AT THE Y&J VINA CO.LTD

STUDENTS


Mai Hoàng Thúy Vy
18158173


Võ Minh Thông
18158161


Huỳnh Thị Thanh Mỹ
18158141

Teacher: Th.s Cao Xuân Vũ

Year: 2018 - 2022

Implementation support unit:
Y&J VINA CO.LTD

INTRODUCTION

The fulte-laminating carton pakaging process is a necessary job for today's paper box packaging, but still not much attention has been paid to quality control issues. The impact of factors on paper (moisture, bursting, pin adhension and glue (viscosity) also greatly affects the production process, leading to unsatisfactory finished product quality.

Each company only checks for objective quality based on the available conditions and perceives it visually, but besides that, they still ensures the quality of the product to their customers

CONCLUSION

Some causes can affect the high moisture content of paper such as:

- The adjustment of the glue supply batch, the amount of glue that makes the inside surface wet, takes longer to dry.
- For flute-laminating carton packaging E, the amount of glue on the lot should be adjusted less than that of B flute-laminating carton packaging.
- For glue of 20% - 40% H2O, wave E has good stickiness after backing, the measured moisture content of 40% H2O sticky paper is low and stable. However the high water ratio, more conditions have been taken place cure paper.
- For flute-laminating carton packaging B , if 40% H2O glue is used, the stickiness is not reached, so it is necessary to use a glue with a mixing ratio of 20 - 30% H2O to achieve the required stickiness for the product and reduce the curved paper after fulte-laminating.

➔ In order to choose a common glue for backing parts, it is necessary to be based on the sensory criteria of stickiness after flute-laminating, paper moisture stability, improvement of previous errors and not use cost of glue increased too much. The company requested that the difference in water ratio compared to the previously mixed glue be allowed to increase in the range of 2-5%, so the team give a proposal to apply glue with a mixing ratio of 30% H2O.

EXPERIENCE

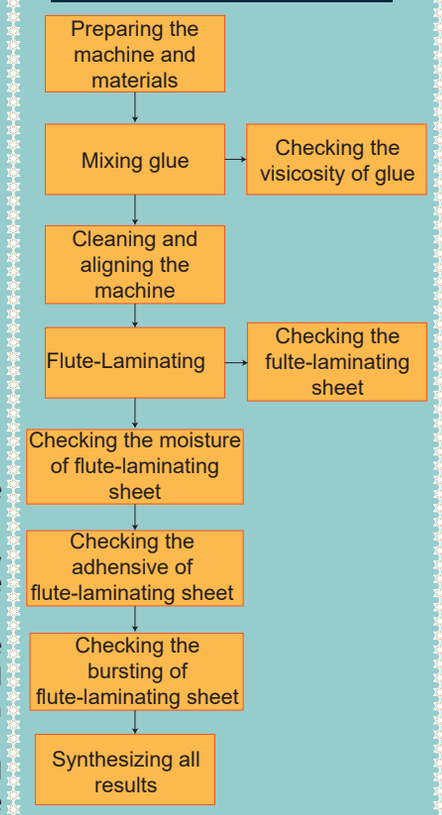

RESULT

Experiencing and evaluating the capacity of the flute-laminating carton packaging.

Establishing the standard control based on experimental conditions.

Comparing and evaluating the results of applying established standards for the flute-laminating carton packaging.

Establishing the sheets control and posters describing hand hygiene in contact with PVAc glue at the filling site have been established.




UP-DEVELOPMENTAL OF TOPIC

- Practising on different types of paper and flutes as it also has similar conditions.
- Development on automated machines and experiment for a longer time to get better results.
- In addition, it is necessary to check other requirements of the flute-laminating carton packaging quality control such as: Edge and Flat Crush Test; Bending stiffness (of the carton); Tensile Strength Test, Ply Bond Test, Puncture Strength Test; Humidnity and air environment for testing.

The study of the characteristics and printing quality of offset inks based on palm oil

Wannarat Wirachkul, Suchapa Netpradit and Juntira Komasatith

Department of Printing and Packaging Technology,
Faculty of Industrial Education and Technology, King Mongkut's University of Technology Thonburi
126 Pracha Uthit Rd., Bang Mod, Thung Khru, Bangkok 10140, Thailand

BACKGROUND

The offset printing technology uses solvent-based inks that are oil-based, and historically, petroleum was the oil that was most commonly utilized in these inks. However, the property of petroleum oil is that it contains odorous, environmentally hazardous volatile compounds. Nowadays, people pay more attention to the environment, so petroleum-based ink does not meet consumer demand because of the environmental unfriendliness of petroleum solvents. Environmental issues are an important issue along with print quality. Therefore, vegetable oil-based ink was invented and developed by using soybean oil to replace and had been accepted. In addition to soybean oil-based inks, other types of vegetable oils are also used to improve the properties of printing inks. In the printing process, they can be used for offset printing systems and can also produce beautiful print quality with bright, high color intensity, and with shiny texture. In addition to the environmental friendliness of soybean oil-based ink, this ink extends the life of the printer and reduces printing costs in the long run [1]. But soybean oil used as a solvent in printing inks to replace petroleum oil is quite expensive because soybean oil is not produced in Thailand, so soybean oil must be imported into the country.

In this regard, the study anticipated the issue of somewhat expensive soybean oil-based ink and considered testing out palm oil-based ink. Based on a survey, there is a large quantity because it is a Thai economic crop with high production capacity [2] to be mixed into an eco-friendly vegetable oil base ink as another alternative. Palm oil is a less expensive vegetable oil than other vegetable oils and in Thailand, the palm is mainly cultivated. Since more than 70% of the ink composition is solvent, if the cost of the solvent in the ink can be reduced, the ink price will be lower, and most importantly, the palm-oil-based ink is also environmentally friendly that does not cause pollution as well.

METHOD

1 VARNISH Prodection Process
2 VARNISH Property Test
3 INK Property Test
4 INK Prodection Process
5 Layer of INK Property

RESULTS

1. Varnish property test

a. Tack value of varnish

Type of varnish	tack value (GM.)
Soy	9.7
Palm	10.9

b. Viscosity of varnish

Type of varnish	viscosity (Pa.s.)
Soy	23.42
Palm	62.49

c. The flow rate of varnish

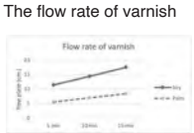

d. Spread flow of varnish

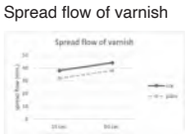

2. Ink property test

a. Fineness of grind

Soybean oil-based inks and palm kernel oil-based ink showed that the resolution of soybean oil-based inks and palm kernel oil-based ink were the same at 3 micrometers.

b. Tack value of ink

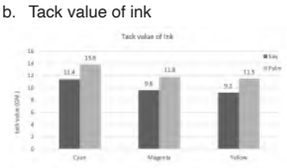

c. Spread flow of ink

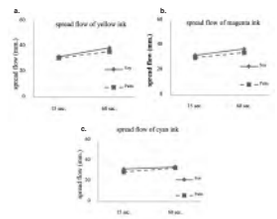

d. Flow rate of ink

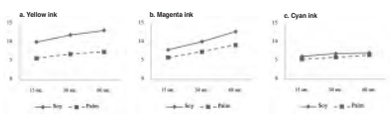

e. Viscosity of ink

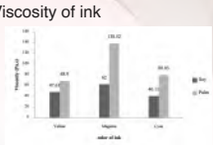

f. Water pickup

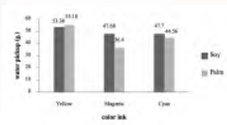

g. Setting time

Palm kernel oil-based ink had a faster setting time than soybean oil-based ink, and Yellow had the slowest setting time of both inks, while Cyan had the fastest setting time of the both types of ink.

3. The Layer of ink property test

a. Gloss test

Palm kernel oil-based ink had a higher gloss value than soybean oil-based ink because the gloss value was related to the drying of the printing ink. The drying time of palm kernel oil-based ink had a faster setting time and therefore higher gloss values.

b. Rub resistance

Palm kernel oil-based ink had a higher degree of rub resistance than soybean oil-based ink because the color of palm kernel oil-based ink had less shedding, while palm kernel oil-based ink with Yellow color had less rub resistance. than soybean oil-based ink.

c. Color different

h. Drying time

Palm kernel oil-based ink had a much slower drying time than soybean oil-based ink compared to other oil-based inks. The structure of the palm kernel oil-based ink was high in saturated fatty acids, where saturated fatty acids are composed of single bonds that did not react with oxygen. At the same time, soybean oil had a high content of polyunsaturated acids, where polyunsaturated fatty acids had multiple double bonds, thus reacting with more oxygen in the air, thus allowing for faster drying.

i. Skinning time

Palm kernel oil-based ink had a much slower skinning time than soybean oil-based ink. The skinning time was based on the structure of both oils as well as the drying time.

The color difference of soybean oil-based inks and palm kernel oil-based inks on coated and uncoated paper showed that the color difference of ink on coated paper was higher than that of uncoated paper. Yellow had the lowest ink color difference on both types of paper, and Magenta on coated paper had the greatest ink color difference.

d. Density

Soybean oil-based ink and palm kernel oil-based ink in all color have similar density values.

CONCLUSION AND DISCUSSION

The soybean-oil-based varnish had better varnish properties than palm-oil-based varnish in terms of toughness, viscosity, flow rate and dispersion because soybean oil is a high polyunsaturated fat, in which this type of fat was a liquid at room temperature and would become solid at lower temperatures. While palm kernel oil was a higher saturated fat, it was solid at room temperature, so the ink properties in terms of toughness, viscosity, flow rate and dispersion were consistent with the properties of the varnish. In terms of ink and water pick up properties, there was a correlation with viscosity. If the viscosity was low, ink and water pick up value would be high. If the viscosity was high, ink and water pick up value would be low. Moreover, palm kernel oil-based ink had better setting, drying and skinning properties than soybean oil-based ink because of the chemical structure of polyunsaturated fat of palm kernel oil, and palm kernel oil-based ink had a higher gloss than soybean oil-based ink which was related to the setting of the ink. For the rub resistance level of palm kernel oil-based ink, most had better rub resistance, better adhesion than soybean oil-based ink. For the color difference of prints printed with both types of ink, Yellow had the lowest ink color difference on both paper types, and Magenta on coated paper had the largest difference in ink color. And the density value on coated paper has similar blackness values for prints printed with both inks. For uncoated paper in Magenta and Cyan color, the density value of palm kernel oil-based ink was lower than that of soybean oil-based ink.

ACKNOWLEDGMENT

We would like to express my sincere thanks to Patum Vegetable Oil Co., Ltd. for providing the palm oils. Many appreciations to Chalerm Chaichan Co., Ltd. for the suggestion and preparing the raw materials and facilities for printing ink mixing. We also appreciate the Foundation of Printing Exhibition Fund of Thailand for support to send one of us to present this work at the ASPT 2022 Symposium in Vietnam.

REFERENCES

1. Smile Siam Printing Service, Smile-Siam.com [Online], Available : https://www.smile-siam.com/printing_content-soy_ink/. [14 May 2021].
2. The Agricultural Research Development Agency (Public Organization), arda.or.th [Online], Available : https ://www.arda.or.th/kasetinfo/south/. [14 May 2021].
3. Ploysri, W.and Charoensopa, K., The production of processed color of offset printing ink from used vegetable oil, Journal of industrial technology Ubon Ratchathani Rajabhat University, vol.10, No. 2, pp. 89-98. (2020)
4. Cem Aydemir, Semiha Yenidoğan, Arif Karademir and Emine Arman Kandirmaz, "The examination of vegetable and mineral oil-based inks' effects on print quality: Green printing effects with different oils", Journal of Applied Biomaterials & Functional Materials, Vol.16, No.3, pp. 137-143. (2018)\

Effect of the spatial frequency of skin texture on the conspicuousness of a pigmented spot

Akane Takahashi[1], Hiromi Sato[2], Yoko Mizokami[2]

[1]Graduate School of Science and Engineering, Chiba University, [2]Graduate School of Engineering, Chiba University

ASPT2022, 9/15
@Ho Chi Minh, Vietnam

Introduction

Pigmented spots of the skin influence to impression such as the age, health, attractiveness. [1)]

There is not much research on how pigmentation appear.

<Previous study>

concentration | number | position | area

The conspicuousness of pigmentation is affected by the difference in lightness between the skin and pigmentation.[2)]

Evaluations for only homogeneous skin only.

Purpose To clarify whether noise on the skin affects the conspicuousness of pigmentation.

Experiment

Stimuli

The average face of Japanese women and a pigmented spot extracted from cheek image were combined.

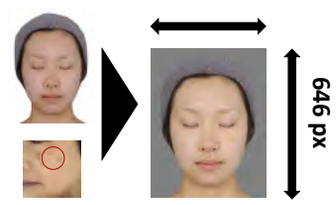

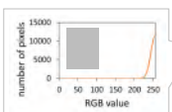

Noise values: The lower half of a normal distribution.

Gaussian noise

Peak frequency [cy/img](cpd)

10 (0.46) 30 (1.39) 50 (2.32) 70 (3.25) 90 (4.18)

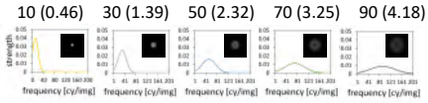

・Normalizing contrast
・Modifying noise color to a high-density melanin chromaticity.

homogeneous

standard comparisons

Skin color modulations (for comparisons)

For all noise conditions

Four types of skin color modulations.

※Contrast btwn the skin and noise/pigmentation was the same.

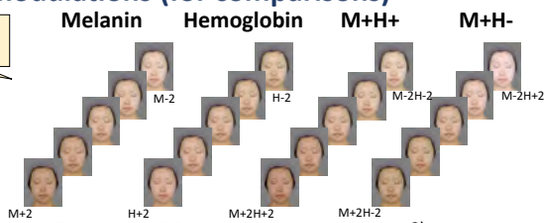

Based on Monte Carlo simulation[3)]

Procedure

Evaluating the conspicuousness of the pigmentation by comparing it with the standard stimulus.

Standard stimulus | Comparison stimuli

Observers
6 students (3 women)
23.7 ±1.63

Result and Discussion

Average evaluation score

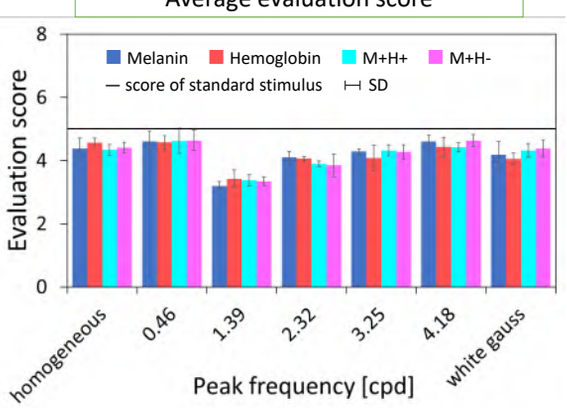

Compared to the homogeneous patterns, most noise patterns had smaller evaluation scores.

In the condition with a peak frequency of 1.39 cpd, the evaluation score was significantly lower.

There was no significant difference in scores by skin color.

Spectrum × CSF(MTF)[4)]

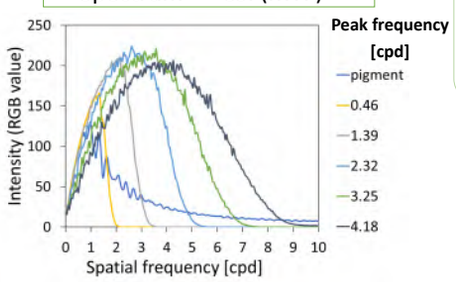

Profile of RGB value around the pigmentation

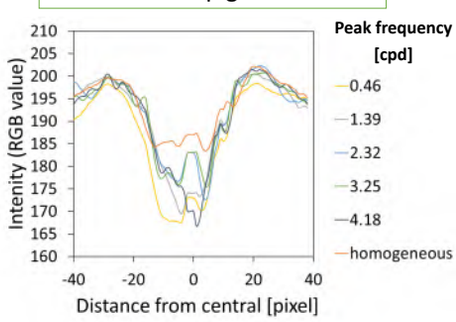

Mathematical CSF model

$A(f) = 75 f^{0.8} e^{0.2f}$

A: CSF
f: Spatial frequency [cpd]

The spectra with a peak frequency of 0.46 and 1.39 cpd are similar to pigmentation but inconsistent with evaluation score.

Peak frequency : 1.39 cpd
➡The area of intensity reduction is narrow.
➡Pigmentation spot appear smaller.

Future work
Varying pigmentation size to clarify the relationship between spatial frequency components and conspicuousness.

Conclusion

Noise on the skin reduces the conspicuousness of pigmented spots.
A specific spatial frequency component of facial noise markedly reduces the conspicuousness of pigmented spots.
Facial color does not affect the conspicuousness of pigmented spots if their contrasts are the same.

1) Stephen et al., Handbook of Color Psychology (A. J. Elliot et al.), 585-602, 2015
2) Takahashi et al., The 43rd ECVP, Perception, 50(1S), 112 (2021)
3) Maeda et al., Optical Review, 17(3), 223-229 (2010)
4) Movshon et al., JOSA, A, 5(12), 2166-2172 (1988)

Supported by JSPS KAKENHI JP18H04183, JP21H05805, and JSPS Core-to-Core Program (JPJSCCB20220006)

Digital transformation on business operation and internal administration of printing houses focusing on the problem of adjustable work processes of employees

Koravit Sriwongsa, Banchar Arnonkijpanich and Aran Hansuebsai
Department of Imaging and Printing Technology, Faculty of Science, Chulalongkorn University, Bangkok, Thailand 10330.

Abstract

Nowadays, the print media business is in a recession due to an increased quantity of marketing competitors, an increase of specialized entrepreneurs, and a change in consumer behavior from paper-based publications to electronic format. These factors directly affect the business operation of entrepreneurs. We studied a working system of Chulalongkorn University Press relying on conventional and digital printing technologies. To minimize production costs in the printing house, the parameters derived from the constrained optimization problem need to be computed explicitly according to existing employees. The set of parameters corresponds to the number of jobs assigned to conventional and digital systems were observed, including the work efficiency in both systems. An average of the work efficiency levels was needed to define a constraint in an optimization modeling approach. In the experiments, the simulated annealing (SA) algorithm based on evolutionary computation was applied for identifying the parameters of the cost balance model.

Introduction

Chulalongkorn University Press (CUpress) recently invested the web inkjet press in-line with sheet cutting and stacking machines for book printing service while the old offset machines are used for medium and long run printing and cover printing (Figure 1-2). It showed that the inkjet press system used the operators only 2 workers while the conventional system was still run by 12 workers. (pre-press + press + post-press). The question is that how to manage these workers in the conventional system that the CU press should not let them vacant from work. We therefore studied the digital transformation on business operation and internal administration of printing houses focusing on the problem of adjustable work processes of employees in the case of Chulalongkorn University Press.

A model relating to the existing employees was proposed to minimize production costs in the printing house. A set of parameters corresponds to the number of tasks was assigned to both systems to estimate the work efficiency level of each position. An average of the work efficiency levels was needed to define a constraint in an optimization modeling approach. In the experiment, the simulated annealing algorithm based on evolutionary computation was applied for identifying the parameters of the cost balance model.

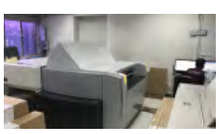
Pre-press (imposition / plate-making)


Press (printing)


Cutting machine


Folding machine


Gathering machine


Glue binding machine

Figure 1 Workers involved in each step in conventional system (Offset printing)

Figure 2 Workers involved in digital web inkjet press + inline sheet cutting and stacking

Experiment

To determine the cost when both systems were simultaneously used, we defined the parameters in the model based on staff working in the two processes as they have obligations with the CU press. The proposed costing models could be summarized in linear equation as followings :

$$C^s_o = w_a a_s a_o + w_b b_s b_o + w_c c_{fp} c_o + w_d d_s d_o + w_e e_s e_o + w_f f_s f_o + w_g g_s g_o + w_h h_s h_o \quad \text{.....(1)}$$

$$C^s_n = w_a a_s a_n + w_b b_s b_n + w_c c_s c_n + w_d d_s d_n + w_e e_s e_n + w_f f_s f_n + w_g g_s g_n + w_h h_s h_n \quad \text{..... (2)}$$

where C^s_o : cost of staff in conventional system

C^s_n : cost of staff in digital system

a_o / a_n : number of editorial staff in conventional and digital systems

b_o / b_n : number of designer in conventional and digital systems

c_o / c_n : number of prepress staff in conventional and digital systems

d_o / d_n : number of printer in conventional and digital systems

e_o / e_n : number of folding machine staff in conventional system

f_o / f_n : number of cutting machine staff in conventional system

g_o / g_n : number of gathering machine staff in conventional system

h_o / h_n : number of binding machine staff in conventional and digital systems

$a_s / b_s / c_s / d_s / e_s / g_s / h_s$: salary for each staff

$w_a / w_b / w_c / w_d / w_e / w_f / w_g / w_h$: workload of each staff

As the staff can work in both systems. Accordingly, the cost based on working staff would be:

$$C^s = \alpha C^s_o + \beta C^s_n \quad \text{.....(3)}$$

where α and β were the ratio of job allocation between two systems.

$$\alpha + \beta = 1.0 \quad \text{.....(4)}$$

In case of variable cost, we could explain it in a linear equation as given in Equation 5.

$$C^p = \alpha C^p_o + \beta C^p_n \quad \text{.....(5)}$$

The total cost will be:

$$C^T = C^s + C^p \quad \text{.....(6)}$$

This research was to find the **optimal solution** of these parameters to achieve the lowest total cost (C^T). MATLAB was used as a tool to calculate. In addition, the cost estimation should be determined under the condition that working efficiency of CUpress (ϖ) should not less than that of defined criteria (γ).

$$\varpi > \gamma \quad \text{.....(7)}$$

Where $\varpi = (w_a + w_b + \cdots + w_h)/8$

Finally, constrained optimization was applied as follows:

$$\min_p T(P)$$

$$\text{s.t. } 0 < \propto, \beta < 1$$

$$\propto + \beta = 1$$

Results and Discussion

Table 1 shows the number of staff working in the conventional and web inkjet printing systems, including their salary. The parameters obtained from the SA analysis under the present situation were as follows:

- job allocation in conventional system ($\propto$) = 0.599984 (60%)
- job allocation in digital system (β) = 0.400016 (40%)
- average working efficiency (ϖ) 0.95015979
- Total cost (C^T) 2,072,845 THB/month (C^s = 452,845 THB, C^p = 1,620,000 THB)
- C^s calculated from full workload of working staff
- C^p_o 975,000 THB / C^p_n 650,000 THB

Table 1 Number of staff working in the conventional and digital printing systems

Staff (position)	Conventional printing system	Digital printing system	Salary (THB)
editorial	x	x	28,500/28,500
Designer1	x	x	30,500/27,650
Designer 2	x		26,000
Press operator 1	x	x	36,650/16,500
Press operator 2	x	x	20,000/21,500
Press operator 3	x		21,650
Pre-press 1	x		25,745
Pre-press 2	x		24,650
Cutting machine operator	x		19,500
Folding machine operator 1	x		19,500
Folding machine operator 2	x		21,000
Gathering machine operator 1	x		24,000
Gathering machine operator 2	x		18,500
Binding machine operator 1	x	x	24,000
Binding machine operator 2	x	x	18,500

It is shown that more job are allocated to the conventional system as most of the employees are still working with the CUpress. However, the CUpress has to accept the situation that the click charge payment for digital system must pay at the minimum amount. Some months are loss, some months are gain!

We predicted in the next five years after the retirement of several staff of conventional production. We obtained the optimal parameters as given in Table 2. Evolutional computing by random technique was applied step by step in order to observe the improvement of these parameters and total cost (CT). It appears that the job allocation can be forwarded more to digital system. For the work in conventional process, the CUpress may recruit the employees from other department instead.

Table 2 Prediction of optimal solution of book production at the CUpress using the combination of conventional and digital systems

iteration = 89,104,677
total cost (C^T) = 1,642,172.50 THB/Month (C^s : 273,497.50 THB, C^p : 1,430,000 THB)
α = 0.4000 (40%)
β = 0.5999 (60%)
working efficiency (ϖ) = 95.030141 %

Full digital transformation

In the case of full digital transformation, this means that we stop using conventional system. The cost of staff will be based on only six staff with full workload (136,650 THB/month). While the production cost depends on the number of jobs from the sale department which at least minimum click charge. By SA analysis, the total cost (CT) will down to below one million THB/month including the materials cost (ink and paper). This represents the success of digital transformation at the CUpress in the future when the organization is leaned.

Conclusions

It was shown that digital transformation with the web inkjet press allowed publishing houses to repurpose their business by combining with conventional production, depending on the adjustable work processes of employees. Its benefit was to be able to reduce the total cost which is important to get more jobs. To approve the assumption, the simulated annealing algorithm based on evolutionary computation was applied for identifying the parameters of the cost balance model. Optimal solution showed that the total cost could decrease to the level of CUpress be able to compete in the book printing market. Interestingly, the success of digital transformation will be seen concretely when the CUpress stops using conventional production in the future after the retirement of employees.

Investigation on the effect of different papers on the total area coverage of inks in offset color printing

Anh Tuan Phung, Truong Trong Tung

Affiliations: Department of Printing Technology, Hanoi University of Science and Technology
Address: No 1, Dai Co Viet str., Hanoi, Vietnam

Abstract

The total area coverage is the maximum total dot percentage of cyan (C), magenta (M), yellow (Y) and black (K) ink used in the darkest areas. It generally depends on the printing process and the type of paper. The most important parameters that have a significant influence on the TAC values are the papers, inks and printing press specifications. In case of incorrect values usage at relatively high or low levels of TAC, press problems such as the big amount of ink consumption, poor ink trapping, back transfer and set-off due to insufficient ink drying might be encountered. The goal of this study is to define the total area coverage of inks on coated and uncoated papers in a sheet-fed offset press. For this study, we have used a particular test form containing different control strips for densitometric. According to the measurement of the density of test charts, we have determined the TAC values with other papers. The results achieved are necessary to determine the optimal values of color separation parameters for each ink/paper/printing press combination.

Keywords: Total area coverage, Total ink limit, Gracol7, Dotgain.

Properties of Gravure Inks for Printing on Biodegradable Plastic Film

Suchapa Netpradit, Ratsamee Narktabtim,
Jadetarin Tanglertthanasap and Vachira Kuptavetin

Department of Printing and Packaging Technology, Faculty of Industrial Education and Technology, King Mongkut's University of Technology Thonburi
126 Pracha Uthit Rd., Bang Mod, Thung Khru, Bangkok 10140, Thailand

Abstract

The purposes of this project were 1) to determine the adhesion properties of solvent-based, alcohol-based, and water-based inks on biodegradable plastic films, 2) to study the physical properties in resistance of heat, cold and oil, and 3) to compare the print density and color difference between inks printed on biodegradable plastic film and polyethylene film. There were 5 types of gravure printing inks to applied by bar coater on the Polylactic acid (PLA) film with and without corona surface treatment for surface energy increasement. The results showed that all printing ink types had a printability on the PLA film with the same print density as the polyethylene film, especially for solvent-based and alcohol-based ink. The adhesion levels were tested by the Tape Test method according to ASTM D 3395, found that the solvent-based inks had the best adhesion, the alcohol-based ink and the water-based ink was good on the treated film. The heat resistance of samples was tested by placing on the hot plate heated at 60-65°C for 15 minutes. The results showed that 3 types of printing inks also had the same good adhesion levels. After the cold resistance testing by placing the samples in a freezer at temperature of -6°C for 24 hours, the solvent-based ink for treated film and alcohol-based ink for untreated film had the best adhesion. The water-based inks had poorer adhesion or ink peel off especially for untreated film. For the oil resistance of samples tested in vegetable oil for 24 hours, the solvent-based ink and the water-based ink on treated film did not peel off but the alcohol-based ink was peeled off. Therefore, the alcohol-based ink could be applied on the untreated PLA film for eco-friendly with an acceptable color difference (ΔE_{ab}=3.76) from the printed polyethylene. However, the water-based ink could be applied to print on the treated PLA film with enough adhesion level.

Keywords: Alcohol-Based Ink/ Biodegradable Plastic/ Corona Surface Treatment/ Solvent-Based Ink/ Water-Based Ink

.

Identification of DNA from Japanese Traditional Paper, *Washi*, to Trace Diversity of Paper Mulberry Species.

Shin Min Soo

Master program in Agro-Bioresources Science and Technology, Univ. of Tsukuba
University of Tsukuba, Tennodai 1-1-1, Tsukuba, Ibaraki, 305-8572, Japan

Abstract

Paper Mulberry including *Broussonetia kazinoki* and *Broussonetia papyrifera* has been historically used for papermaking and is a species native to Asian countries. Especially, *B.kazinoki* is a species inherent in Japan, Korea, and China, while the *B.papyrifera* species is found also in Southeastern Asian countries. In recent decades, the hybrid species of *B.papyrifera* hybridized with *B.kazinoki* has become the majority of paper mulberry species. To originate the paper mulberry biodiversity, the Japanese traditional paper, *Washi*, is a significant source of identification of inherent or hybridized DNA. Due to the mild alkaline condition and relatively low temperature of industrialized papermaking technique, the DNA available within traditional paper remains throughout the papermaking process. Parenchyma tissues containing DNA were observed through acetocarmine staining in a digested tree bark. DNA extraction of tree bark samples and traditional paper is optimized through different methods. The DNA structure was analyzed by UV-visible spectroscopy. The allele sizes of extracted DNA in a bark from a freshly harvested tree and in a product of traditional paper were compared through a polymerase chain reaction and agarose gel electrophoresis.

Advancement of Paper-based Eco-friendly Material Sciences

Division of Biomaterial Engineering, Faculty of Life and Environmental Sciences

Toshiharu Enomae, Shalida Rosnan, Kotchaporn Thangunpai, Kong Peifu, Shin Min Soo, Megumi Kitamura, Toshiaki Hayashi

Biomaterial Engineering, Faculty of Life and Environmental Sciences, University of Tsukuba Tennodai 1-1-1, Tsukuba, Ibaraki 305-8572, Japan

Abstract

In the laboratory of Paper device and Eco-friendly materials, many types of biomass have been intended to be utilized for paper product (1) During the production of cardboard gift boxes, laser cutting processes were introduced for flexible design of the packaging shape and function. To minimize the carbonization near the kerf edges due to thermal decomposition, the cutting speed and laser power ratio was successfully optimized through the measurement of the area of the heat-affected (blackened) zones (HAZ) using the suitable binarization filtering (Otsu technique) applied to the micrograph images of HAZ. (2) A composite of wood pulp fibers and poly-ε-caprolactone (PCL) was produced to create hydrophobic paper keeping biodegradability. For better miscibility between the two components, maleic anhydride was hydrophilically grafted onto PCL. (3) Essential oils (EOs) from aromatic plants possess antimicrobial activities but are volatile. To apply EOs to food packaging paper, microencapsulation with β-cyclodextrin to embed EOs was successfully conducted. (4) Agricultural wastes like rice and barley straws were tried to be applied to papermaking and paper was successfully produced especially after digestion with sodium hydroxide. Those types of pulps seem to be valuable to replace plastics and even wood pulps for sustainable development.

Combined effects of lighting diffuseness, object surface and curvature on the object impression

Haruya Shiba[1], Hiromi Sato[2], Yoko Mizokami[2]

[1]Graduate school of Science and Engineering, Chiba University, Japan
[2]Graduate school of Engineering, Chiba University, Japan
[1, 2]1-33, Yayoicho, Inage-ku, Chiba-shi, Chiba, Japan

Abstract

Factors that influence the impression of an object surface include illumination, object shape, material, and reflectance. It has been shown that the gloss and roughness impression of an achromatic plate stimulus tends to weaken when the diffuseness of the illumination becomes stronger. The effect also depended on the surface gloss and roughness conditions. On the other hand, the gloss impression of cylindrical stimuli tended to be notably strengthened in some conditions, suggesting the combined effects of the object surface and curvature conditions. In this study, we investigated the effect of curvature on the impression of objects under lighting with different diffuseness conditions. We used achromatic half cylindrical stimuli with a sinusoidal wave surface. The curvature (1/mm) was varied in four steps, 0, 1/25, 1/16.25, and 1/15. Observers viewed each stimulus under three levels of diffuseness conditions and evaluated the gloss and roughness. As a result, the overall roughness impression decreased as the diffuseness increased. In addition, the gloss impression for glossy stimuli with low-frequency waves became higher with increasing diffuseness when the curvature was larger than 0. These results indicate the combined effects of surface conditions and curvature on the impression of the object's surface.

The 12th Asian Symposium on Printing Technology (ASPT 2022)

September 15th and 16th, 2022

Sponsored by:

Fuji Seal

CUULONG TRADING CORP. GROUP

FUJIFILM

ANVI

THE PRINT FACTORY VIETNAM BY NQH

TAC TOTAL PRINT Toàn Ấn Co.,Ltd.

CP PAPER

IN SINCE 1977

SCGP

DIAMIC

VINATAM©

AN NHAN DESIGN & PRINTING

Ho Chi Minh City University of Technology and Education
Thu Duc City, Ho Chi Minh City, Vietnam